K. F. J. Heinrich, Ed., *Microbeam Analysis – 1982*

RARE-EARTH PYROSILICATES ($RE_2Si_2O_7$) AS POTENTIAL ELECTRON MICROPROBE STANDARDS

J. A. Speer and T. N. Solberg

Microprobe analyses involving rare earth elements (REE) lag behind those of other elemments because of the numerous interfering x-ray spectra and the lack of comparable standards for all the REE. Little can be done about the x-ray spectra (Fig. 1), but the standards are amenable to improvement. Previous standards have included metals, oxides,[1] REE-doped anorthite glass,[2] analyzed minerals, and a limited number of synthetics such as REE-aluminate garnets. Problems with these standards include oxidation of the metals, hygroscopism of some oxides, and (for the minerals and glasses) limited quantities and the necessary testing for homogenization and actual amounts present.

One of the REE silicate compounds[3] appeared to be a promising standard. They contain significant amount of REE are stoichiometric, have high thermal stabilities, and can be manufactured when needed. The simplest compound appeared to be the REE analogs of the minerals thortveitite ($Sc_2Si_2O_7$) and thalenite ($Y_2Si_2O_7$). The $RE_2Si_2O_7$ compounds are known in all the binary REE_2O_3-SiO_2 systems and they show extensive polymorphism.[4]

The members of the REE pyrosilicates have been prepared by direct sintering of the oxides[5,6,7] or by growth from various fluxes.[8,9,10] In this study, the flux method for growing REE pyrosilicates was used and thus allowed relatively large, stoichiometric crystals to form.

The REE pyrosilicates were grown from molten Li_2MoO_4-MoO_3 or Li_2MoO_4-SiO_2 fluxes at approximately 850°C. The starting materials were 99.9% REE oxides and 99.95% SiO_2. All chemicals were from Apache Chemicals, Inc., Seward, Illinois. The charge consisted of between 5 and 10 wt-% of stoichiometric $RE_2O_3 \cdot 2SiO_2$ in the flux, well mixed in a platinum crucible. The charge was held at temperature in a muffle furnace for 4 to 5 days. The charge and crucible were air cooled and the flux was dissolved away in hot water.

The REE pyrosilicates grown thus far are the Pr, Nd, Sm, Tb, Er, Tm, and Y compounds (Fig. 2). The crystals have been as large as 4 mm in the case of Pr and Nd, but most are between 0.5 and 1 mm. X-ray powder and single-crystal work show the crystals to be one of the number of various polymorphs that are possible with these compounds. They are stable under the electron beam and microprobe analyses of the Nd pyrosilicate (Table 1) would suggest near ideal composition.

TABLE 1.--Microprobe analysis of flux-grown Nd-pyrosilicate.

	Flux-grown*	Ideal $Nd_2Si_2O_7$
SiO_2	27.12	26.32
Nd_2O_3	73.49	73.68
	100.61	100.00

*average of 6 analyses. Si-standard, quartz (SiO_2); Nd-standard, Nd-Ga garnet ($Nd_3Ga_5O_{12}$).

The authors are at the Department of Geological Sciences of the Virginia Polytechnic Institute and State University, Blacksburg, VA 24061-0976.

UNIVERSITÉ PIERRE ET MARIE CURIE
LABORATOIRE DE PÉTROLOGIE MINÉRALOGIQUE
4, place Jussieu, 75252 Paris Cedex 05
Tour 26, 3e étage
43 36 25 25, poste 51.88
Télex UPMC Six 200145 F

Michel F I A L I N

Pa ris, February 2, 1988

Dr J.A. SPEER
Department of Geological of the
Virginia Polytechnic Institute
and State University
BLACKSBURG VA 24061-0976
Etats-Unis.

Dear Dr Speer,

I have read with great interest your short note on "Rare-Earth pyrosilicates ($R_2Si_2O_7$)* as potential electron microprobe standards" I would be most interested in obtaining a few grains of any of the pyroxilicates that would be available.

Sincerely,

Michel FIALIN

* + $Y_2Si_2O_7$

North Carolina State University
School of Physical and Mathematical Sciences

Department of Marine, Earth and Atmospheric Sciences
(919) 737-3711

Box 8208, Raleigh, NC 27695-8208

Dept. Marine, Earth and Atmospheric Sciences
Box 8208
North Carolina State University
Raleigh, NC 27695-8208 USA
March 11, 1988

Dr. Michel Fialin
Laboratoire de Pétrologie Minéralogique
Université Pierre et Marie Curie
4, place Jussieu, 75252
Paris Cedex 05
France

Dear Dr. Fialin:

Thank you for letter expressing interest in our paper on rare-earth pyrosilicates. A copy is enclosed.

During the last year I have moved from the Virginia Polytechnic Institute to the North Carolina State University. As there are not extensive microprobe facilities here, I left most of the synthetic microprobe standards I grew, including all of the REE pyrosilicates with my coauthor at VPI - Todd N. Solberg. Todd operates the electron microprobe facility there. I would suggest writing him as to what is available, though he may not be prompt in answering his mail.

Sincerely yours,

J. Alexander Speer

Sc - thortveitite

$Sc_2Si_2O_7$

Sc_2O_3	53.44
SiO_2	46.56
	100.00

Journal of the Less-Common Metals
Elsevier Sequoia S.A., Lausanne – Printed in The Netherlands

THE POLYMORPHS OF THE RARE-EARTH PYROSILICATES $R.E._2Si_2O_7$, [R.E.: La, Ce, Pr, Nd, Sm]

J. FELSCHE AND W. HIRSIGER
Institut für Kristallographie und Petrographie der ETH, Zürich (Switzerland)
(Received January 31st, 1969)

SUMMARY

The low- and high-temperature forms of the isostructural pyrosilicate compounds are described in terms of single crystal- and powder X-ray data. The low-temperature form is tetragonal, space group $P4_1$, or $P4_122$. Crystals of the high-temperature form show orthorhombic symmetry, possible space group $Pna2_1$, or *Pnma*. Cell dimensions and indexed *d*-spacings of all compounds are given.

The polymorphs are isostructural with the α- and β-form of the pyrophosphates $M_2P_2O_7$, [M = Ca, Sr, (Ba)].

INTRODUCTION

The existence of rare-earth pyrosilicates, in addition to the known minerals thortveitite, $Sc_2Si_2O_7$, and thalenite, $Y_2Si_2O_7$, has been established by recent phase diagram studies of various of the binary systems $R.E._2O_3$–SiO_2[1,2].

The pyrosilicates of the 14 lanthanide elements have been classified into three different groups according to their different vibration spectra in the 450–1050 cm^{-1} region[3,4] and their different X-ray powder patterns[5]. These diffraction patterns could not be indexed however because of the absence of structural information on all of the compounds.

The pyrosilicates of the elements lanthanum through holmium exhibit polymorphism with a transition point of the two phases reported to be at about 1275°C, and an incongruent melting point at about 1760°C[5].

The polymorphs of the first group of rare-earth pyrosilicates, which include the elements La → Sm will be described in this paper crystallographically, in terms of single crystal- and powder X-ray data.

EXPERIMENTAL

The high-temperature form of the pyrosilicate group was obtained by solid-state reaction of the lanthanide oxides with a fine-grained quartz powder in the temperature range 1550°–1600°C. The starting materials in the case of La, Nd and Sm were the sesquioxides; Ce and Pr however were used in the form of CeO_2 and

Pr_6O_{11}, respectively. All the compounds were prepared in air under atmospheric pressure, with the exception of $Ce_2Si_2O_7$ and $Pr_2Si_2O_7$. These two compounds were highly sensitive to atmospheric oxygen unless quenched. In the case of $Ce_2Si_2O_7$, slow cooling from the formation temperature led to decomposition and subsequent formation of CeO_2, cristobalite and a glass. However, high-temperature $Ce_2Si_2O_7$ was prepared without any difficulty in an inert atmosphere as well as under high-vacuum conditions.

More detailed information about the kinetics of formation of $Ce_2Si_2O_7$, starting with $2CeO_2+2SiO_2$, was obtained by a thermogravimetric study. According to the expected reduction of $Ce^{4+} \rightarrow Ce^{3+}$ the oxygen was given off in two steps. The O_2-gas was analyzed by a high-resolution mass spectrometer, which was connected to the reaction chamber. As shown in Fig. 1, the first reaction occurs at 700°–900°C.

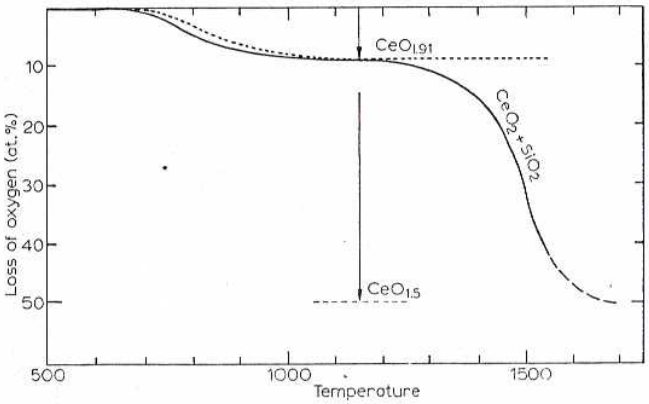

Fig. 1. Thermal decomposition of pure CeO_2 (dotted line), and of CeO_2 in the presence of SiO_2 (heavy line). Nitrogen atmosphere, normal pressure, heating rate: 4°/min.

(This was also observed with pure CeO_2 only.) It results in the formation of the grey-blue phase $CeO_{1.91}$ which is supposed still to have the fluorite type structure of CeO_2, with anion vacancies[6]. The large reduction step at 1500°C however occurs in the presence of SiO_2 only, *i.e.*, with the simultaneous formation of $Ce_2Si_2O_7$. Hence the reaction equation is:

$$2CeO_2+2SiO_2 \xrightarrow{800^\circ C} 2CeO_{1.91}+2SiO_2+O_{0.18}\uparrow$$

$$\xrightarrow{1500^\circ C} Ce_2O_3+2SiO_2+O_{0.82}\uparrow \rightarrow Ce_2Si_2O_7.$$

In the synthesis of $Pr_2Si_2O_7$, the thermal reduction under normal atmosphere of $Pr_6O_{11} \rightarrow Pr_2O_3$ was completed before the formation temperature of $Pr_2Si_2O_7$ at 1560°C was reached.

The low-temperature compounds were formed by cooling the samples gradually (0.5°/min) from 1600°C to 1200°C and subsequent annealing at 1200°C for about 100 h. Structurally, this means that the high-temperature form was converted to the low-temperature phase. But under normal atmospheric (air) pressure this procedure was succesful only for the pyrosilicates of the smaller lanthanide atoms, neodymium and samarium. The low-temperature forms of $La_2Si_2O_7$ and $Pr_2Si_2O_7$ were prepared in a similar way but under high-vacuum conditions. The high-temperature form of $Ce_2Si_2O_7$ could not be transformed to the low-temperature phase by these methods.

The transformation obviously involves a reaction of the first kind, *i.e.*, the breaking of lanthanide–oxygen bonds and a reconstruction of the coordination polyhedra. The transition, studied in a Mettler thermoanalyzer (20 μV sensitivity), did not show any DTA signal in the temperature range 20°C–1550°C employing heating rates of 0.1°C through 15°C per minute. However the high-temperature form was always observed at temperatures above 1350°C on the basis of its X-ray pattern.

The chemical composition of the compounds was checked with the electron microprobe analyzer. Within the limits of error the theoretical composition $R.E._2O_3 \cdot 2SiO_2$ was confirmed. Single crystals selected for the X-ray investigation on the precession camera were analyzed and showed an atomic ratio of R.E.: Si = 0.98 ± 0.03.

RESULTS

Single crystals about 0.2 × 0.15 × 0.1 mm in size were used to determine the lattice symmetry of the two polymorphic forms. The *d*-spacings were obtained by Guinier $FeK\alpha$-photographs.

TABLE I

CELL DIMENSIONS AND DENSITIES OF THE ORTHORHOMBIC HIGH-TEMPERATURE FORMS

Standard deviations are given in parentheses in units of the last decimal place (Z = formula units per unit cell).

	$La_2Si_2O_7$	$Ce_2Si_2O_7$	$Pr_2Si_2O_7$	$Nd_2Si_2O_7$	$Sm_2Si_2O_7$
a (Å)	8.794 (2)	8.722 (1)	8.674 (1)	8.630 (2)	8.564 (7)
b (Å)	13.201 (2)	13.056 (2)	12.996 (2)	12.945 (2)	12.855 (9)
c (Å)	5.409 (1)	5.401 (1)	5.405 (1)	5.391 (1)	5.383 (5)
V (Å^3)	627.95 (8)	615.09 (7)	609.40 (7)	602.37 (7)	592.61
Z	4	4	4	4	4
ϱ_o (gcm^{-3})	4.702 (6)	4.812 (7)	4.900 (9)	5.011 (6)	5.219 (7)
$\varrho_{calc.}$ (gcm^{-3})	4.718	4.842	4.905	5.044	5.233

TABLE II

CELL DIMENSIONS AND DENSITIES OF THE TETRAGONAL LOW-TEMPERATURE FORMS

Standard deviations are given in parentheses in units of the last decimal place (Z = formula units per unit cell).

	$La_2Si_2O_7$	$Pr_2Si_2O_7$	$Nd_2Si_2O_7$	$Sm_2Si_2O_7$
a (Å)	6.7945 (9)	6.7657 (6)	6.7405 (6)	6.6933 (8)
c (Å)	24.871 (8)	24.608 (4)	24.524 (4)	24.384 (9)
V (Å^3)	1148.1 (9)	1126.4 (2)	1114.3 (2)	1092.4 (3)
Z	8	8	8	8
ϱ_o (gcm^{-3})	5.112 (9)	5.266 (8)	5.382 (6)	5.672 (7)
$\varrho_{calc.}$ (gcm^{-3})	5.159	5.306	5.443	5.701

d-SPACINGS OF THE ORTHORHOMBIC HIGH-TEMPERATURE FORMS AND RELATIVE INTENSITIES OF THE OBSERVED REFLECTIONS (*hkl*)

(Reflections with $I/I_0 < 2$ are neglected.)

hkl	I/I_0*	$La_2Si_2O_7$	$Ce_2Si_2O_7$	$Pr_2Si_2O_7$	$Nd_2Si_2O_7$	$Sm_2Si_2O_7$
110	31	7.32	7.25	7.21	7.18	7.13
020	20	6.61	6.53	6.50	6.47	6.43
120	3	5.28	5.27	5.20	5.17	5.14
200	8	4.39	4.36	4.33	4.31	4.29
111	7	4.35	4.33			
121	3	3.77	3.70	3.74	3.73	3.71
201	100	3.41	3.39	3.38	3.37	3.35
031						
211	29	3.30	3.28	3.27	3.26	3.24
040	2		3.26	3.25	3.24	3.21
131	13	3.18	3.15	3.15	3.14	3.12
230	16	3.112	3.081	3.065	3.05	3.029
140	5	3.094	3.057	3.042	3.030	3.009
310	9	2.861	2.838	2.822	2.808	2.787
002	30	2.704	2.700	2.703	2.696	2.692
231	4	2.697	2.676	2.666	2.656	2.640
141	15	2.686	2.660	2.651	2.642	2.627
320	6	2.679	2.656	2.641	2.629	2.609
240	3	2.642	2.613	2.600	2.589	2.570
112	3	2.536	2.530	2.531	2.524	2.518
311	14	2.529	2.512	2.502	2.491	2.474
150	4	2.532	2.501	2.490	2.479	2.462
330	2	2.440	2.418	2.405	2.392	2.375
122	3	2.407	2.399	2.398		2.384
321	2	2.401	2.383	2.373	2.363	2.347
241	2	2.374	2.351	2.343	2.333	2.320
051						
202	2	2.303	2.296	2.294	2.286	2.279
400	21	2.199	2.178	2.167	2.157	2.144
060				2.162		
222	4	2.175	2.166			
410	16	2.168	2.151	2.139	2.128	2.112
160	5	2.137	2.111	2.102	2.093	2.079
251	3	2.088	2.069	2.059	2.049	2.040
420						2.031
232	20	2.041	2.030	2.027	2.020	2.012
142	11	2.030	2.023	2.021	2.014	2.006
401	3			2.012	2.003	1.989
341	2	2.032	2.014	2.006	1.997	1.984
411	2	2.013	1.998	1.989	1.980	1.966
421	7	1.940	1.932	1.923	1.914	1.901
322	4	1.903	1.893	1.889	1.882	1.873
242	5	1.889	1.877	1.874	1.867	1.859
152	6	1.843	1.835	1.831	1.825	1.817
431	8			1.824	1.817	1.805
261	8	1.851	1.831			
351	4	1.845	1.828	1.820	1.812	1.800
171	2	1.748	1.728	1.721	1.714	1.704
441	5	1.734	1.718	1.710	1.703	1.691
342	2	1.703	1.692	1.687	1.681	1.672
412	3	1.692	1.682	1.677	1.670	1.662
450	3	1.690	1.674	1.665	1.658	1.645
203	20	1.668	1.663	1.664	1.659	1.655
033						
213	3	1.655	1.651	1.650	1.646	1.642
521	5	1.621	1.609	1.601	1.593	1.582

* Measurement on $Ce_2Si_2O_7$.

The intensity data of the other compounds deviate $\leq 6\%$.

Crystals of the high-temperature form have orthorhombic symmetry. Sets of precession photographs showed the extinction rules:

$$okl\colon\ k+l=2n$$

$$hol\colon\quad h=2n.$$

This indicates the possible space groups $Pna2_1$ and $Pnma$.

The low-temperature structures showed tetragonal symmetry. Systematic absences of the reflections $(00l)$ with $l \neq 4$ were observed, indicating a space group $P4_1$ or $P4_122$.

TABLE IV

d-SPACINGS OF THE TETRAGONAL LOW-TEMPERATURE FORMS AND RELATIVE INTENSITIES OF THE OBSERVED REFLECTIONS (*hkl*)

(Reflections with $I/I_1 < 2$ are neglected.)

hkl	I/I_1*	$La_2Si_2O_7$	$Pr_2Si_2O_7$	$Nd_2Si_2O_7$	$Sm_2Si_2O_7$
004	3	6.21	6.15	6.13	6.10
012	6	5.96	5.93	5.91	5.87
013	8	5.26	5.22	5.20	5.17
110	23	4.80	4.78	4.76	4.74
112	24	4.48	4.46	4.44	4.41
113	48	4.15	4.13	4.12	4.09
015	8	4.01	3.98	3.96	3.94
016	10	3.54	3.51	3.49	3.47
115	23	3.46	3.43	3.42	3.39
020	12	3.40	3.38	3.37	3.34
021	15	3.37	3.35	3.33	3.31
022	39	3.28	3.26	3.25	3.22
023	39	3.143	3.127	3.116	3.095
116	13	3.136	3.114	3.103	3.084
008	100	3.109	3.078	3.067	3.047
121	27	3.016	3.004	2.993	2.971
024	9	2.981	2.966	2.953	2.934
122	13	2.952	2.938	2.927	2.908
123	30	2.853	2.837	2.829	2.809
117	3	2.857	2.832	2.822	
025	25	2.805	2.787	2.779	2.760
124	13	2.730	2.716	2.705	2.687
026	10	2.628	2.609	2.600	2.584
125	14	2.593	2.576	2.569	2.552
221	16	2.391	2.381	2.372	2.356
119	9	2.395	2.373	2.365	2.351
028	8	2.293	2.276	2.268	2.254
031	14	2.255	2.246	2.237	2.223
033	10	2.185	2.175	2.167	2.152
034	33	2.128	2.118	2.109	2.096
132	13	2.117	2.108	2.100	2.089
129	14	2.044	2.029	2.021	2.009
134	12	2.030	2.021	2.013	1.999
0210	7	2.007	1.989	1.983	1.971
227	17	1.990	1.978	1.970	1.957
232	13	1.863	1.855	1.848	1.835
229	17	1.813	1.799	1.793	1.782
336	11	1.715	1.707	1.699	1.688

* Measurement on $Nd_2Si_2O_7$. The intensity data of the other compounds deviate $< 8\%$.

The cell dimensions and their standard deviations given in the Tables were obtained by the normal procedure of least-squares refinement on data taken from the Guinier $FeK\alpha$-photographs. The densities given (g/cm^3) were measured by the flotation method (ϱ_0); the calculated values ($\varrho_{calc.}$) are based on 4 or 8 formula units per unit cell.

The powder diffraction patterns of all compounds were indexed unambiguously. The intensity of the reflections (*hkl*) were measured both with a Siemens densitometer and with a Philips diffractometer.

DISCUSSION

Previous results with the rare-earth pyrosilicates, which indicate that the first lanthanide elements form one structurally similar group, are substantiated for the elements La → Sm by this study.

Both the high- and low-temperature forms show a decreasing cell volume in accord with the lanthanide contraction. Furthermore it is evident from the crystal data that these compounds are isostructural with the polymorphs of the pyrophosphates $M_2P_2O_7$, [M = Ca, Sr, (Ba)]. Two new members therefore are added to the large family of analogous silicate–phosphate structures.

One of the analogous structure types, the high-temperature form of $Sr_2P_2O_7$, has been described recently by GRENIER AND MASSE[7], who found for it the space group $Pna2_1$ and the cell dimensions a, 8.87 Å; b, 13.27 Å and c, 5.39 Å. Comparing the earlier powder data of the pyrophosphate group[8] with our (*hkl*)-intensities the structural analogy is confirmed and we arrive at the following description for the pyrosilicate structure.

The most remarkable feature of the high-temperature structure is the grouping of the $[Si_2O_7]^{6-}$ double tetrahedra around the two rare-earth atoms which occupy two nonequivalent positions in the cell. This grouping results in an eightfold coordination. So far coordination numbers of 6, 7, 9 and 12 are known for the trivalent ion only. The 8 oxygens in the present case are located at the corners of a slightly distorted cube centered by the lanthanide atom. The distortion is mainly caused by two oxygens of two different $[Si_2O_7]^{6-}$-double tetrahedra.

This type of coordination polyhedron in the pyrosilicate structure accounts for the structural relationship to the fluorite-related oxide phases of the rare earth elements. The length of the c-axis of the silicate structure (5.40–5.38 Å) corresponds closely to the cell constant $a_0 = 5.41$ Å of the dioxide structures (*e.g.*, CeO_2, Pr_6O_{11}), which represents just twice the length of a coordination cube edge. This type of coordination polyhedron is maintained in the C-type structure of the sesquioxides but with 2 positions at the corners of the cube vacant.

The crystal structure of the low-temperature form may be best described in terms of the data given by WEBB[9] on β-$Ca_2P_2O_7$. He found the structure of this compound to have tetragonal symmetry, space group $P4_1$, the cell containing 8 formula units with $a = 6.684$ Å and $c = 24.144$ Å.

The heavy atoms of the structure occur in 4 pairs of layers along the c axis. The layers are separated by approximately $\frac{1}{8}$ of the c-axis which is indicated by the strong (008)-reflection. Sets of two crystallographically independent groups of $[Si_2O_7]^{6-}$ double tetrahedra form infinite spirals along the fourfold screw axis. The spirals are held together by four independent rare-earth atoms. The different coordination numbers of these atoms are interesting; two of them have seven nearest oxygen neighbours, one has eight and one has nine. All the polyhedra may be described as octahedra distorted by the additional oxygens.

ACKNOWLEDGEMENTS

The authors thank Prof. F. LAVES for his interest in this work, Dr. M. CORLETT for the microprobe work and Owens–Illinois Inc., Toledo, for financial support.

REFERENCES

1 N. A. TOROPOV AND J. A. BONDAR, *Izv. Akad. Nauk SSSR, Otd. Khim. Nauk*, *4* (1961) 544; *5* (1961) 739; *8* (1961) 1372.
2 N. A. TOROPOV, F. A. GALAKOV AND S. F. KONOVALOVA, *Izv. Akad. Nauk SSSR, Otd. Khim. Nauk*, *4* (1961) 539; *8* (1961) 1365.
3 A. N. LAZAREV AND T. F. TENISHEVA, *Izv. Akad. Nauk SSSR, Otd. Khim. Nauk*, *6* (1961) 964.
4 A. N. LAZAREV, T. F. TENISHEVA, J. A. BONDAR AND L. N. KOROLEVA, *Izv. Akad. Nauk SSSR, Otd. Khim. Nauk*, *4* (1962) 557.
5 J. WARSHAW AND R. ROY, in L. EYRING (ed.), *Progress in the Science and Technology of the Rare Earths*, Pergamon, Oxford, 1964, p. 215.
6 G. BRAUER AND K. A. GINGERICH, *J. Inorg. Nucl. Chem.*, *16* (1960) 87.
7 J. C. GRENIER AND R. MASSE, *Bull. Soc. Franç. Minéral. Crist.*, *15* (1967) 285.
8 P. W. RANBY, D. H. MASH AND S. T. HENDERSON, *Brit. J. Appl. Phys. Suppl.*, *4* (1965) 18, 25.
9 N. C. WEBB, *Acta Cryst.*, *21* (1966) 85

Journal of Crystal Growth 46 (1979) 671–680

FLUX GROWTH OF POLYMORPHIC RARE-EARTH DISILICATES, $R_2Si_2O_7$ (R = Tm, Er, Ho, Dy)

A. MAQSOOD *, B.M. WANKLYN and G. GARTON
Clarendon Laboratory, Department of Physics, University of Oxford, Oxford, UK

Received 28 September 1978

Optically clear single crystals of the polymorphic rare-earth disilicates $R_2Si_2O_7$ (R = Tm, Er, Ho, Dy) have been produced by the flux method. The single crystal growth of $R_2Si_2O_7$ (R = Tm, Ho, Dy) has not been reported previously. Wanklyn's generalised pseudoternary composition model was used successfully for the prediction of favourable starting compositions. Crystals of $Er_2Si_2O_7$ and $Ho_2Si_2O_7$ of both C- and D-types were obtained. Indexed X-ray powder pattern data is given for C-type $R_2Si_2O_7$ (R = Er, Ho) and D-type $Dy_2Si_2O_7$, and the antiferromagnetic transition temperatures of C- and D-$Er_2Si_2O_7$ are reported. Substitutional flux impurity levels have been determined by electron probe micro-analysis (EPMA).

1. Introduction

When prepared by reaction of the component oxides, the rare-earth disilicates have structures which vary as a function of two parameters, the size of the cation and the temperature of synthesis [1,2]. It has been established by X-ray analysis that the compounds undergo a series of phase transformations between 1000 and 1600°C. Each subsequent crystal modification with a larger cation has the high temperature structure of the preceding cation of smaller ionic radius, as is seen in fig. 1 [1,2].

Rare-earth compounds are of technological and research interest on account of their magnetic, electrical and optical properties. Although the structures and phase transitions of the rare-earth disilicates prepared by sintering the components have been extensively investigated [3–5], and Felsche [6] has reviewed their structures and polymorphism, no other physical properties have previously been reported.

Some members of the series $R_2Si_2O_7$ (R = Yb, Er, Gd, Nd) have been prepared as single crystals by the Verneuil method [5]. The growth of $Yb_2Si_2O_7$ crystals from KF flux [7] and the growth of $Er_2Si_2O_7$ by the "vapour-flux" technique [8] and by the flux method [9] have been reported. The present paper describes the crystal growth of $R_2Si_2O_7$ from several flux systems, and the investigation of the polymorphic forms by X-ray methods.

2. Nomenclature

Ito and Johnson [1], as well as Warshaw and Roy [10] used the Greek letters α, β and δ for distinguishing the polymorphic forms of the rare-earth disilicates. Felsche [2,6] followed the nomenclature of the polymorphs of the rare-earth sesquioxides, designating the various structure types by the capital letters A, B, C, D, E, F, G, the method also followed here.

3. Materials and equipment

The chemicals were: Rare Earth Products 99.9% pure R_2O_3 (R = Tm, Er, Ho, Dy); BDH "Analar" MoO_3, PbO, K_2CO_3; BDH "extra pure" PbF_2; BDH silica gel, 60–120 mesh. The SiO_2, which contained 12 wt% H_2O, was calcined at 1000°C and then kept in a desiccator. V_2O_5 was melted prior to use. The furnaces have been described previously [11], and the

* Physics Department, Quaid-i-Azam University, Islamabad, Pakistan.

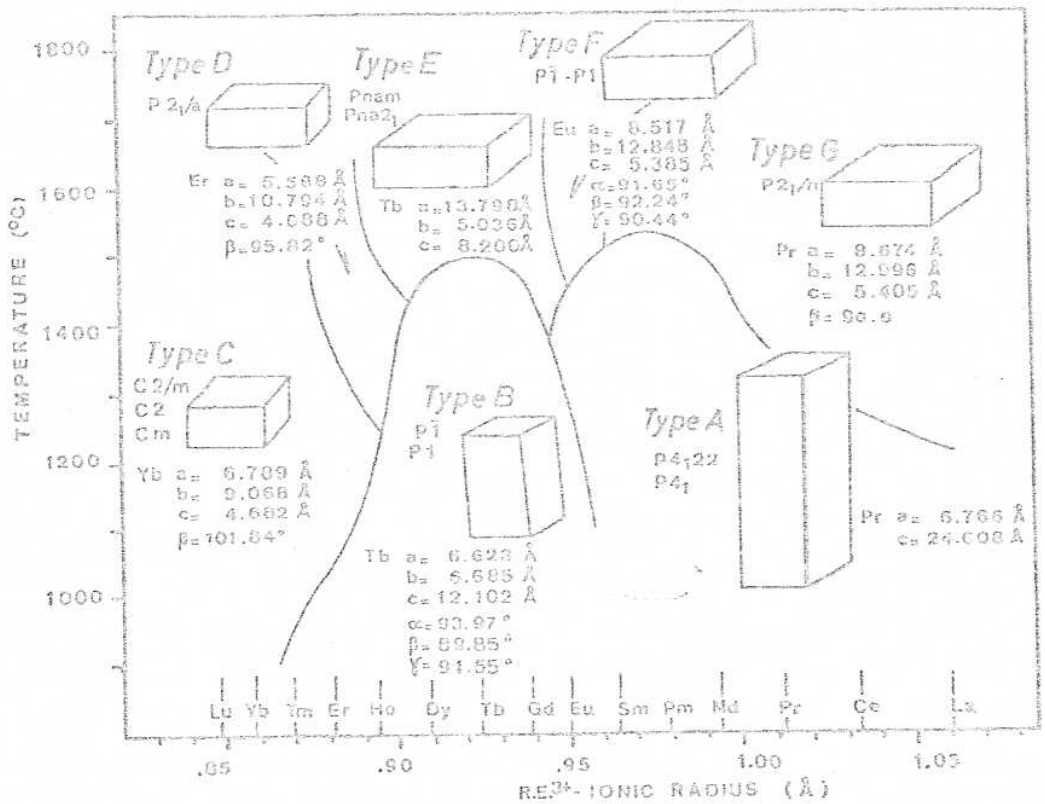

Fig. 1. Stability range of sinters and crystal data on the structure types A to G of the rare-earth disilicates [2]. (By courtesy of the Editor, J. Less Common Metals.)

crucibles were of pure platinum, of 10, 20 or 50 cm^3 capacity, and of 0.50 mm wall thickness.

4. Calculation of starting compositions

Wanklyn has pointed out that starting compositions for the flux growth of compounds consisting of a refractory oxide and an acidic oxide require an excess of the acidic oxide component, as shown in the generalised pseudoternary composition diagram (fig. 2) [12]. The apices A, B and C represent respectively the refractory oxide, the basic oxide or oxide plus fluoride, and the acidic and/or amphoteric oxide components. The distance of PQ from BC represents the molar solubility of the refractory oxide in the system at the soak temperature. The advantage of this model is that compositions in only a relatively small area require investigation, first along the line PQ to find O, where the phase with the most suitable habit from crystallises, then along the line NOM to determine the amount of refractory oxide that can be

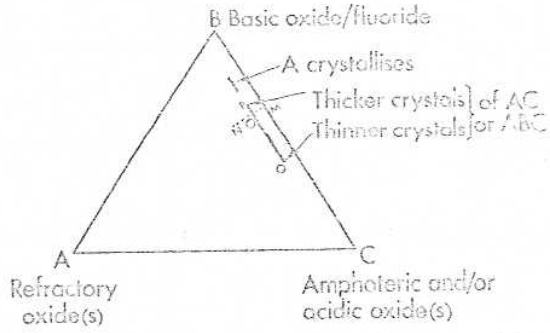

Fig. 2. Generalised pseudoternary composition diagram [12].

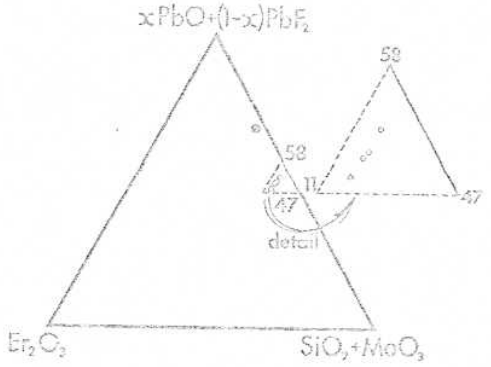

Fig. 3. Diagram showing starting compositions for the growth of C-$Er_2Si_2O_7$ (soak temperature, 1270 ± 5°C); (●) compositions resulting in either C-$Er_2Si_2O_7$ or Er_2SiO_5; (○) compositions resulting in larger crystals of C-$Er_2Si_2O_7$; (▽) compositions resulting in smaller crystals of C-$Er_2Si_2O_7$.

completely dissolved in the system at a convenient soak temperature.

For such compounds, it is also suggested that the acidic or amphoteric component in the generalised pseudoternary system can be replaced in part by another acidic oxide, provided no undesired compound results. $Er_2Si_2O_7$ falls into this class of compounds, and thus an excess of the acidic oxide component is required. However, a high concentration of SiO_2 leads to an inconveniently high viscosity, and on the basis of previous work [13], part of the excess SiO_2 in the system Er_2O_3–$(PbO + PbF_2)$–SiO_2 has been replaced by MoO_3. Similarly, in the system R_2O_3–Bi_2O_3–SiO_2, part of the excess SiO_2 has been replaced by V_2O_5. In addition to reducing the viscosity, V_2O_5 has been found effective in reducing the attack on platinum which occurs when free bismuth is produced by thermal dissociation [14]:

$$3\ V_2O_5 + 2\ Bi \rightleftharpoons Bi_2O_3 + 3\ V_2O_4\ .$$

It has also been shown previously that part of the PbO/PbF_2 component can be replaced by K_2O/KF, sometimes with advantageous results [9].

Tables 1a, b and c give starting compositions in the above systems, furnace programmes and crystal products. The experiments are representative of a much larger number performed. Starting compositions which yielded the crystals indicated are shown in fig. 3.

5. Experimental

For mixture containing Bi_2O_3–$(SiO_2 + V_2O_5)$, the crucible lids were loosely fitted and the furnace was heated at rather a slow rate, 88 K h^{-1}, to allow complete oxidation of the contents. To minimize evaporation losses for the $(PbO + PbF_2)$–$(SiO_2 + MoO_3)$ fluxes, the crucibles were provided with tightly fitting lids, and the furnace was heated at 176 K h^{-1}. Since the crystals reacted with even very dilute acid, the flux was separated by hot-pouring the melts while still molten [15], leaving the crystals attached to the crucible base and walls. The crystal products were identified by comparing their X-ray powder patterns with published data. In the experiments described in sections 5.1 and 5.2, it was frequently noted that the number of crystals was six or fewer, exceptionally low for growth by spontaneous nucleation.

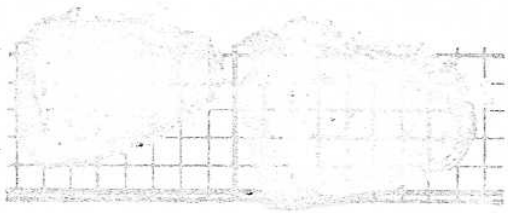

Fig. 4. Platelets of C-$Er_2Si_2O_7$ grown from $(PbO + PbF_2)$–$(SiO_2 + MoO_3)$ flux (mm grid).

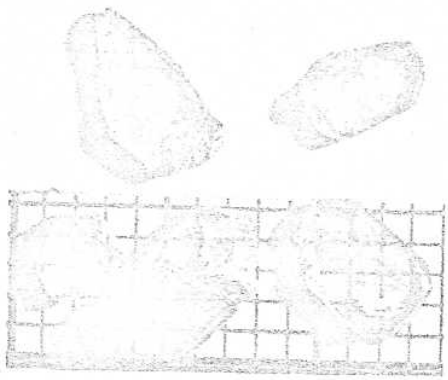

Fig. 5. Faceted crystals of C-$Tm_2Si_2O_7$ grown from $(PbO + PbF_2)$–$(SiO_2 + MoO_3)$ flux (mm grid).

Table 1

(a) Starting compositions and experimental conditions for the growth of $Er_2Si_2O_7$ and $Tm_2Si_2O_7$ from $(PbO + PbF_2)$–$(SiO_2 + MoO_3)$ flux

Phase obtained	Batch No.	Starting composition (mole%)					Crucible volume (cm^3)	Initial temp. (°C)	Soak period (h)	Cooling rate ($K\ h^{-1}$)	Final temp. (°C)	Notes on the crystals
		R_2O_3	SiO_2	MoO_3	PbF_2	PbO						
C-$Er_2Si_2O_7$	1	5.65	17.66	26.38	20.37	30.03	20	1270	24	2.4	1020	A few platy crystals up to 7 mm × 5 mm × 1 mm (fig. 4)
	2	5.81	17.49	26.40	20.25	30.04	20	1270	24	1.0	800	Optically clear, faceted crystals up to 2 mm × 3 mm × 2 mm
	3	2.86	5.99	22.18	35.00	39.97	20	1270	24	1.0	800	Small crystals of C-$Er_2Si_2O_7$ or larger, equidimensional Er_2SiO_5
C-$Tm_2Si_2O_7$		2.90	6.00	22.10	35.00	34.00	20	1270	24	2.4	950	Faceted crystals up to 3 mm × 2 mm × 1 mm, as shown in fig. 5

(b) Effects of replacing part of $(PbO + PbF_2)$ by $(K_2O + KF)$

Phase obtained	Starting composition (mole%)							Crucible volume (cm^3)	Initial temp. (°C)	Soak period (h)	Cooling rate ($K\ h^{-1}$)	Final temp. (°C)	Notes on the crystals
	R_2O_3	SiO_2	MoO_3	PbF_2	PbO	K_2O	KF						
C-$Er_2Si_2O_7$	5.75	15.17	25.31	13.99	25.22	0	14.55	20	1270	24	2.4	850	Six faceted crystals, up to 4 mm × 3 mm × 2 mm
D-$Er_2Si_2O_7$ or C-$Er_2Si_2O_7$	5.71	16.87	23.45	14.35	23.65	5.01	10.96	20	1270	24	2.4	900	Three out of ten batches resulted in the D-form; in one case, only one triangular plate of D-type, 14 mm × 8 mm × 3 mm
C-$Er_2Si_2O_7$	5.71	16.87	23.45	14.35	23.65	5.01	10.96	20	1260	24	2.4	900	Thick, nearly equidimensional crystals of C-type only
C-$Tm_2Si_2O_7$	5.80	16.89	23.40	14.40	23.71	4.8	11.00	20	1260	24	2.4	900	Platy crystals, up to 3 mm × 2 mm × 1.5 mm

Table 1 (continued)
(c) Starting compositions and experimental conditions for crystal growth of $R_2Si_2O_7$ (R=Tm, Er, Ho, Dy) from Bi_2O_3--(SiO_2 + V_2O_5) flux

Phase obtained	Starting composition (mole%)					Crucible volume (cm^3)	Initial temp. (°C)	Soak period (h)	Cooling rate ($K\,h^{-1}$)	Final temp. (°C)	Notes on the crystals
	R_2O_3	SiO_2	Bi_2O_3	V_2O_5	B_2O_3						
C-$Tm_2Si_2O_7$	6.83	21.98	56.67	14.52		10	1240	20	3	1120	Clear platy crystals up to 4 mm × 3 mm × 1 mm at the base of the crucible
D-$Er_2Si_2O_7$	6.75	22.00	56.60	14.65		20	1242	20	1.5	950	Clear platelets up to 8 mm × 6 mm × 2 mm
C-$Ho_2Si_2O_7$	10.68	33.34	42.94	4.40	8.68	15	1240	20	5	1120	3 mm × 3 mm × 0.2 mm platelets on the surface of the melt
D-$Ho_2Si_2O_7$	7.02	21.94	56.56	14.48		50	1240	20	1.5	1050	Optically clear, faceted crystals up to 6 mm × 3 mm × 1 mm grew at the sides of the crucible; some are shown in fig. 6
E-$Dy_2Si_2O_7$	7.14	21.43	57.15	14.28		15	1250	18	1.5	960	Faceted rods up to 10 mm × 2 mm × 2 mm grew across the melt and thin platelets up to 4 mm × 3 mm × 0.2 mm at the surface (fig. 7)
D-$Ho_2Si_2O_7$ and apatite	8.67	21.55	55.55	14.23		10	1240	20	1.5	980	Large platy crystals of D-phase and hexagonal apatite rods, 2 to 3 mm in length
D-$Ho_2Si_2O_7$ and apatite	10.18	21.20	54.64	13.99		10	1240	20	1.5	980	Apatite rods up to 3 mm × 1 mm × 1 mm and D-$Ho_2Si_2O_7$ in powder form (solution was incomplete)

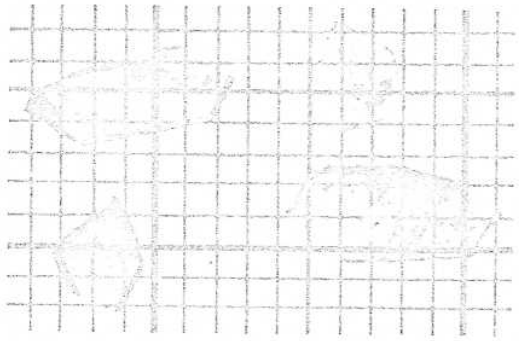

Fig. 6. Platelets of D-$Ho_2Si_2O_7$ grown from Bi_2O_3–(SiO_2 + V_2O_5) flux (mm grid).

5.1. Experiments in the systems R_2O_3–(PbO + PbF_2)–(SiO_2 + MoO_3). (R = Tm, Er)

Fig. 3 shows starting compositions which yielded C-$Er_2Si_2O_7$ and C-$Tm_2Si_2O_7$, and fig. 4 shows some of the crystals. Composition 3, in table 1, resulted sometimes in Er_2SiO_5, and is evidently near the boundary between the regions where $Er_2Si_2O_7$ and Er_2SiO_5 are the primary phases. The crucibles containing composition 3 frequently leaked because of the relatively high PbO content, which increased during slow cooling because of evaporation and hydrolysis of PbF_2.

The loss by evaporation from compositions which yielded $Er_2Si_2O_7$ was 30 to 60 wt%. Initially, many batches yielded rare-earth apatites [16], and it was found that these were obtained when the weight loss

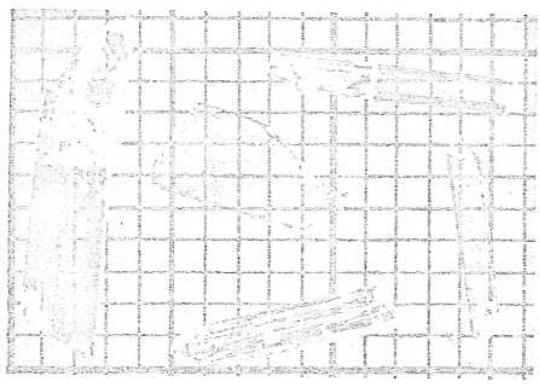

Fig. 7. Rods of E-$Dy_2Si_2O_7$ grown from Bi_2O_3–(SiO_2 + V_2O_5) flux (mm grid).

was low, as a result of relatively fast cooling (4 to 8 K h^{-1}) or very tightly-fitted lids. The apatites are of variable formula, such as $Pb_{1.4}Er_{7.93}Si_{3.6}O_{13}$ [16], and, since they contain lead, may be expected to crystallise from melts with a lower concentration of R_2O_3 in a lower temperature range. On the other hand, batches which yielded $Er_2Si_2O_7$ became more concentrated by evaporation, so that growth occurred at a higher temperature.

5.2. Experiments with (K_2O + KF) in the flux

In some experiments, (PbO + PbF_2) was partly replaced by equimolar amounts of (K_2O + KF), as shown in table 1b. When the soak temperature was above 1260°C, D-$Er_2Si_2O_7$ resulted in three out of ten batches. With lower soak temperatures, C-$Er_2Si_2O_7$ was always obtained. The C- and D-type crystals did not occur together in a crucible, and there was no sign, such as twin domains, of crystallographic transitions having occurred.

EPMA, given in table 2, shows that in C- and D-$Er_2Si_2O_7$ the flux impurity levels are similarly low; it is thus improbable that the substitutional incorporation of K^+ in the lattice can account for the fact that the D-type phase was obtained only when K^+ was present in the melt. Instead, since the D-form was not obtained in the absence of K^+, it may be that the complex ions present at the nucleation stage determine the polymorph that is formed. As shown in table 1b, the temperature at which D-$Er_2Si_2O_7$ is produced from the fluxed melt is very different from that which applies to the formation of D-$Er_2Si_2O_7$ as a sinter. Ito and Johnson found that the C to D transformation in sintered material occurred at 1400 ± 10°C [1].

5.3. Growth of $R_2Si_2O_7$ (R = Tm, Er, Ho and Dy) from Bi_2O_3–(SiO_2 + V_2O_5)

The flux system (PbO + PbF_2)–(SiO_2 + MoO_3) did not yield $R_2Si_2O_7$ with rare-earth ions larger than Er^{3+}; rare-earth apatites were instead produced. The only good alternative flux appeared to be Bi_2O_3–(SiO_2 + V_2O_5), although fluxes containing Bi_2O_3 are normally avoided, if possible, because the use of Bi_2O_3 reduces the life of platinum crucibles and also because Bi^{3+}, being similar in size and charge to R^{3+},

Table 2
Substitutional flux impurities in $R_2Si_2O_7$ crystals, determined by EPMA

Crystal	Cooling rate ($K\ h^{-1}$)	Pb (%)	K (%)	V (%)	Bi (%)
C-$Er_2Si_2O_7$	2.4	0.04	0.01	–	–
D-$Er_2Si_2O_7$	2.4	0.06	0.01	–	–
D-$Er_2Si_2O_7$	1.5	–	–	0.07	1.0
C-$Ho_2Si_2O_7$	5	–	–	0.05	2.0
D-$Ho_2Si_2O_7$	5	–	–	0.06	1.7
D-$Ho_2Si_2O_7$	1.5	–	–	0.3	1.6
E-$Dy_2Si_2O_7$	1.5	–	–	0.04	4.5

readily substitutes for it in the crystal lattice.

It was found that $Ho_2Si_2O_7$ and $Dy_2Si_2O_7$ crystallised from this system, though apatite crystals were occasionally obtained.EPMA shows that, as may be expected, the substitutional Bi content increased as the ionic radius of the rare-earth ion approached that of Bi^{3+}. Reducing the rate of cooling from 5 to 1.5 K h^{-1} did not appreciably reduce the percentage of Bi in the $Ho_2Si_2O_7$ crystals.

The solubility of Ho_2O_3 in Bi_2O_3–(V_2O_5 + SiO_2) has been determined by thermogravimetry (TGA) [17] and in these experiments the D-form was obtained in the range 1150 to 1350°C. Similar compositions yielded C-$Tm_2Si_2O_7$, D-$Er_2Si_2O_7$ and E-$Dy_2Si_2O_7$. However, when B_2O_3 was included in the starting composition, C-$Ho_2Si_2O_7$ was obtained, as indicated in table 1c.

The TGA experiments showed a temperature difference of 50 ± 5°C between the crystallization and the solubility temperatures, and this is taken into account in the crystallization ranges indicated in table 3. Although the supercooling has not been determined for the melts with ($PbO + PbF_2$), it has been assumed to have a similar effect on the crystallization temperatures from these compositions, given in table 3. The difference in the temperatures of formation of the polymorphs produced from the flux, as compared with the stability ranges of the sinters, is very marked, as table 3 makes clear.

5.4. Seeding experiments

To check whether the introduction of seed crystals would induce the formation of the corresponding polymorph, a series of experiments under similar conditions were performed. For example, seeds of E-$Dy_2Si_2O_7$ were added to a composition which normally produced D-$Ho_2Si_2O_7$. In every case, the result was negative, the added seeds evidently having no influence on the phase formed.

6. Notes on the crystals

The crystals have the colours of the corresponding rare-earth ions, except for $Dy_2Si_2O_7$, the pale green colour of which may be attributable to traces of V^{3+}

Table 3
Stability range of sintered polymorph, compared with temperature range for growth of the same crystal from the flux

Polymorph	Stability range for sinter (°C)	Temperature range in which polymorph was obtained from the flux (°C)	Flux components
C-$Tm_2Si_2O_7$	1000–1650	1220–1020 (in 2 batches)	($PbO + PbF_2$)–($SiO_2 + MoO_3$)
		1190–1120 (in 3 batches)	Bi_2O_3–($SiO_2 + V_2O_5$)
C-$Er_2Si_2O_7$	1050–1400	1220–800 (in 19 batches)	($PbO + PbF_2$)–($SiO_2 + MoO_3$)
D-$Er_2Si_2O_7$	1400–1700	1220–900 (in 3 out of 10 batches)	($PbO + PbF_2 + K_2O + KF$)–($SiO_2 + MoO_3$)
C-$Er_2Si_2O_7$	1050–1400	1220–900 (in 7 out of 10 batches)	($PbO + PbF_2 + K_2O + KF$)–($SiO_2 + MoO_3$)
C-$Er_2Si_2O_7$	1050–1400	1210–900 (in 6 batches)	($PbO + PbF_2 + K_2O + KF$)–($SiO_2 + MoO_3$)
D-$Er_2Si_2O_7$	1400–1700	1190–950 (in 4 batches)	Bi_2O_3–($SiO_2 + V_2O_5$)
C-$Ho_2Si_2O_7$	1200–1260	1190–1120 (one batch only)	Bi_2O_3–($SiO_2 + B_2O_3 + V_2O_5$)
D-$Ho_2Si_2O_7$	1260–1500	1190–1050 (in 10 batches)	Bi_2O_3–($SiO_2 + V_2O_5$)
E-$Ho_2Si_2O_7$	1450–1700	1190–960 (in 4 batches)	Bi_2O_3–($SiO_2 + V_2O_5$)

in the lattice. All the crystals showed simultaneous extinction under the polarising microscope. Thus there was no sign of structural transitions having occurred.

Only one form was present in each batch. In table 3, the conditions under which each form was obtained are compared with the temperature ranges in which the sintered materials have been reported to exist [2,6].

6.1. C-$R_2Si_2O_7$ (R = Tm, Er, Ho)

The X-ray powder patterns corresponded closely to the data for C-$Tm_2Si_2O_7$ [2]. The structure is that of the mineral thortveitite. Powder patterns of single crystal C-$Er_2Si_2O_7$ and C-$Ho_2Si_2O_7$ have been indexed according to the reported lattice parameters and space group, and the data are given in table 4.

Table 4
X-ray powder pattern data for C-$R_2Si_2O_7$ (R = Er, Ho)

I_{est}	hkl	$Er_2Si_2O_7$		$Ho_2Si_2O_7$	
		d_{calc} (Å)	d_{obs} (Å)	d_{calc} (Å)	d_{obs} (Å)
M	110	5.36	5.36	5.38	5.38
M	001	4.62	4.62	4.63	4.63
VW	020	4.46	4.47	4.48	4.47
VW	11$\bar{1}$	3.82	3.83	3.83	3.82
VW	200	3.35	3.35	3.36	3.36
M	111	3.25	3.25	3.26	3.25
VS	021	3.21	3.21	3.22	3.22
S	20$\bar{1}$	3.027	3.027	3.028	3.027
M	130	2.739	2.738	2.740	2.739
M	220	2.682	2.684	2.692	2.694
VW	002	2.312	2.311	2.316	2.316
M	131	2.262	2.262	2.271	2.269
W	221, 310	2.167	2.166	2.177	2.177
VW	31$\bar{1}$	2.134	2.133	2.138	2.134
VW	022	2.053	2.054	2.058	2.056
W	22$\bar{2}$	1.912	1.913	1.916	1.914
a_0(Å)		6.8517(4)		6.8750(9)	
b_0 (Å)		8.9241(5)		8.962(1)	
c_0 (Å)		4.7262(9)		4.7303(6)	
β(deg)		101.66(7)		101.69(6)	

Space groups: C 2/m, Cm, C2.

Table 5
X-ray powder pattern data for E-$Dy_2Si_2O_7$

I_{est}	hkl	d_{calc} (Å)	d_{obs} (Å)
W	110	4.71	4.71
S	002	4.09	4.06
S	210	4.04	4.06
W	211	3.63	3.62
W	400	3.42	3.41
VW	310	3.37	3.37
VW	401	3.15	3.14
S	112	3.090	3.084
VS	212	2.778	2.782
W	402	2.625	2.625
W	312	2.604	2.602
VW	020	2.509	2.510
M	120	2.468	2.468
VW	510	2.403	2.401
VW	013	2.397	2.397
VW	220	2.356	2.358
VW	412	2.326	2.326
VW	213	2.264	2.262
a_0 (Å)			13.686(8)
b_0 (Å)			5.019(3)
c_0 (Å)			8.185(6)

Space groups: Pnam, $Pna2_1$.

6.2. D-$R_2Si_2O_7$ (R = Er, Ho)

These compounds are the only two members of the series which possess the monoclinic P 21/b $Y_2Si_2O_7$ structure [5,18]. The crystals grew at the base of the crucible, with the c-axis perpendicular to the plane of the platelets.

6.3. E-$Dy_2Si_2O_7$

The X-ray powder pattern data was very similar to that for E-$Tb_2Si_2O_7$ [2], and has been indexed according to the reported cell dimensions and space group, as shown in table 5.

7. Magnetic transitions

These were determined for $Er_2Si_2O_7$. C-$Er_2Si_2O_7$ became antiferromagnetic at 2.50 ± 0.05 K, and D-$Er_2Si_2O_7$ at 1.71 ± 0.05 K. These temperatures are

exceptionally high for compounds of erbium. Details of the magnetic anisotropy and optical absorption spectra will be published.

8. Discussion

As shown in fig. 1, the lowest temperature polymorph, the B-phase, was obtained by sintering. However, it has not been observed in the preparation of any of the compounds by the flux method. Two polymorphs of each of $Er_2Si_2O_7$ and $Ho_2Si_2O_7$ were obtained, as shown in tables 1 and 3.

Similar effects have been observed in other polymorphic materials. $ThGeO_4$ has two tetragonal polymorphs, scheelite and zircon-type. Harris and Finch [19], in a phase stability study, found that only zircon-type crystallised from $(Li_2O + 2MoO_3)$ or $(Li_2O + 2WO_3)$ fluxes between 750 and 1420°C. They found that sintering experiments gave the scheelite form at 1050°C, but when a mineralizer was added, it converted to zircon-type at 750°C and above. $ThSiO_4$ also has two forms, tetragonal thorite and monoclinic huttonite. Flux growth experiments in the systems $(Li_2O + 2WO_3)$, $(Li_2O + 2MoO_3)$ and $(Na_2O + 2WO_3)$ produced thorite below 1225 ± 10°C, and huttonite above this temperature [20]. However, Wanklyn [21] obtained only huttonite, using $(PbO + PbF_2)$–$(SiO_2 + MoO_3)$ as flux, even when the soak temperature was as low as 1180°C.

All these observations indicate that the formation of the various polymorphs of $R_2Si_2O_7$, and also of $ThSiO_4$ and $ThGeO_4$, from fluxed melts depends not only on the temperature range in which the crystals grow but also on the chemical composition of the flux, which probably determines the form of the polymorph at the stage of nucleation.

9. Conclusion

Flux growth studies in the systems Er_2O_3–$(PbO + PbF_2)$–$(SiO_2 + MoO_3)$ and R_2O_3–Bi_2O_3–$(SiO_2 + V_2O_5)$, which resulted in crystals of the polymorphs of $R_2Si_2O_7$ (R = Tm, Er, Ho, Dy), have been described. An excess of the acidic oxide component over that required by the formula was necessary for the phase to crystallise, as was predicted from the generalised composition diagram for compounds of refractory and acidic oxides [12].

The temperature at which the polymorphs were obtained differed considerably from those previously reported for sintered materials and depended on the flux compositions. Thus it is doubtful whether flux growth is a useful technique for the determination of structural transitions, as proposed by Finch et al. [20]. However, this method has been shown to be very appropriate for the preparation of various polymorphs in single crystal form.

Acknowledgements

The authors express their thanks to Dr. S.H. Smith, especially for assistance with TGA, and to Mr. B.J. Garrard and Mr. F.R. Wondre for helpful discussions. They are also indebted to Mr. W. Davison of the School of Physics, University of Newcastle upon Tyne, for EPMA, and to Mr. Peter Clack for equipment building and platinum work. This study was supported in part by the Science Research Council. A.M. wishes also to thank the British Council for financial support.

References

[1] J. Ito and H. Johnson, Am. Mineralogist 53 (1968) 1940.
[2] J. Felsche, J. Less-Common Metals 21 (1970) 1.
[3] Yu.I. Smolin and Yu.F. Shepelev, Inorg. Mater. 4 (1967) 992.
[4] R.D. Shannon and C.T. Prewitt, J. Solid State Chem. 2 (1970) 199.
[5] Yu.I. Smolin and Yu.F. Shepelev, Acta Cryst. B26 (1970) 484.
[6] J. Felsche, The Crystal Chemistry of the Rare Earth Silicates, in: Structure and Bonding, Vol. 1, (Springer, New York, 1973) p. 99.
[7] I.A. Bondar, L.N. Koroleva and N.A. Toropov, in: Rost Kristallov, Vol. 6 (Inst. Krist., Akad. Nauk SSSR, Moscow, 1965) p. 111.
[8] B.M. Wanklyn, F.R. Wondre, G.B. Ansell and W. Davison, J. Mater. Sci. 9 (1974) 2007.
[9] B.M. Wanklyn, J. Crystal Growth 43 (1978) 336.
[10] I. Warshaw and R. Roy, in: Progress in the Science and Technology of the Rare Earths, Vol. 1 (Pergamon, (1964) p. 203.
[11] G. Garton, S.H. Smith and B.M. Wanklyn, J. Crystal Growth 13/14 (1972) 588.

[12] B.M. Wanklyn, J. Crystal Growth 37 (1977) 334.
[13] B.M. Wanklyn, F.R. Wondre, G.B. Ansell and W. Davison, J. Mater. Sci. 10 (1975) 1492.
[14] B.M. Wanklyn, J. Crystal Growth 7 (1970) 368.
[15] B.M. Wanklyn, in: Crystal Growth, Ed. B.R. Pamplin (Pergamon, 1975) 217.
[16] B.M. Wanklyn, F.R. Wondre, G.B. Ansell and W. Davison, J. Mater. Sci. 10 (1975) 1494.
[17] S.R. Smith and D. Elwell, J. Mater. Sci. 2 (1967) 297.
[18] N.G. Batalieva and Yu.A. Pyatenko, Zh. Strukt. Khim. 8 (1967) 548.
[19] L.A. Harris and C.B. Finch, Am. Mineralogist 57 (1972) 1894.
[20] C.B. Finch, L.A. Harris and G.W. Clark, Am. Mineralogist 49 (1964) 782.
[21] B.M. Wanklyn, J. Crystal Growth 37 (1977) 51.

alex - I hope you hadn't seen this (ie I hope I'm being redundant?) Zoe

Journal of Crystal Growth 46 (1979) 671–680

FLUX GROWTH OF POLYMORPHIC RARE-EARTH DISILICATES, $R_2Si_2O_7$ (R = Tm, Er, Ho, Dy)

A. MAQSOOD *, B.M. WANKLYN and G. GARTON
Clarendon Laboratory, Department of Physics, University of Oxford, Oxford, UK

Received 28 September 1978

Optically clear single crystals of the polymorphic rare-earth disilicates $R_2Si_2O_7$ (R = Tm, Er, Ho, Dy) have been produced by the flux method. The single crystal growth of $R_2Si_2O_7$ (R = Tm, Ho, Dy) has not been reported previously. Wanklyn's generalised pseudoternary composition model was used successfully for the prediction of favourable starting compositions. Crystals of $Er_2Si_2O_7$ and $Ho_2Si_2O_7$ of both C- and D-types were obtained. Indexed X-ray powder pattern data is given for C-type $R_2Si_2O_7$ (R = Er, Ho) and E-type $Dy_2Si_2O_7$, and the antiferromagnetic transition temperatures of C- and D-$Er_2Si_2O_7$ are reported. Substitutional flux impurity levels have been determined by electron probe micro-analysis (EPMA).

1. Introduction

When prepared by reaction of the component oxides, the rare-earth disilicates have structures which vary as a function of two parameters, the size of the cation and the temperature of synthesis [1,2]. It has been established by X-ray analysis that the compounds undergo a series of phase transformations between 1000 and 1600°C. Each subsequent crystal modification with a larger cation has the high temperature structure of the preceding cation of smaller ionic radius, as is seen in fig. 1 [1,2].

Rare-earth compounds are of technological and research interest on account of their magnetic, electrical and optical properties. Although the structures and phase transitions of the rare-earth disilicates prepared by sintering the components have been extensively investigated [3–5], and Felsche [6] has reviewed their structures and polymorphism, no other physical properties have previously been reported.

Some members of the series $R_2Si_2O_7$ (R = Yb, Er, Gd, Nd) have been prepared as single crystals by the Verneuil method [5]. The growth of $Yb_2Si_2O_7$ crystals from KF flux [7] and the growth of $Er_2Si_2O_7$ by the "vapour-flux" technique [8] and by the flux method [9] have been reported. The present paper describes the crystal growth of $R_2Si_2O_7$ from several flux systems, and the investigation of the polymorphic forms by X-ray methods.

2. Nomenclature

Ito and Johnson [1], as well as Warshaw and Roy [10] used the Greek letters α, β and δ for distinguishing the polymorphic forms of the rare-earth disilicates. Felsche [2,6] followed the nomenclature of the polymorphs of the rare-earth sesquioxides, designating the various structure types by the capital letters A, B, C, D, E, F, G, the method also followed here.

3. Materials and equipment

The chemicals were: Rare Earth Products 99.9% pure R_2O_3 (R = Tm, Er, Ho, Dy); BDH "Analar" MoO_3, PbO, K_2CO_3: BDH "extra pure" PbF_2; BDH silica gel, 60–120 mesh. The SiO_2, which contained 12 wt% H_2O, was calcined at 1000°C and then kept in a desiccator. V_2O_5 was melted prior to use. The furnaces have been described previously [11], and the

* Physics Department, Quaid-i-Azam University, Islamabad, Pakistan.

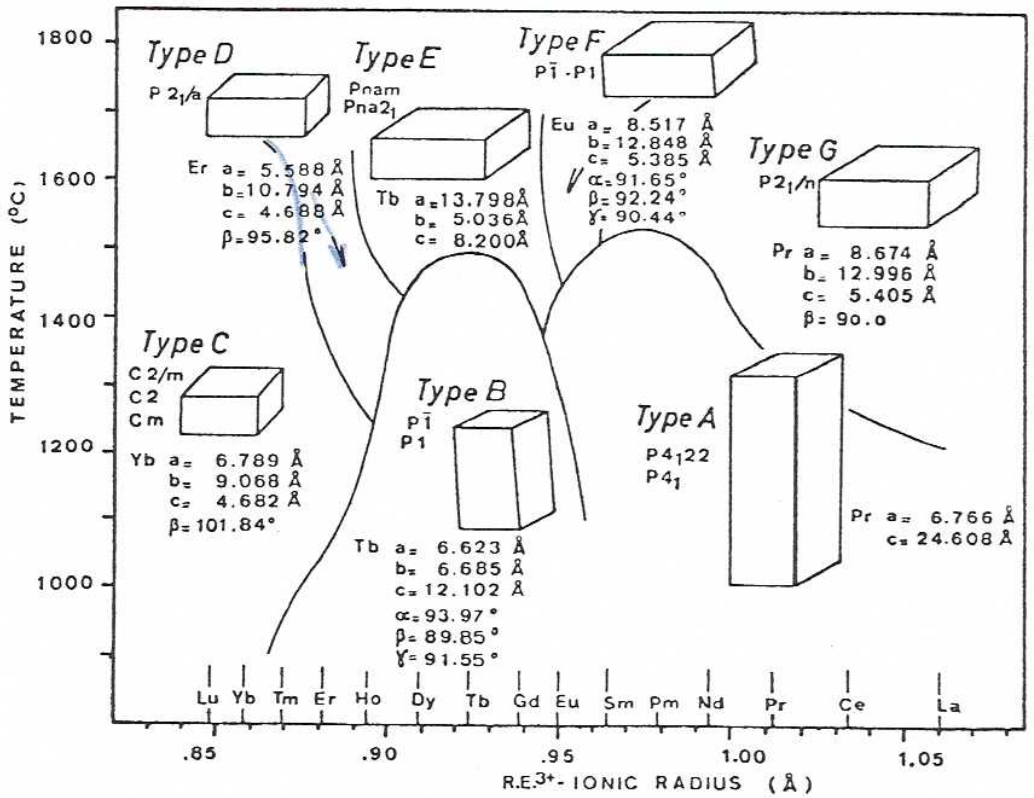

Fig. 1. Stability range of sinters and crystal data on the structure types A to G of the rare-earth disilicates [2]. (By courtesy of the Editor, J. Less Common Metals.)

crucibles were of pure platinum, of 10, 20 or 50 cm^3 capacity, and of 0.50 mm wall thickness.

4. Calculation of starting compositions

Wanklyn has pointed out that starting compositions for the flux growth of compounds consisting of a refractory oxide and an acidic oxide require an excess of the acidic oxide component, as shown in the generalised pseudoternary composition diagram (fig. 2) [12]. The apices A, B and C represent respectively the refractory oxide, the basic oxide or oxide plus fluoride, and the acidic and/or amphoteric oxide components. The distance of PQ from BC represents the molar solubility of the refractory oxide in the system at the soak temperature. The advantage of this model is that compositions in only a relatively small area require investigation, first along the line PQ to find O, where the phase with the most suitable habit from crystallises, then along the line NOM to determine the amount of refractory oxide that can be

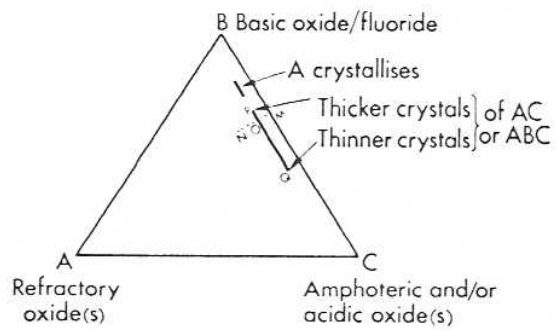

Fig. 2. Generalised pseudoternary composition diagram [12].

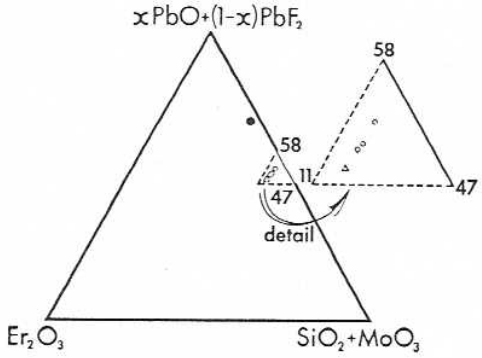

Fig. 3. Diagram showing starting compositions for the growth of C-$Er_2Si_2O_7$ (soak temperature, 1270 ± 5°C); (•) compositions resulting in either C-$Er_2Si_2O_7$ or Er_2SiO_5; (○) compositions resulting in larger crystals of C-$Er_2Si_2O_7$; (▽) compositions resulting in smaller crystals of C-$Er_2Si_2O_7$.

completely dissolved in the system at a convenient soak temperature.

For such compounds, it is also suggested that the acidic or amphoteric component in the generalised pseudoternary system can be replaced in part by another acidic oxide, provided no undesired compound results. $Er_2Si_2O_7$ falls into this class of compounds, and thus an excess of the acidic oxide component is required. However, a high concentration of SiO_2 leads to an inconveniently high viscosity, and on the basis of previous work [13], part of the excess SiO_2 in the system Er_2O_3–$(PbO + PbF_2)$–SiO_2 has been replaced by MoO_3. Similarly, in the system R_2O_3–Bi_2O_3–SiO_2, part of the excess SiO_2 has been replaced by V_2O_5. In addition to reducing the viscosity, V_2O_5 has been found effective in reducing the attack on platinum which occurs when free bismuth is produced by thermal dissociation [14]:

$$3\,V_2O_5 + 2\,Bi \rightleftharpoons Bi_2O_3 + 3\,V_2O_4\,.$$

It has also been shown previously that part of the PbO/PbF_2 component can be replaced by K_2O/KF, sometimes with advantageous results [9].

Tables 1a, b and c give starting compositions in the above systems, furnace programmes and crystal products. The experiments are representative of a much larger number performed. Starting compositions which yielded the crystals indicated are shown in fig. 3.

5. Experimental

For mixture containing Bi_2O_3–$(SiO_2 + V_2O_5)$, the crucible lids were loosely fitted and the furnace was heated at rather a slow rate, 88 K h^{-1}, to allow complete oxidation of the contents. To minimize evaporation losses for the $(PbO + PbF_2)$–$(SiO_2 + MoO_3)$ fluxes, the crucibles were provided with tightly fitting lids, and the furnace was heated at 176 K h^{-1}. Since the crystals reacted with even very dilute acid, the flux was separated by hot-pouring the melts while still molten [15], leaving the crystals attached to the crucible base and walls. The crystal products were identified by comparing their X-ray powder patterns with published data. In the experiments described in sections 5.1 and 5.2, it was frequently noted that the number of crystals was six or fewer, exceptionally low for growth by spontaneous nucleation.

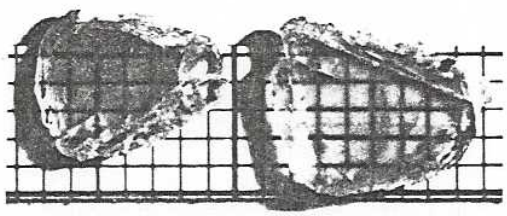

Fig. 4. Platelets of C-$Er_2Si_2O_7$ grown from $(PbO + PbF_2)$–$(SiO_2 + MoO_3)$ flux (mm grid).

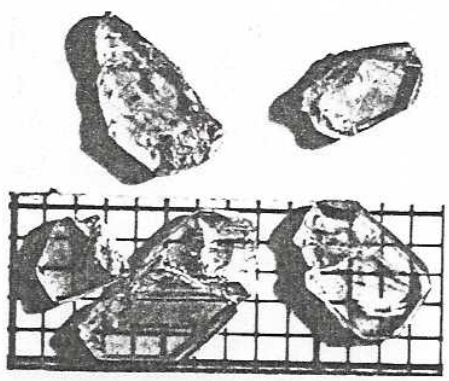

Fig. 5. Faceted crystals of C-$Tm_2Si_2O_7$ grown from $(PbO + PbF_2)$–$(SiO_2 + MoO_3)$ flux (mm grid).

Table 1

(a) Starting compositions and experimental conditions for the growth of $Er_2Si_2O_7$ and $Tm_2Si_2O_7$ from $(PbO + PbF_2)$–$(SiO_2 + MoO_3)$ flux

Phase obtained	Batch No.	Starting composition (mole%)					Crucible volume (cm^3)	Initial temp. (°C)	Soak period (h)	Cooling rate (K h^{-1})	Final temp. (°C)	Notes on the crystals
		R_2O_3	SiO_2	MoO_3	PbF_2	PbO						
C-$Er_2Si_2O_7$	1	5.65	17.66	26.38	20.37	30.03	20	1270	24	2.4	1020	A few platy crystals up to 7 mm × 5 mm × 1 mm (fig. 4)
	2	5.81	17.49	26.40	20.25	30.04	20	1270	24	1.0	800	Optically clear, faceted crystals up to 2 mm × 3 mm × 2 mm
	3	2.86	5.99	22.18	35.00	39.97	20	1270	24	1.0	800	Small crystals of C-$Er_2Si_2O_7$ or larger, equidimensional Er_2SiO_5
C-$Tm_2Si_2O_7$		2.90	6.00	22.10	35.00	34.00	20	1270	24	2.4	950	Faceted crystals up to 3 mm × 2 mm × 1 mm, as shown in fig. 5

(b) Effects of replacing part of $(PbO + PbF_2)$ by $(K_2O + KF)$

Phase obtained	Starting composition (mole%)							Crucible volume (cm^3)	Initial temp. (°C)	Soak period (h)	Cooling rate (K h^{-1})	Final temp. (°C)	Notes on the crystals
	R_2O_3	SiO_2	MoO_3	PbF_2	PbO	K_2O	KF						
C-$Er_2Si_2O_7$	5.75	15.17	25.31	13.99	25.22	0	14.55	20	1270	24	2.4	850	Six faceted crystals, up to 4 mm × 3 mm × 2 mm
D-$Er_2Si_2O_7$ or C-$Er_2Si_2O_7$	5.71	16.87	23.45	14.35	23.65	5.01	10.96	20	1270	24	2.4	900	Three out of ten batches resulted in the D-form; in one case, only one triangular plate of D-type, 14 mm × 8 mm × 3 mm
C-$Er_2Si_2O_7$	5.71	16.87	23.45	14.35	23.65	5.01	10.96	20	1260	24	2.4	900	Thick, nearly equidimensional crystals of C-type only
C-$Tm_2Si_2O_7$	5.80	16.89	23.40	14.40	23.71	4.8	11.00	20	1260	24	2.4	900	Platy crystals, up to 3 mm × 2 mm × 1.5 mm

						1260	24	2.4	900	crystals of C-type only	Platy crystals, up to 3 mm × 2 mm × 1.5 mm

Table 1 (continued)
(c) Starting compositions and experimental conditions for crystal growth of $R_2Si_2O_7$ (R=Tm, Er, Ho, Dy) from Bi_2O_3–(SiO_2 + V_2O_5) flux

Phase obtained	Starting composition (mole%)					Crucible volume (cm^3)	Initial temp. (°C)	Soak period (h)	Cooling rate ($K\,h^{-1}$)	Final temp. (°C)	Notes on the crystals
	R_2O_3	SiO_2	Bi_2O_3	V_2O_5	B_2O_3						
C-$Tm_2Si_2O_7$	6.83	21.98	56.67	14.52		10	1240	20	3	1120	Clear platy crystals up to 4 mm × 3 mm × 1 mm at the base of the crucible
D-$Er_2Si_2O_7$	6.75	22.00	56.60	14.65		20	1242	20	1.5	950	Clear platelets up to 8 mm × 6 mm × 2 mm
C-$Ho_2Si_2O_7$	10.68	33.34	42.94	4.40	8.68	15	1240	20	5	1120	3 mm × 3 mm × 0.2 mm platelets on the surface of the melt
D-$Ho_2Si_2O_7$	7.02	21.94	56.56	14.48		50	1240	20	1.5	1050	Optically clear, faceted crystals up to 6 mm × 3 mm × 1 mm grew at the sides of the crucible; some are shown in fig. 6
E-$Dy_2Si_2O_7$	7.14	21.43	57.15	14.28		15	1250	18	1.5	960	Faceted rods up to 10 mm × 2 mm × 2 mm grew across the melt and thin platelets up to 4 mm × 3 mm × 0.2 mm at the surface (fig. 7)
D-$Ho_2Si_2O_7$ and apatite	8.67	21.55	55.55	14.23		10	1240	20	1.5	980	Large platy crystals of D-phase and hexagonal apatite rods, 2 to 3 mm in length
D-$Ho_2Si_2O_7$ and apatite	10.18	21.20	54.64	13.99		10	1240	20	1.5	980	Apatite rods up to 3 mm × 1 mm × 1 mm and D-$Ho_2Si_2O_7$ in powder form (solution was incomplete)

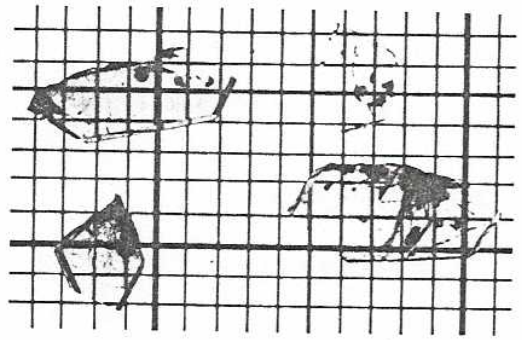

Fig. 6. Platelets of D-$Ho_2Si_2O_7$ grown from Bi_2O_3–(SiO_2 + V_2O_5) flux (mm grid).

5.1. Experiments in the systems R_2O_3–(PbO + PbF_2)–(SiO_2 + MoO_3), (R = Tm, Er)

Fig. 3 shows starting compositions which yielded C-$Er_2Si_2O_7$ and C-$Tm_2Si_2O_7$, and fig. 4 shows some of the crystals. Composition 3, in table 1, resulted sometimes in Er_2SiO_5, and is evidently near the boundary between the regions where $Er_2Si_2O_7$ and Er_2SiO_5 are the primary phases. The crucibles containing composition 3 frequently leaked because of the relatively high PbO content, which increased during slow cooling because of evaporation and hydrolysis of PbF_2.

The loss by evaporation from compositions which yielded $Er_2Si_2O_7$ was 30 to 60 wt%. Initially, many batches yielded rare-earth apatites [16], and it was found that these were obtained when the weight loss was low, as a result of relatively fast cooling (4 to 8 K h^{-1}) or very tightly-fitted lids. The apatites are of variable formula, such as $Pb_{1.4}Er_{2.93}Si_{3.6}O_{13}$ [16], and. since they contain lead, may be expected to crystallise from melts with a lower concentration of R_2O_3 in a lower temperature range. On the other hand, batches which yielded $Er_2Si_2O_7$ became more concentrated by evaporation, so that growth occurred at a higher temperature.

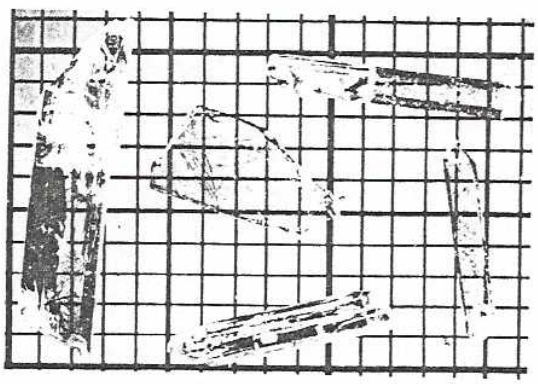

Fig. 7. Rods of E-$Dy_2Si_2O_7$ grown from Bi_2O_3–(SiO_2 + V_2O_5) flux (mm grid).

5.2. Experiments with (K_2O + KF) in the flux

In some experiments, (PbO + PbF_2) was partly replaced by equimolar amounts of (K_2O + KF), as shown in table 1b. When the soak temperature was above 1260°C, D-$Er_2Si_2O_7$ resulted in three out of ten batches. With lower soak temperatures, C-$Er_2Si_2O_7$ was always obtained. The C- and D-type crystals did not occur together in a crucible, and there was no sign, such as twin domains, of crystallographic transitions having occurred.

EPMA, given in table 2, shows that in C- and D-$Er_2Si_2O_7$ the flux impurity levels are similarly low; it is thus improbable that the substitutional incorporation of K^+ in the lattice can account for the fact that the D-type phase was obtained only when K^+ was present in the melt. Instead, since the D-form was not obtained in the absence of K^+, it may be that the complex ions present at the nucleation stage determine the polymorph that is formed. As shown in table 1b, the temperature at which D-$Er_2Si_2O_7$ is produced from the fluxed melt is very different from that which applies to the formation of D-$Er_2Si_2O_7$ as a sinter. Ito and Johnson found that the C to D transformation in sintered material occurred at 1400 ± 10°C [1].

5.3. Growth of $R_2Si_2O_7$ (R = Tm, Er, Ho and Dy) from Bi_2O_3–(SiO_2 + V_2O_5)

The flux system (PbO + PbF_2)–(SiO_2 + MoO_3) did not yield $R_2Si_2O_7$ with rare-earth ions larger than Er^{3+}; rare-earth apatites were instead produced. The only good alternative flux appeared to be Bi_2O_3–(SiO_2 + V_2O_5), although fluxes containing Bi_2O_3 are normally avoided, if possible, because the use of Bi_2O_3 reduces the life of platinum crucibles and also because Bi^{3+}, being similar in size and charge to R^{3+},

Table 2
Substitutional flux impurities in $R_2Si_2O_7$ crystals, determined by EPMA

Crystal	Cooling rate ($K\ h^{-1}$)	Pb (%)	K (%)	V (%)	Bi (%)
C-$Er_2Si_2O_7$	2.4	0.04	0.01	–	–
D-$Er_2Si_2O_7$	2.4	0.06	0.01	–	–
D-$Er_2Si_2O_7$	1.5	–	–	0.07	1.0
C-$Ho_2Si_2O_7$	5	–	–	0.03	2.0
D-$Ho_2Si_2O_7$	5	–	–	0.06	1.7
D-$Ho_2Si_2O_7$	1.5	–	–	0.3	1.6
E-$Dy_2Si_2O_7$	1.5	–	–	0.04	4.5

readily substitutes for it in the crystal lattice.

It was found that $Ho_2Si_2O_7$ and $Dy_2Si_2O_7$ crystallised from this system, though apatite crystals were occasionally obtained.EPMA shows that, as may be expected, the substitutional Bi content increased as the ionic radius of the rare-earth ion approached that of Bi^{3+}. Reducing the rate of cooling from 5 to 1.5 K h^{-1} did not appreciably reduce the percentage of Bi in the $Ho_2Si_2O_7$ crystals.

The solubility of Ho_2O_3 in Bi_2O_3–(V_2O_5 + SiO_2) has been determined by thermogravimetry (TGA) [17] and in these experiments the D-form was obtained in the range 1150 to 1350°C. Similar compositions yielded C-$Tm_2Si_2O_7$, D-$Er_2Si_2O_7$ and E-$Dy_2Si_2O_7$. However, when B_2O_3 was included in the starting composition, C-$Ho_2Si_2O_7$ was obtained, as indicated in table 1c.

The TGA experiments showed a temperature difference of 50 ± 5°C between the crystallization and the solubility temperatures, and this is taken into account in the crystallization ranges indicated in table 3. Although the supercooling has not been determined for the melts with ($PbO + PbF_2$), it has been assumed to have a similar effect on the crystallization temperatures from these compositions, given in table 3. The difference in the temperatures of formation of the polymorphs produced from the flux, as compared with the stability ranges of the sinters, is very marked, as table 3 makes clear.

5.4. Seeding experiments

To check whether the introduction of seed crystals would induce the formation of the corresponding polymorph, a series of experiments under similar conditions were performed. For example, seeds of E-$Dy_2Si_2O_7$ were added to a composition which usually produced D-$Ho_2Si_2O_7$. In every case, the result was negative, the added seeds evidently having no influence on the phase formed.

6. Notes on the crystals

The crystals have the colours of the corresponding rare-earth ions, except for $Dy_2Si_2O_7$, the pale green colour of which may be attributable to traces of V^{3+}

Table 3
Stability range of sintered polymorph, compared with temperature range for growth of the same crystal from the flux

Polymorph	Stability range for sinter (°C)	Temperature range in which polymorph was obtained from the flux (°C)	Flux components
C-$Tm_2Si_2O_7$	1000–1650	1220–1020 (in 2 batches) 1190–1120 (in 3 batches)	($PbO + PbF_2$)–($SiO_2 + MoO_3$) Bi_2O_3–($SiO_2 + V_2O_5$)
C-$Er_2Si_2O_7$	1050–1400	1220–800 (in 19 batches)	($PbO + PbF_2$)–($SiO_2 + MoO_3$)
D-$Er_2Si_2O_7$	1400–1700	1220–900 (in 3 out of 10 batches)	($PbO + PbF_2 + K_2O + KF$)–($SiO_2 + MoO_3$)
C-$Er_2Si_2O_7$	1050–1400	1220–900 (in 7 out of 10 batches)	($PbO + PbF_2 + K_2O + KF$)–($SiO_2 + MoO_3$)
C-$Er_2Si_2O_7$	1050–1400	1210–900 (in 6 batches)	($PbO + PbF_2 + K_2O + KF$)–($SiO_2 + MoO_3$)
D-$Er_2Si_2O_7$	1400–1700	1190–950 (in 4 batches)	Bi_2O_3–($SiO_2 + V_2O_5$)
C-$Ho_2Si_2O_7$	1200–1260	1190–1120 (one batch only)	Bi_2O_3–($SiO_2 + B_2O_3 + V_2O_5$)
D-$Ho_2Si_2O_7$	1260–1500	1190–1050 (in 10 batches)	Bi_2O_3–($SiO_2 + V_2O_5$)
E-$Ho_2Si_2O_7$	1450–1700	1190–960 (in 4 batches)	Bi_2O_3–($SiO_2 + V_2O_5$)

in the lattice. All the crystals showed simultaneous extinction under the polarising microscope. Thus there was no sign of structural transitions having occurred.

Only one form was present in each batch. In table 3, the conditions under which each form was obtained are compared with the temperature ranges in which the sintered materials have been reported to exist [2,6].

6.1. C-$R_2Si_2O_7$ (R = Tm, Er, Ho)

The X-ray powder patterns corresponded closely to the data for C-$Tm_2Si_2O_7$ [2]. The structure is that of the mineral thortveitite. Powder patterns of single crystal C-$Er_2Si_2O_7$ and C-$Ho_2Si_2O_7$ have been indexed according to the reported lattice parameters and space group, and the data are given in table 4.

Table 4
X-ray powder pattern data for C-$R_2Si_2O_7$ (R = Er, Ho)

I_{est}	hkl	$Er_2Si_2O_7$		$Ho_2Si_2O_7$	
		d_{calc} (Å)	d_{obs} (Å)	d_{calc} (Å)	d_{obs} (Å)
M	110	5.36	5.36	5.38	5.38
M	001	4.62	4.62	4.63	4.63
VW	020	4.46	4.47	4.48	4.47
VW	11$\bar{1}$	3.82	3.83	3.83	3.82
VW	200	3.35	3.35	3.36	3.36
M	111	3.25	3.25	3.26	3.25
VS	021	3.21	3.21	3.22	3.22
S	20$\bar{1}$	3.027	3.027	3.028	3.027
M	130	2.739	2.738	2.740	2.739
M	220	2.682	2.684	2.692	2.694
VW	002	2.312	2.311	2.316	2.316
M	131	2.262	2.262	2.271	2.269
W	221, 310	2.167	2.166	2.177	2.177
VW	31$\bar{1}$	2.134	2.133	2.138	2.134
VW	022	2.053	2.054	2.058	2.056
W	22$\bar{2}$	1.912	1.913	1.916	1.914
a_0(Å)		6.8517(4)		6.8750(9)	
b_0 (Å)		8.9241(5)		8.962(1)	
c_0 (Å)		4.7262(9)		4.7303(6)	
β(deg)		101.66(7)		101.69(6)	

Space groups: C 2/m, Cm, C2.

Table 5
X-ray powder pattern data for E-$Dy_2Si_2O_7$

I_{est}	hkl	d_{calc} (Å)	d_{obs} (Å)
W	110	4.71	4.71
S	002	4.09	4.06
S	210	4.04	4.06
W	211	3.63	3.62
W	400	3.42	3.41
VW	310	3.37	3.37
VW	401	3.15	3.14
S	112	3.090	3.084
VS	212	2.778	2.782
W	402	2.625	2.625
W	312	2.604	2.602
VW	020	2.509	2.510
M	120	2.468	2.468
VW	510	2.403	2.401
VW	013	2.397	2.397
VW	220	2.356	2.358
VW	412	2.326	2.326
VW	213	2.264	2.262
a_0 (Å)			13.686(8)
b_0 (Å)			5.018(3)
c_0 (Å)			8.185(6)

Space groups: Pnam, $Pna2_1$.

6.2. D-$R_2Si_2O_7$ (R = Er, Ho)

These compounds are the only two members of the series which possess the monoclinic P 21/b $Y_2Si_2O_7$ structure [5,18]. The crystals grew at the base of the crucible, with the *c*-axis perpendicular to the plane of the platelets.

6.3. E-$Dy_2Si_2O_7$

The X-ray powder pattern data was very similar to that for E-$Tb_2Si_2O_7$ [2], and has been indexed according to the reported cell dimensions and space group, as shown in table 5.

7. Magnetic transitions

These were determined for $Er_2Si_2O_7$. C-$Er_2Si_2O_7$ became antiferromagnetic at 2.50 ± 0.05 K, and D-$Er_2Si_2O_7$ at 1.71 ± 0.05 K. These temperatures are

exceptionally high for compounds of erbium. Details of the magnetic anisotropy and optical absorption spectra will be published.

8. Discussion

As shown in fig. 1, the lowest temperature polymorph, the B-phase, was obtained by sintering. However, it has not been observed in the preparation of any of the compounds by the flux method. Two polymorphs of each of $Er_2Si_2O_7$ and $Ho_2Si_2O_7$ were obtained, as shown in tables 1 and 3.

Similar effects have been observed in other polymorphic materials. $ThGeO_4$ has two tetragonal polymorphs, scheelite and zircon-type. Harris and Finch [19], in a phase stability study, found that only zircon-type crystallised from $(Li_2O + 2MoO_3)$ or $(Li_2O + 2WO_3)$ fluxes between 750 and 1420°C. They found that sintering experiments gave the scheelite form at 1050°C, but when a mineralizer was added, it converted to zircon-type at 750°C and above. $ThSiO_4$ also has two forms, tetragonal thorite and monoclinic huttonite. Flux growth experiments in the systems $(Li_2O + 2WO_3)$, $(Li_2O + 2MoO_3)$ and $(Na_2O + 2WO_3)$ produced thorite below 1225 ± 10°C, and huttonite above this temperature [20]. However, Wanklyn [21] obtained only huttonite, using $(PbO + PbF_2)$–$(SiO_2 + MoO_3)$ as flux, even when the soak temperature was as low as 1180°C.

All these observations indicate that the formation of the various polymorphs of $R_2Si_2O_7$, and also of $ThSiO_4$ and $ThGeO_4$, from fluxed melts depends not only on the temperature range in which the crystals grow but also on the chemical composition of the flux, which probably determines the form of the polymorph at the stage of nucleation.

9. Conclusion

Flux growth studies in the systems Er_2O_3–$(PbO + PbF_2)$–$(SiO_2 + MoO_3)$ and R_2O_3–Bi_2O_3–$(SiO_2 + V_2O_5)$, which resulted in crystals of the polymorphs of $R_2Si_2O_7$ (R = Tm, Er, Ho, Dy), have been described. An excess of the acidic oxide component over that required by the formula was necessary for the phase to crystallise, as was predicted from the generalised composition diagram for compounds of refractory and acidic oxides [12].

The temperature at which the polymorphs were obtained differed considerably from those previously reported for sintered materials and depended on the flux compositions. Thus it is doubtful whether flux growth is a useful technique for the determination of structural transitions, as proposed by Finch et al. [20]. However, this method has been shown to be very appropriate for the preparation of various polymorphs in single crystal form.

Acknowledgements

The authors express their thanks to Dr. S.H. Smith, especially for assistance with TGA, and to Mr. B.J. Garrard and Mr. F.R. Wondre for helpful discussions. They are also indebted to Mr. W. Davison of the School of Physics, University of Newcastle upon Tyne, for EPMA, and to Mr. Peter Clack for equipment building and platinum work. This study was supported in part by the Science Research Council. A.M. wishes also to thank the British Council for financial support.

References

[1] J. Ito and H. Johnson, Am. Mineralogist 53 (1968) 1940.
[2] J. Felsche, J. Less-Common Metals 21 (1970) 1.
[3] Yu.I. Smolin and Yu.F. Shepelev, Inorg. Mater. 4 (1967) 992.
[4] R.D. Shannon and C.T. Prewitt, J. Solid State Chem. 2 (1970) 199.
[5] Yu.I. Smolin and Yu.F. Shepeler, Acta Cryst. B26 (1970) 484.
[6] J. Felsche, The Crystal Chemistry of the Rare Earth Silicates, in: Structure and Bonding, Vol. 1, (Springer, New York, 1973) p. 99.
[7] I.A. Bondar, L.N. Koroleva and N.A. Toropoc, in: Rost Kristallov, Vol. 6 (Inst. Krist., Akad. Nauk SSSR, Moscow, 1965) p. 111.
[8] B.M. Wanklyn, F.R. Wondre, G.B. Ansell and W. Davison, J. Mater. Sci. 9 (1974) 2007.
[9] B.M. Wanklyn, J. Crystal Growth 43 (1978) 336.
[10] I. Warshaw and R. Roy, in: Progress in the Science and Technology of the Rare Earths, Vol. 1 (Pergamon, (1964) p. 203.
[11] G. Garton, S.H. Smith and B.M. Wanklyn, J. Crystal Growth 13/14 (1972) 588.

[12] B.M. Wanklyn, J. Crystal Growth 37 (1977) 334.
[13] B.M. Wanklyn, F.R. Wondre, G.B. Ansell and W. Davison, J. Mater. Sci. 10 (1975) 1492.
[14] B.M. Wanklyn, J. Crystal Growth 7 (1970) 368.
[15] B.M. Wanklyn, in: Crystal Growth, Ed. B.R. Pamplin (Pergamon, 1975) 217.
[16] B.M. Wanklyn, F.R. Wondre, G.B. Ansell and W. Davison, J. Mater. Sci. 10 (1975) 1494.
[17] S.H. Smith and D. Elwell, J. Mater. Sci. 2 (1967) 297.
[18] N.G. Batalieva and Yu.A. Pyatenko, Zh. Strukt. Khim. 8 (1967) 548.
[19] L.A. Harris and C.B. Finch, Am. Mineralogist 57 (1972) 1894.
[20] C.B. Finch, L.A. Harris and G.W. Clark, Am. Mineralogist 49 (1964) 782.
[21] B.M. Wanklyn, J. Crystal Growth 37 (1977) 51.

41. *Jørgensen, C. K., Brinen, S.:* Mol. Phys. *6*, 629 (1963).
42. *Loh, E.:* Phys. Rev. *147*, 332 (1966).
43. *Reisfeld, R., Hormodaly, J.:* 9th Rare Earth Conference *1*, 123 (1971).
44. — — *Barnett, B.:* Chem. Phys. Letters (1972).
45. *Ryan, J. L., Jørgensen, C. K.:* J. Phys. Chem. *70*, 2845 (1966).
46. *Blasse, G., Bril, A.:* J. Chem. Phys. *47*, 5139 (1967).
47. *Reisfeld, R., Morag, S.:* Appl. Phys. Letters *21*, (2), 57 (1972).
48. — *Honigbaum, A., Michaeli, G., Harel, L., Ish-Shalom, M.:* Israel J. Chem. *7*, 613 (1970).
49. *Sinha, S. P.:* Europium. Berlin–Heidelberg–New York: Springer 1967.
50. *Hoshina, T., Kuboniwa, S.:* J. Phys. Soc. Japan, *31*, 828 (1971).
51. *Bril, A., Blasse, G., de Poorter, J. A.:* J. Electrochem. Soc., Solid State Sci. *117*, 346 (1970).
52. *Eisenstein, J. C.:* J. Chem. Phys. *25*, 142 (1956).
53. *Jørgensen, C. K., Rittershaus, E.:* Mat. Fys. Medd. Dan. Vid. Selskab. *35*, No. 15 (1967).
54. *Reisfeld, R.:* unpublished results (1972).
55. *Sinha, S. P.:* Complexes of the Rare Earths. Oxford: Pergamon Press, 1966.
56. *Reisfeld, R., Glasner, A.:* J. Chem. Phys. *43*, 2923 (1965).
57. — — J. Chem. Phys. *42*, 2983 (1965).
58. *Lang, R. L.:* Can. J. Res. *14A*, 127 (1930).
59. *Reisfeld, R., Greenberg, E.:* unpublished results (1972).
60. *Blasse, G.:* J. Solid State Chem. *4*, 52 (1972).
61. *Reisfeld, R., Boehm, L., Greenberg, E., Ish-Shalom, M.:* unpublished results (1972).
62. *Duffy, J. A., Ingram, M. D.:* J. Chem. Phys. *52*, 3752 (1970).
63. — — J. Chem. Phys. *54*, 443 (1971).
64. *Förster, Th.:* Discussions Faraday Soc. *27*, 7 (1959).
65. — Ann. Physik *2*, 55 (1948).
66. *Dexter, D. L.:* J. Chem. Phys. *21*, 836 (1953).
67. *Patek, K.:* p. 94, See Ref. 3.
68. *Nakazawa, E., Shionoya, S.:* J. Chem. Phys. *47*, 3211 (1967).
69. *Inokuti, M., Hirayama, F.:* J. Chem. Phys. *43*, 1978 (1965).
70. *Reisfeld, R., Greenberg, E., Velapoldi, R. A., Barnett, B.:* J. Chem. Phys. *56*, 1698 (1971).
71. — *Boehm, L.:* J. Solid State Chem. *4*, 417 (1972).
72. — *Barnett, B.:* unpublished results (1972).
73. *Soules, T. F., Duke, C. B.:* Phys. Rev. B. *3*, 262 (1971).
74. *Fong, F. V., Miller, M. M.:* Chem. Phys. Letters *10*, 408 (1971).
75. *Riseberg, L. A., Gandrud, W. B., Moos, H. W.:* Phys. Rev. *159*, 262 (1967).
76. *Yamada, N., Shionoya, S., Kushida, T.:* J. Phys. Soc. Japan *30*, 1507 (1971).
77. *Miyahawa, T., Dexter, D. L.:* Phys. Rev. B. *1*, 2961 (1970).
78. *Moos, M. W.:* J. Luminescence *1*, 2, 406 (1970).
79. *Weber, M. J.:* Phys. Rev. *157*, 262 (1967); Phys. Rev. *171*, 283 (1968).

Received July 7, 1972

KEVIN: write in the book ref:

F2-1

the Pribbe

The Crystal Chemistry of the Rare-Earth Silicates

J. Felsche

Institut für Kristallographie der ETH, Zürich, Switzerland

Structure and Bonding (1973) Vol. 13, 100-197

ORTHOSILICATES GARNETS

Table of Contents

to discuss this effect on silicate structures with special attention to possible discontinuities along the series of rare-earth elements. Compounds of the binary systems RE_2O_3—SiO_2 are of special interest because their properties should show a closer relationship with the lanthanide periodicity than is the case with more complex compounds. Therefore, some charateristics and the history of the investigation of these systems will be given first, followed by brief comments on ternary rare-earth silicate compounds.

Pure rare-earth compounds are unknown in nature; minerals (see also appendix I) usually contain groups of rare earths because of their nearly identical chemical character. It is not surprising, therefore, that a systematic investigation of the individual binary silicate systems RE_2O_3—SiO_2 revealed a large number of new phases and unknown structural types. These experiments were started about 15 years ago, when modern methods of ion separation were developed and provided very pure rare-earth elements.

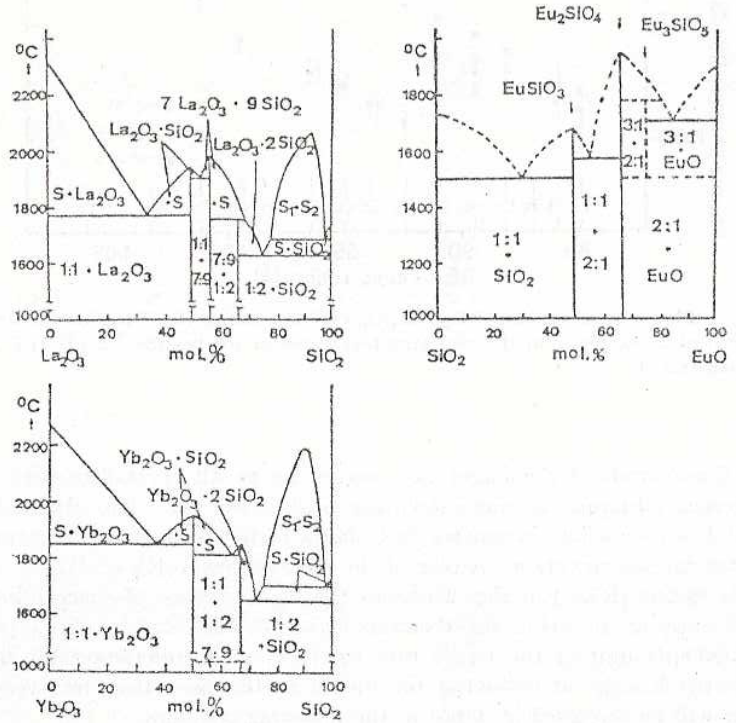

Fig. 1. The Systems of La_2O_3—SiO_2 and Yb_2O_3—SiO_2 after Ref. (*81*) and of EuO—SiO_2 after Ref. (*36*).

First results on the complete binray systems RE_2O_3—SiO_2 were published about ten years ago by Russian authors, essentially (*1—9*). The phase diagrams of La_2O_3—SiO_2 and Yb_2O_3—SiO_2, as shown in Fig. 1, are from a recent review made by this group of authors of their own work in the rare-earth silicate field (*81*). The phase diagrams have been slightly revised as compared to the data from the early period of investigation. Originally, silicates of composition $1\ RE_2O_3 \cdot 1\ SiO_2$, $2\ RE_2O_3 \cdot 3\ SiO_2$ and $1\ RE_2O_3 \cdot 2\ SiO_2$ were described. The existence of these compounds was suggested by various X-ray powder patterns of a rather complicated character, vibration spectra or optical data, but with hardly any single-crystal information. Data of this quality were published in a first survey of the rare-earth silicate compounds (*10*). The introduction of single-crystal X-ray methods into this field led to some progress in understanding the highly polymorphic character of the compounds.

Analysis of the crystal structure of compounds $2\ RE_2O_3 \cdot 3\ SiO_2$ revealed the true composition to be $7\ RE_2O_3 \cdot 9\ SiO_2$ (*11*). The crystals represent a cation-deficient type of oxyapatite structure $RE_{9.33}\square_{0.67}(SiO_4)_6O_2$. Subsequently the crystal structures of 1:1 and 1:2 rare-earth silicate compounds were studied. The single-crystal information led to reinterpretation of the powder diffraction patterns of the samples prepared during the first stage of phase diagram investigation. The X-ray powder diffraction patterns of the single phases are shown in Appendix II. Two different structure types were identified in 1:1 compounds of type $RE_2(SiO_4)O$ (*12, 13*). Seven polymorphic forms were found of the compounds $1\ RE_2O_3 \cdot 2\ SiO_2$, largely of the type $RE_2(Si_2O_7)$ (*14—21*). Consequently, some major changes had to be introduced into the original version of the RE_2O_3—SiO_2 phase diagrams; Fig. 1 shows the revised data.

Many of the binary compounds were prepared by solid-state reaction of corresponding oxide mixtures, to some extent by the employment of flux methods. Some ternary compounds were synthesized under hydrothermal conditions. These compounds are polymorphic $NaRE(SiO_4)$, $Na_3RE(Si_2O_7)$ (*29—31*) and a garnet-type $Mg_3RE_2(SiO_4)_3$ (*32*). The synthesis of borosilicates $RE\ B(SiO_4)O$ showing the stillwellite structure (*58*) was accomplished by solid-state reaction (*80*). Various compounds containing divalent rare earths were reported in the systems RE O—SiO_2 for Sm, Eu and Yb, largely based on X-ray powder data (*33—37*). The phase diagram EuO—SiO_2 after (*36*) is shown in Fig. 1. Dimorphic $Eu_2(SiO_4)$ (*59, 60*) and $Eu_3(SiO_4)O$ (*62*) were shown by structural analysis to be isostructural with polymorphic $Ca_2(SiO_4)$ and $Sr_3(SiO_4)O$, respectively.

It is proposed to present in this article a detailed structural description of all rare-earth silicate compounds known so far. Compounds more

Table 1. *Cell dimensions of compounds $RE_2[SiO_4]O$. Structure type A of monoclinic symmetry, space group $P2_1/c$ and $Z = 4$ for compounds La, ... Tb. Structure type B of monoclinic symmetry space group $B2/b$ and $Z = 8$ for compounds of Dy, ... Lu*

	a_0[Å]	b_0[Å]	c_0[Å]	β[Å]	V[Å^3]
$La_2[SiO_4]O$	9.420 (9)	7.398 (7)	7.028 (7)	108.21 (6)	465.2 (9)
$Pr_2[SiO_4]O$	9.253 (9)	7.301 (8)	6.934 (8)	108.15 (9)	445.1 (8)
$Nd_2[SiO_4]O$	9.250(11)	7.258(10)	6.886 (9)	108.30(11)	439.3 (6)
$Sm_2[SiO_4]O$	9.161 (9)	7.112 (9)	6.821 (7)	107.51 (9)	424.4 (7)
$Eu_2[SiO_4]O$	9.142 (8)	7.054 (6)	6.790 (6)	107.53 (9)	417.9 (8)
$Gd_2[SiO_4]O$	9.131 (7)	7.045 (6)	6.749 (5)	107.52 (7)	414.0 (9)
$Tb_2[SiO_4]O$	9.083(22)	6.990(11)	6.714(10)	107.31(21)	406.1(42)
	a[Å]	b[Å]	c[Å]	γ[Å]	V[Å^3]
$Dy_2[SiO_4]O$	14.38 (2)	10.42 (2)	6.74 (1)	122.0 (3)	856.5(72)*
$Ho_2[SiO_4]O$	14.35 (2)	10.37 (2)	6.71 (1)	122.2 (3)	843.0(38)*
$Er_2[SiO_4]O$	14.32 (2)	10.35 (2)	6.69 (1)	122.3 (3)	836.7(41)*
$Tm_2[SiO_4]O$	14.302(9)	10.313(9)	6.662 (6)	122.21 (9)	828.5 (9)
$Yb_2[SiO_4]O$	14.28 (1)	10.28 (1)	6.653 (5)	122.2 (1)	824.0 (7)*
$Lu_2[SiO_4]O$	14.254(9)	10.241(8)	6.641 (7)	122.20 (8)	819.3(10)

* Data from Ref. (*13*).

Table 2. *Atomic parameters of $Gd_2(SiO_4)O$*

Atom	x	y	z	B[Å^2]
Gd(1)	0.11453(5)	0.14600(6)	0.41628(1)	0.48
Gd(2)	0.52458(5)	0.62451(6)	0.23428(1)	0.40
Si	0.2020 (3)	0.5876 (3)	0.4598 (6)	0.30
O(1)	0.2032 (9)	0.4302(10)	0.6453(18)	0.58
O(2)	0.1317 (8)	0.4587 (9)	0.2520(17)	0.48
O(3)	0.3839 (8)	0.6361 (9)	0.5059(16)	0.45
O(4)	0.0941 (9)	0.7681(11)	0.4507(18)	0.73
O(5)	0.3837 (8)	0.3782 (9)	0.0487(16)	0.49

After Ref. (*13*).

2.1.1. Structure Type A, (La, ... Tb)$_2$(SiO$_4$)O, '(RE Oxy (A)'

The structure of the larger rare-earth compounds consists of isolated (SiO_4) tetrahedra, extra, not silicon-bonded oxygens, and two crystallographically independent RE atoms (Fig. 3). The extra oxygens are located at the centre of RE^{3+}-cation tetrahedra. These (O—RE_4) tetrahedra form a two-dimensional network parallel to the (*100*) plane, as shown in the lower illustration in Fig. 3. Sheet-like packing of the structure is

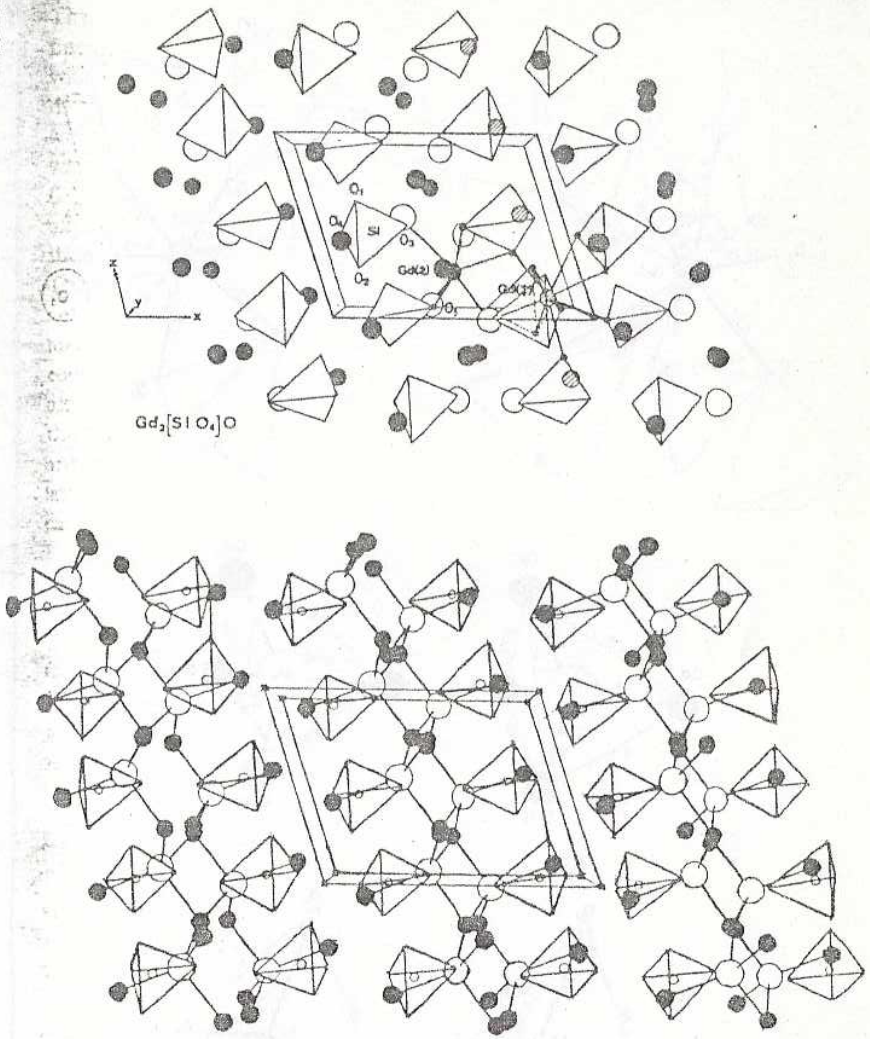

Fig. 3. Crystal structure of $Gd_2[SiO_4]O$

achieved by the introduction of (SiO_4) tetrahedra into the wide meshes of this net. This ensures charge balance and connection to the parallel-running units which are all just one a_0 translation wide. The atomic parameters for $Gd_2(SiO_4)O$ are given in Table 2.

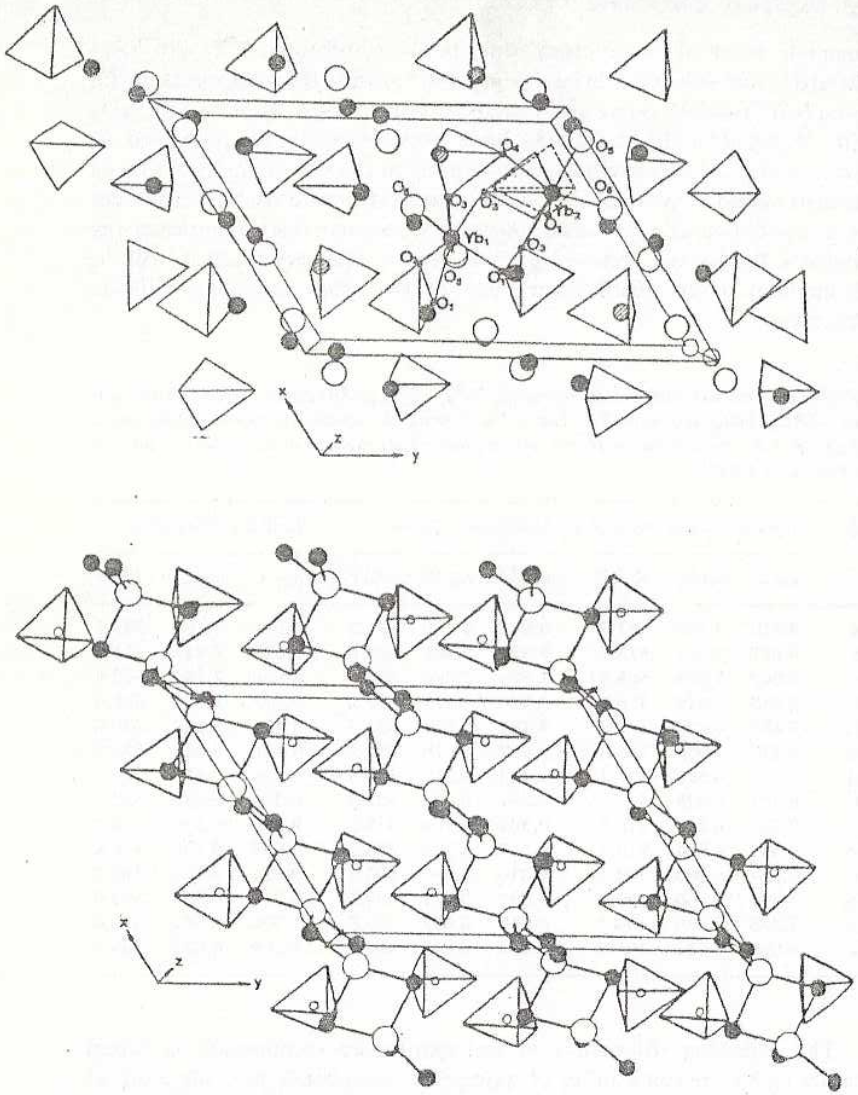

Fig. 5. Crystal structure of $Yb_2[SiO_4]O$

As illustrated in Fig. 5, this structure type also has ionic units consisting of isolated (SiO_4)tetrahedra and the other type of anion, the 'extra', not silicon-bonded oxygens. These oxygens are also surrounded by four rare-earth cations in the shape of a slightly distorted tetrahedron,

Table 3. *Atomic parameters of* $Yb_2(SiO_4)O$

Atom	x	y	z	B[Å^2]
Yb(1)	0.46638(4)	0.53709(3)	0.75564(8)	0.338
Yb(2)	0.66416(4)	0.35892(3)	0.87736(8)	0.340
Si	0.6928 (3)	0.3182 (2)	0.4085 (6)	0.237
O(1)	0.6747 (7)	0.3787 (5)	0.2103(16)	0.586
O(2)	0.8618 (7)	0.4122 (5)	0.4941(16)	0.596
O(3)	0.6769 (6)	0.2029 (5)	0.3535(14)	0.406
O(4)	0.5627 (9)	0.2987 (6)	0.5710(17)	0.886
O(5)	0.8965 (6)	0.5177 (5)	0.9052(16)	0.412

After Ref. (*14*).

and thus, in this case too, the main structural motifs might very well be described in terms of the arrangement of (SiO_4) and (O—RE_4)tetrahedra. In contrast to the structure of the larger rare-earth compounds, here the (O—RE_4)tetrahedra form, not a two-dimensional network, but chains and (O_2—RE_6)double tetrahedra running in the a_0 direction. The infinite chains of edge-sharing (O—RE_4)tetrahedra are connected to the (O_2—RE_6) groups by isolated (SiO_4)tetrahedra. This arrangement is, however, less intensively-filling than the other type found in the 'RE Oxy A' structure. The effect of these two types of packing on the cell volume has already been shown in Fig. 2. Some further details will illustrate the difference between the two structures.

As can be seen from Fig. 6, the coordination around the heavy atoms is somewhat different with respect to the degree of bond-length variation from that observed in the larger rare earth type of structure. Actually, both of the independent rare-earth cations suggest oxygen coordination number 6 instead of 7 for Yb(1). Four silicon-bonded oxygens and two not silicon-bonded oxygens form the shells. Assuming coordination number 6 for both the heavy atoms, a model of a fairly ideal closest packing of the oxygens has been suggested (*38*) with two of the five available octahedral sites occupied by the two heavy atoms and three of the octahedral holes left vacant. However, this interpretation of the structure neglects the fact that one of the rare-earth cations, Yb(1), actually shows CN 7, with the additional oxygen present at a fairly close distance of 2.63 Å. A discussion of polyhedra packing in terms of distorted octahedra, heptahedra and (SiO_4) tetrahedra is, however, much more difficult. Moreover, it fails to explain the different degree of space-filling in the two analogous structure types, as shown in Fig. 2.

The mean Yb—O distance in the oxygen polyhedron of the sevenfold coordinated Yb(1) is 2.33 Å, as compared to 2.23 Å of the sixfold coor-

data. It seems worthwhile, however, to give the general impression from the numerous papers published recently on multivalent charge-couple substitution in apatites. It is tempting during synthesis experiments to establish the chemical formula of a new apatite-like compound from the overall chemical analysis, or even from the composition of the starting material as soon as the X-ray examination provides the apatite diffraction pattern. The temptation is especially strong because the apatite structure is known to be extremely tolerant to any type of charge-coupled cation and anion substitution, as well as to cation and probably also anion deficiency. It should be realized, however, that the stoichiometry of apatite is extremely complicated and that, because solid solutions and mixed phases of different degrees of crystallinity may form, reliable data can only be obtained from the analysis of single crystals.

Data on cation substitution will be presented in the following chapter, but only if they are likely to be in agreement with the given requirement. The structural interpretation of the crystal data on mixed cation apatites will be of the preliminary state. The rather anisotropic response of the unit cell dimensions suggests that cation distribution on the (4*f*) and (6*h*)lattice sites may vary in many cases. However, most of these conclusions have to be confirmed by structural analysis.

2.2.1. Binary Compounds $RE_{9.33}\square_{0.67}(SiO_4)_6O_2$

Compounds 7 $RE_2O_3 \cdot 9\,SiO_2$ were shown to crystallize with the apatite structure of space group $P6_3/m$. The cation-deficient oxyapatite structure was established by structural analysis for La, Sm (*11*) and confirmed also for the Gd analogue (*47*). Taking into account all atoms per unit cell, the nature of this structure might best be described in terms of the formula $^{IX}(RE_{3.33}\square_{0.67})\,^{VII}RE_6(^{IV}Si\,^{IV}O_4)_6\,^{III}O_2$, which makes special allowance for the coordination around each atom (Roman numbers above the elements give the coordination number, CN). The

Table 5. *Atomic parameters of* $Gd_{9.33}\square_{0.67}(SiO_4)_6O_2$

Atom	*x*	*y*	*z*	B(Å^2)
Gd(1)	0.24001(7)	0.23321(7)	0.75	0.67
Gd(2)	0.66666	0.33333	0.0	0.76
Si	0.4001 (3)	0.3721 (3)	0.25	0.71
O(1)	0.3178 (7)	0.4872 (7)	0.25	1.00
O(2)	0.6002 (7)	0.4740 (7)	0.25	1.10
O(3)	0.3418 (5)	0.2497 (5)	0.0575(1)	1.40
O(4)	0.0	0.0	0.25	1.09

After Ref. (*47*).

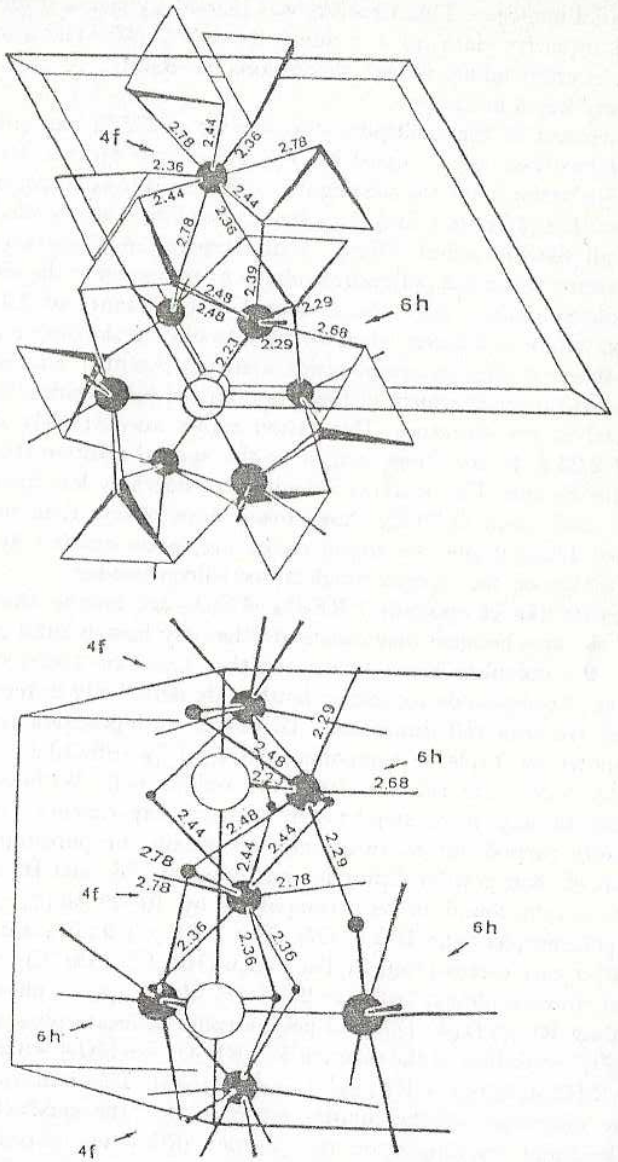

Fig. 7. Perspective view of the structure of rare-earth silicate oxyapatites $(RE_{3.33}\square_{0.67})RE_6(SiO_4)_6O_2$ along [OOl] and [lOO]. Interatomic distances from data on the Gd analogue (*47*) with e.s.d.'s ranging from 0.002 Å to 0.008 Å. Black balls: rare earths in the special positions (4*f*) and (6*h*), white balls: 'free', not silicon-bonded oxygen, solid (SiO_4) tetrahedra

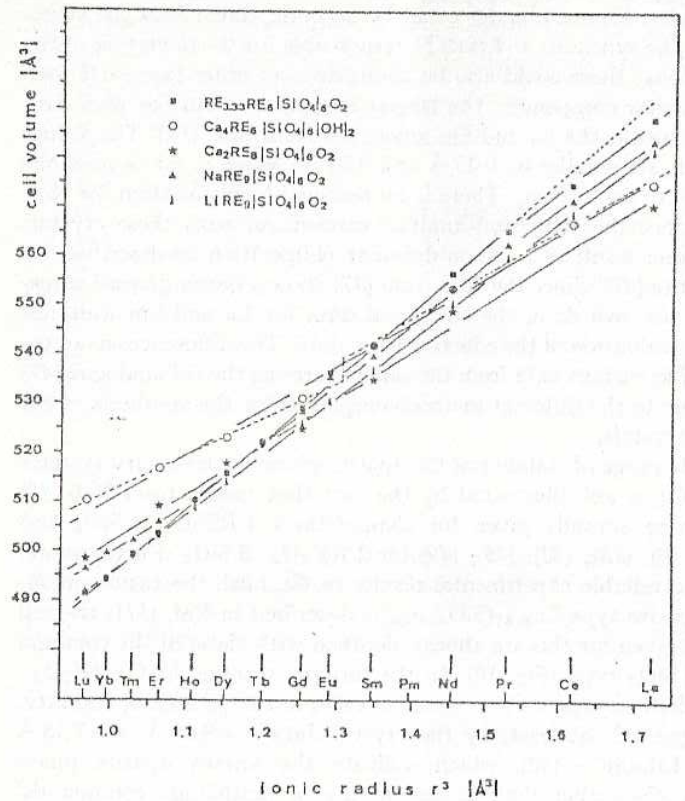

Fig. 9. Cell volume V vs. r^3 (RE^{3+} ionic radii) of rare-earth silicate apatites showing different mixed cation ratios 1:9, 2:8, 4:6 as compared to the binary cation-deficient compound $(RE_{8.33}\square_{0.67})RE_6(SiO_4)_6O_2$. Data of $Ca_2RE_8(SiO_4)_6O_2$ and $Ca_4RE_6(SiO_4)_6O_2$ from (*44*). E.s.d.'s of the cell volume are = height of the symbols

The experiment was controlled in a simultaneous TGA/DTA run. The partial reduction of $Eu^{3+} \rightarrow Eu^{2+}$, corresponding to -0.78% loss of the total starting weight, occurred at 1050 °C:

$$5\ Eu_2O_3 + 6\ SiO_2 \longrightarrow Eu_2^{2+}Eu_8^{3+}(SiO_4)_6O_2 + 0.5\ O_2\uparrow .$$

The microprobe examination carried out on crystals $\sim$0.05 mm in diameter gave $RE:Si = 1.661 \pm 0.002$, which agrees quite well with the theoretical value of 1.666 for the given formula.

To study a possible effect of the lanthanide periodicity on the apatite structure, plots were made of unit-cell volumes vs. ionic radii, $r^3(RE^{3+})$, and plots of cell dimensions a_0 and c_0 vs. ionic radii, $r(RE^{3+})$. To obtain these plots, the experimental values of RE—O bond lengths of the Gd apatite structure served to determine the effective ionic radii of the RE^{3+} cations in this structure type. Since the effective radius of any ion depends on the coordination numbers of both cation and anion, the mean RE^{3+} radii in the apatite structure were evaluated from the seven- and ninefold oxygen-coordinated Gd cations in the following way. The refined values of the Gd—O distances show e.s.d.'s of the order of 0.008 Å, corresponding to the overall R value for the structure of 6.5% (*47*). The average Gd—O distances in the '(4*f*)polyhedron' with CN 9 and in the '(6*h*)polyhedron' with CN 7 are 2.53 Å and 2.40 Å, respectively. The 24 silicon-bonded oxygens per unit cell are surrounded by four cations, whereas the two 'free' oxygens have three rare-earth neighbours. Thus, with the average oxygen radius of 1.38 Å (*54*), the effective Gd^{3+}—(4*f*) and Gd^{3+}—(6*h*) ionic radii are 1.15 Å and 1.02 Å. From these data the weighted mean value of the Gd^{3+} ionic radius in the apatite structure was determined as 1.08 Å.

Fig. 9 is the plot of apatite cell volumes vs. $r^3(RE^{3+})$. The relative scale of the trivalent rare-earth radii was maintained from the known RE^{3+} series with CN 6 (*48*). The complete set was shifted to the values $r(Gd^{3+}) = 1.08$ Å and $r^3(Gd^{3+}) = 1.26$ Å, respectively. The correlation is quite linear with small deviations from $r^3(La^{3+})$ and $r^3(Ce^{3+})$. These should be corrected to slightly smaller values corresponding to ionic radii of 1.19 Å and 1.17 Å. The special situation of the Eu analogue, which is also off the straight line, probably arises from mixed valence Eu^{2+}—Eu^{3+}, as already suggested from the chemical analysis on this compound. The plots of the individual cell dimensions of the apatite compounds vs. ionic radii (RE^{3+}) revealed some interesting details about the response of the structure to rare earth substitution. As shown in Fig. 10, the shrinkage of the c_0 dimension of the apatite cell is much more pronounced than that of the a_0 dimension. As compared with the La analogue, the structure of the Lu apatite shows a shrinkage of 9.6% along the c direction as compared to 4.7% along the a_0 axis. This is best understood in terms of the Gd—O interatomic distances given in Fig. 7. The shortest Gd—O bonds are directed essentially along [*001*] from both the cation positions (4*f*) and (6*h*).

Another interesting feature of Fig. 10 is that the changes in slope and intersections occur at different positions along a_0 and c_0. The c_0 axis indicates the three groups Lu—Er, Ho—Nd, and Nd—La, as commonly known in rare-earth chemistry, whereas a_0 shows only one intersection between Gd and Eu. This feature, for which either a change in occu-

listed in Table 4. The composition of these crystals and of some samples of compounds $M_2RE_8(SiO_4)_6O_2$ with M:Mg,Ca,Sr,Ba, which will be introduced later, was confirmed by microprobe analysis. Singel-crystal X-ray examination indicated space group $P6_3/m(P6_3)$ for these ternary rare-earth silicate oxyapatites, too. Reflections $[00l]$ and $[hkl]$ with $l \neq 2n$ were found to be absent on MoKα-precession photographs in the case of $[hkl]$, if $h-k=3n$.

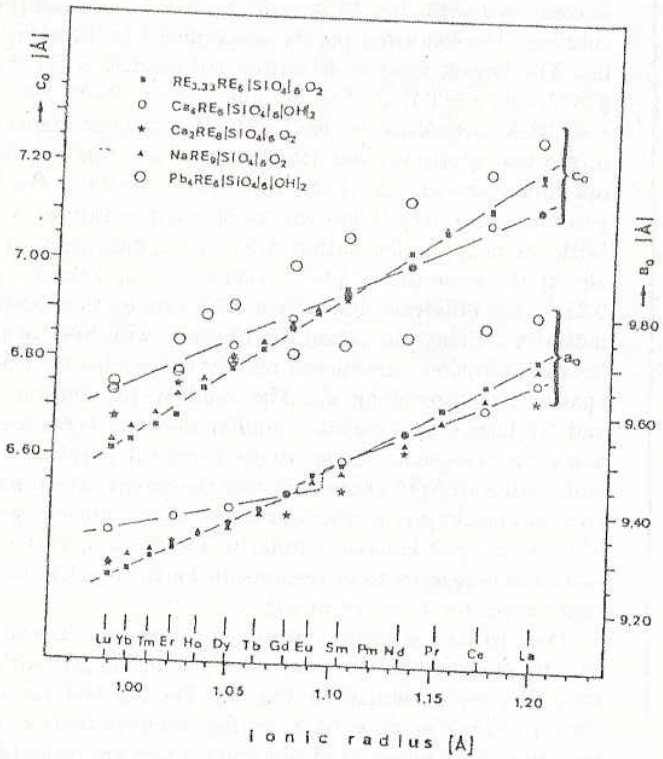

Fig. 11. Survey of cell dimensions a_0 and c_0 vs. r (RE^{3+}) of some representative RE silicate apatites showing different mixed cation ratios 1:9, 2:8, 4:6 as compared to the binary cation-deficient apatite $(RE_{3.33}\square_{0.67})RE_6(SiO_4)_6O_2$. Data for Ca and Pb analogues from Ref. (*44*) with e.s.d.'s of $\sim$0.01 Å (private communication)

In the following chapters the crystal data of mixed-cation oxyapatites of different stoichiometry will be discussed in relation to the cation distribution on the (4*f*) and (6*h*) lattice sites and the lanthanide period-

icity. The general impression which emerges from the data in Figs. 9 to 11 (which also include compounds $M_4RE_6(SiO_4)_6(OH)_2$ in order to emphasize the correlation) is this: The declining slope in the ratio apatite cell volume vs. $r^3(RE^{3+})$ (Fig. 9) of compounds with an increasing proportion of foreign (not RE) cations relative to the pure binary rare-earth apatites, signifies the decreasing influence of the rare-earth periodicity on the structure. The distinct anisotropic response of apatite cell dimensions, as observed in the binary apatites (Fig. 10), is modified or vanishes completely with mixed-cation substitution. This impression will be substantiated in chapters 2.2.2.1 and 2.2.2.2.

2.2.2.1. Ternary Compounds $RE_9Alk(SiO_4)_6O_2$. Compounds $LiRE_9(SiO_4)_6O_2$ show an even more ideal linear relationship between cell volume and cubic RE^{3+} radius (see Fig. 9) than the pure rare-earth apatites. The sodium analogues, however, exhibita change in slope beyond Ho. It is interesting to see from Fig. 10 that the pronounced breaks in the curves a_0 and c_0 vs. r of the pure rare-earth apatites vanish on the introduction of a single small, but different, cation per cell. It appears to be due to this moderator function of the alkali atom that the c_0 dimension of the $LiRE_9$ apatites varies linearly with r along the complete rare-earth series; no subdivision shows up along c_0. A slight change in the slope of a_0, however, is indicated at Ho. This change in the slope at Ho of a_0 is even more pronounced with the compounds $NaRE_9(SiO_4)_6O_2$, whereas their absolute a_0 values with the larger rare earths beyond Dy are about the same. For La to Gd, c_0 for the sodium analogues is about the same as for the pure rare-earth apatite, whereas the c_0 values of the smaller $NaRE_9$ apatites are significantly larger. Since the single alkali atom per cell formally substitutes for the combination $(^1/_3\,RE + ^2/_3\,\square)^{1+}$, it seems likely that the small alkali prefers the smaller space of the (6*h*) position in a statistical distribution. This is suggested by the significant change in slope of a_0 vs. r in Fig. 10. It occurs at a place where the Na^{1+} radius becomes competitive with the rare earths around Ho—Dy. It is apparent from Fig. 7 that the variation of the a_0 axis should depend mostly on a corresponding substitution into the (6*h*)lattice sites rather than into the (4*f*) ones. This is because the (6*h*)position has the tighter bonds in directions $[hk0]$ (2.23 Å, 2.39 Å, 2.68 Å) than the (4*f*) cation with three 2.78 Å Gd—O distances.

2.2.2.2. Ternary Compounds $RE_8M_2(SiO_4)_6O_2$. In order to follow the correlation between cation substitution and variation of cell dimensions in 2:8 mixed-cation apatites, we bring forward crystal data for 4:8 hydroxy apatites from (*44*). It is especially atractive to introduce the 4:6 apatite compounds into the discussion of crystal chemistry because their mixed-cation ratio exactly corresponds to the ratio of the symmetry-

from Ref. (*51*) which describes two different types of deficient apatite structures, in addition to the known cation-deficient apatite $RE_{9.33}\square_{0.67}(SiO_4)_6O_2$, by the formulas $Sr_2La_{6.67}(SiO_4)_6$, $Sr_3La_6(SiO_4)_6$, $Sr_4La_{5.33}(SiO_4)_6$ (↑) and $Sr_4La_6(SiO_4)_6O$ (/). However, no reliable experimental data exist, so far to confirm these types of oxygen deficiency in the silicate apatite structure. The criticism concerning $La_{8.67}(SiO_4)_6O$ from the same source (*51*) applies to $La_{9.33}\square_{0.67}(SiO_4)_6O_2$ too, since the cell dimensions given for the various Sr–La apatites indicate that only one type of compound is present, namely $Sr_2La_8(SiO_4)O_2$ (↑). The arguments are restricted by the limits of accuracy indicated for the data given.

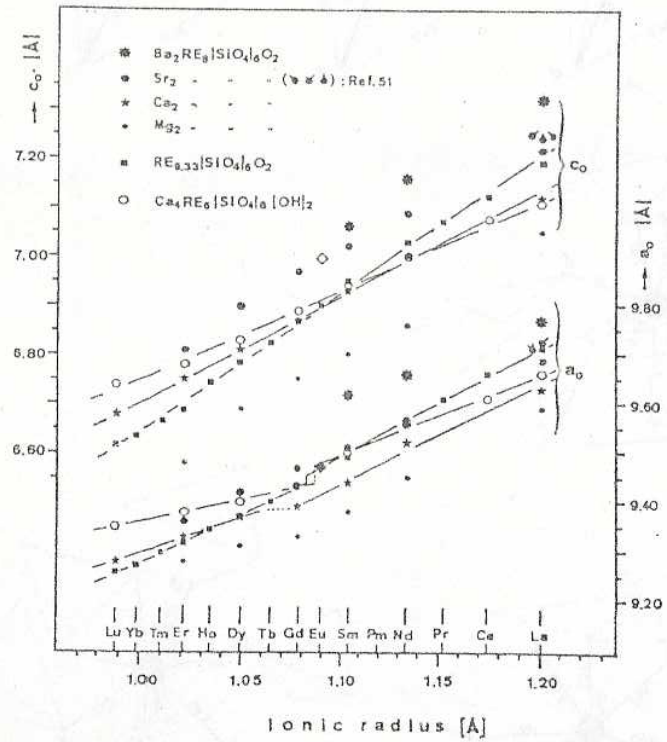

Fig. 13. Cell dimensions a_0 and c_0 vs. r (RE^{3+}) of rare-earth silicate oxyapatite with mixed-cation ratio 2:8 from Ref. (*44*) with e.s.d.'s ~0.01 Å (private communication) compared with the binary rare-earth silicates (own data) and the Ca hydroxyapatites with mixed-cation ratio 4:6, also from (*44*). The rhombus-like symbol represents cell dimensions of $Eu_2^{2+}Eu_8^{3+}(SiO_4)_6O_2$

2.3. *Mixed-Cation Compounds RE $M^{1+}(SiO_4)$*

Three different types of structure are known for ternary compounds RE $Na(SiO_4)$. They were obtained by hydrothermal synthesis in the systems Na_2O–RE_2O_3–SiO_2–H_2O largely at a pressure of 1000 atm. at 450 °C (*29–31*). The order of their occurrence along the rare-earth series is given in Table 6 together with some crystal data.

Table 6. *Distribution of structure types in $RENa(SiO_4)$ compounds*

RE	Structure Type	Cell Dimensions	Space Group	Z	$\varrho_{exp.}$ (g/cm³)
(La) Ce Pr Nd	Na RE A	$a = 20.00$ Å, $b = 9.28$ Å, $c = 5.45$ Å	$Pna2_1$	12	5.1
Nd Sm (Eu) Gd (Tb) Dy Ho	Na RE B	$a = 11.84$ Å, $c = 5.45$ Å	$I4/m$	8	4.7
Er Yb Tm Lu	Na RE C	$a = 5.09$ Å, $b = 10.96$ Å, $c = 6.35$ Å	$Pbn2_1$	4	

Phase formation during the hydrothermal experiments, which also yielded compounds $Na_3RE(Si_2O_7)$, is apparently controlled mainly by the Na(OH) reduction in each run. Analogous potassium-containing compounds have not been obtained during the corresponding experiments. However, an isostructural group of Li-containing compounds seems to exist for the smaller rare earths with the orthorhombic structure of type C $NaRE(SiO_4)$ (*52*).

Structurally all compounds of type $NaRE(SiO_4)$ are related to polymorphic $Ca_2(SiO_4)$. This supports the general feature, often described in geochemistry, of a $Na^{1+}RE^{3+} \longleftrightarrow 2\,Ca^{2+}$ substitution. This is found in many minerals (see also Appendix I).

Table 7. *Atomic parameters of $NaNd(SiO_4)$*

Atom	x	y	z	Atom	x	y	z
Nd(1)	0.0	0.198	0.052	O (3)	0.166	0.437	0.533
Nd(2)	0.167	0.302	0.0	O (4)	0.442	0.070	0.017
Nd(3)	0.334	0.198	0.0	O (5)	0.235	0.166	0.737
Si(1)	0.091	0.416	0.517	O (6)	0.235	0.165	0.238
Si(2)	0.258	0.084	0.493	O (7)	0.332	0.063	0.533
Si(3)	0.424	0.416	0.500	O (8)	0.276	0.430	0.953
Na(1)	0.111	0.072	0.506	O (9)	0.402	0.333	0.253
Na(2)	0.278	0.428	0.483	O(10)	0.403	0.334	0.753
Na(3)	0.445	0.075	0.517	O(11)	0.0	0.064	0.450
O(1)	0.070	0.333	0.277	O(12)	0.109	0.070	0.040
O(2)	0.069	0.333	0.774				

After Ref. (*55*).

The structure is illustrated in Fig. 14: it contains olivine-like ribbons extending to [*100*]. These ribbons have a core of Nd polyhedra and edges of Na polyhedra and are linked by (SiO_4) tetrahedra and by shared corners. The three crystallographically independent Nd cations show an eightfold coordination in the shape of trigonal prisms with additional oxygens outside the midpoints of the three prism faces (Fig. 15). The structure of $NaNd(SiO_4)$ is apparently not very stable since it shows extensive morphologic twinning. Another structural feature indicating considerable instability is the joining of Nd polyhedra into a strip by face-to-face contact. $NaNd(SiO_4)$ forms a second modification of tetragonal symmetry. This structure is described in 2.3.2.

2.3.2. Compounds (Nd, ... Ho)$Na(SiO_4)$

The crystal structure of $NaSm(SiO_4)$ represents the structural type of the medium-sized rare earths in compounds of composition $NaRE(SiO_4)$. The crystal structure of space group I4/m has $Z=8$ formula units of $NaSm(SiO_4)$ in the unit cell with $a=11.89$ Å and $c=5.45$ Å. The structure was determined by 3-dimensional X-ray intensity film data and refined to an R value of 14%, which corresponds to standard deviations in the oxygen cation distances of about 0.03 Å. The atomic parameters without individual temperature factors are given in Table 8 after (*55*).

The main structural features are shown in Fig. 16. The structure appears to be determined by fourfold rings of Sm—O polyhedra of CN 6 arranged on two levels in the centered cell along [*001*]. The individual polyhedra are linked by their vertical edges and have the shape of fairly undistorted trigonal prisms. However, these fourfold rings of Sm—O prisms do not form a continuous three-dimensional spatial linkage.

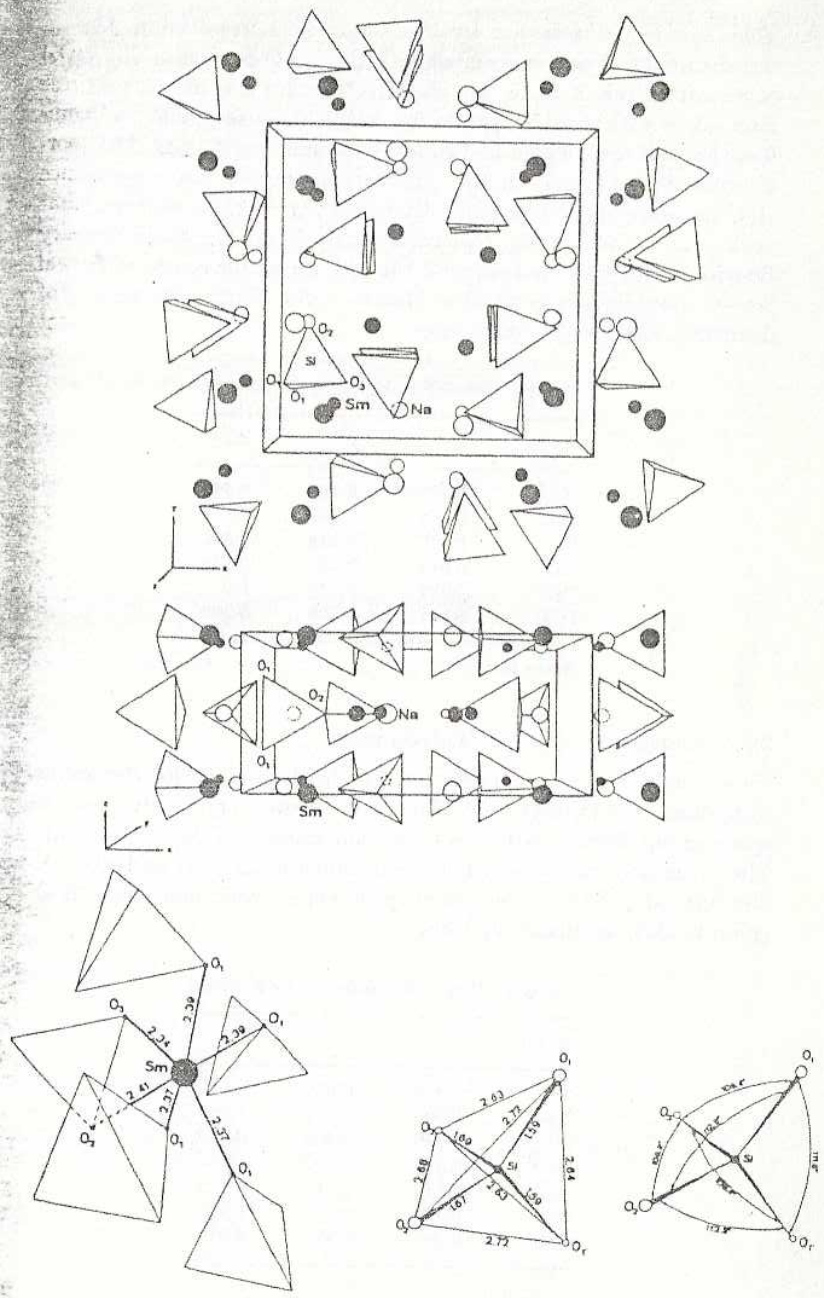

Fig. 16. Crystal structure of $NaSm(SiO_4)$

octahedra are located within the rods while the somewhat smaller Y ions lie in the projections. The reason for this apparently is that Na^{1+} differs considerably in charge from Y^{3+}, which means that the rare-earth cations must be as far apart as possible. Isostructural compounds of Li(Y,Ho ... Lu) (SiO_4) have been prepared by solid-state reaction of the corresponding oxide mixtures at 1050 °C (*52*). The cell dimensions given there for $LiY(SiO_4)$ are $a = 4.94$ Å, $b = 10.68$ Å and $c = 6.29$ Å.

2.3.4. Stillwellite, Ce $B(SiO_4)O$

The crystal structure of stillwellite, a well-known rare-earth boron-silicate mineral, was determined by three-dimensional diffractometer single-crystal intensity data (*58*). The trigonal structure of space group $P3_1$ contains three formula units $CeB(SiO_4)O$ in the unit cell of dimensions $a = 6.85$ Å, and $c = 6.70$ Å. The final R value in the refinement corresponding to the atomic parameters (given in Table 10) is 9.2% for (*hko*) and 12.8% for (*okl*) reflections.

Table 10. *Atomic parameters of* $CeB(SiO_4)O$

Atom	*x*	*y*	*z*
Ce	0.587	0.0	0.0
Si	0.585	0.0	0.500
B	0.113	0.0	0.973
O(1)	0.339	0.194	0.023
O(2)	0.195	0.339	0.310
O(3)	0.613	0.464	0.320
O(4)	0.464	0.614	0.014
O(5)	0.051	0.051	0.781

After Ref. (*58*).

The main structural elements are (SiO_4)tetrahedra, (BO_4) tetrahedra and ninefold-coordinated Ce polyhedra, as illustrated in Fig. 18. The main 'architectural' detail of the structure is apparently determined by the infinite helical chains of (BO_4)tetrahedra parallel to the 3_1-axis. Each (BO_4)tetrahedron of the chain is connected by its two free vertices to two (SiO_4) tetrahedra. Furthermore, it shares two edges with the polyhedra of ninefold-coordinated Ce, which are also arranged in parallel [*001*] columns. Analogous compounds RE $B(SiO_4)O$ of La, Ce, Pr, and Nd were prepared by solid-state reaction starting from the oxides at temperatures around 1100 °C (*50*).

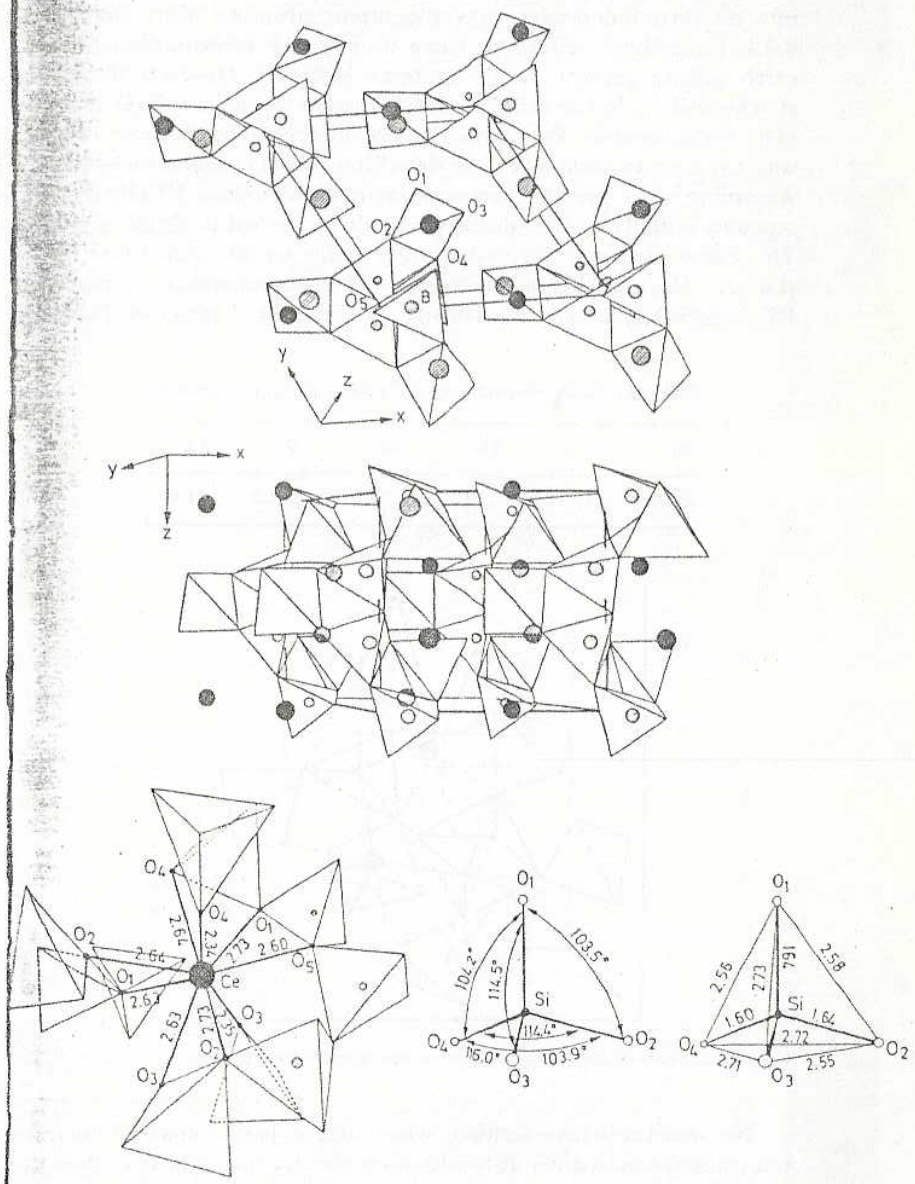

Fig. 18. Crystal Structure of $CeB(SiO_4)O$

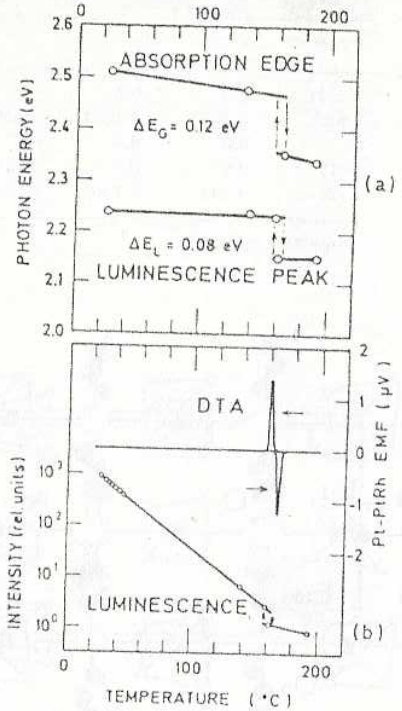

Fig. 20. Phase transition of dimorphic $Eu_2(SiO_4)$

Table 12. *Atomic parameters of monoclinic low* $Eu_2(SiO_4)$

Atom	x	y	z	B[Å²]
Eu(1)	0.9282(2)	0.0011(1)	0.6976(1)	0.42 (4)
Eu(2)	0.6604(2)	0.3424(1)	0.6976(1)	0.55 (4)
Si	0.676 (1)	0.767 (1)	0.419 (1)	0.39 (6)
O(1)	0.795 (4)	0.723 (2)	0.320 (2)	0.62(15)
O(2)	0.368 (4)	0.678 (2)	0.356 (2)	0.98(19)
O(3)	0.652 (4)	0.006 (2)	0.430 (2)	0.65(14)
O(4)	0.883 (4)	0.680 (2)	0.572 (2)	0.94(17)

After Ref. (*60*).

crystals confirmed an isostructural relation with β-$Ca_2(SiO_4)$ (*60*). Because of the fact that no correction for absorption could be carried out, the R value of 8.9% indicates to a relatively high standard deviation (0.02 Å) for the mean cation-oxygen distances.

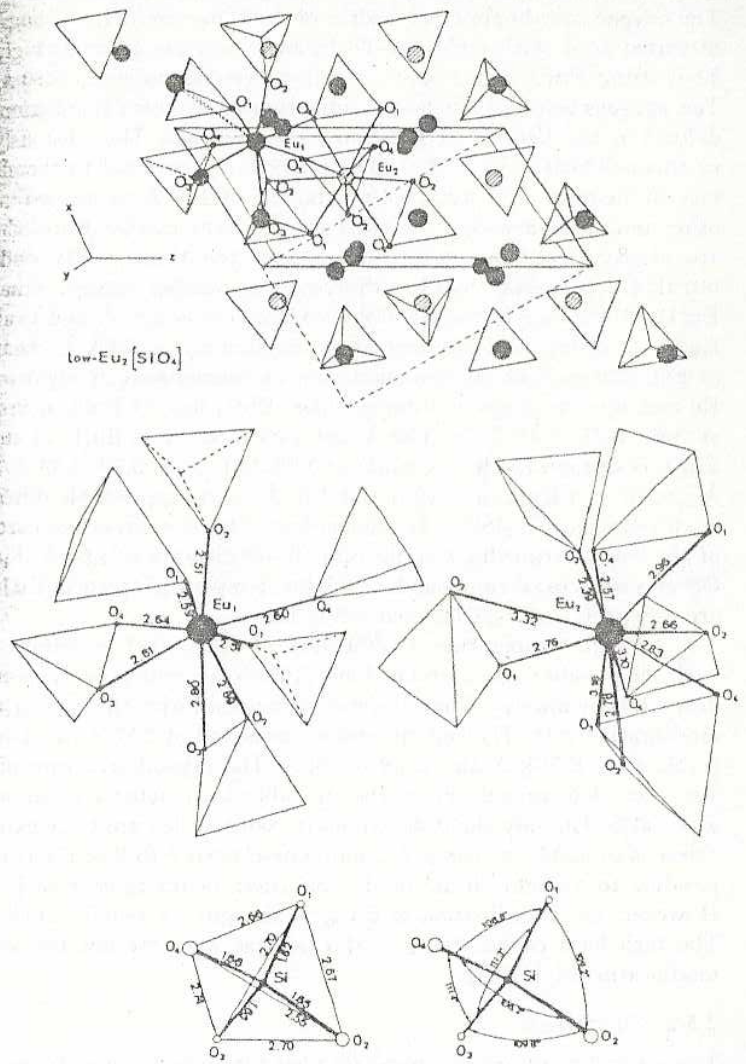

Fig. 21. Crystal structure of low $Eu_2(SiO_4)$

The structure consists of isolated (SiO_4)tetrahedra and two kinds of crystallographically independent Eu atoms. Viewing along [*010*], as in Fig. 21, reveals a pseudo-hexagonal arrangement of strings containing (SiO_4)tetrahedra alternating with Eu(2) atoms, which show CN 10.

is the (SiO_4)tetrahedron and the other is the isolated, not silicon-bonded oxygen O(1). There exist two crystallographically independent types of Eu cations which show not however eight- and tenfold oxygen coordination, as observed in the monoclinic structure of $Eu_2(SiO_4)$ (*60*) but octahedral coordination. Eu(1) is surrounded by two O(1) at 2.69 Å and by four O(2) at 2.70 Å, Eu(2) by two O(1) at 2.52 Å and four O(2) at 2.47 Å and 2.67 Å, respectively. As shown in Fig. 22a, a reasonable description of the structure is obtained in terms of (SiO_4) tetrahedra and $(O—Eu_6)$octahedra. In the latter, the 'extra' oxygen O(1) is octahedrally surrounded by four Eu(2) and two Eu(1) cations.

Like $Sr_3(SiO_4)O$, which crystallizes in space group $P4/ncc$ (*63*), these $(O—Eu_6)$octahedra form a three-dimensional framework in which the (SiO_4)tetrahedra are located for charge balance. The corner-sharing

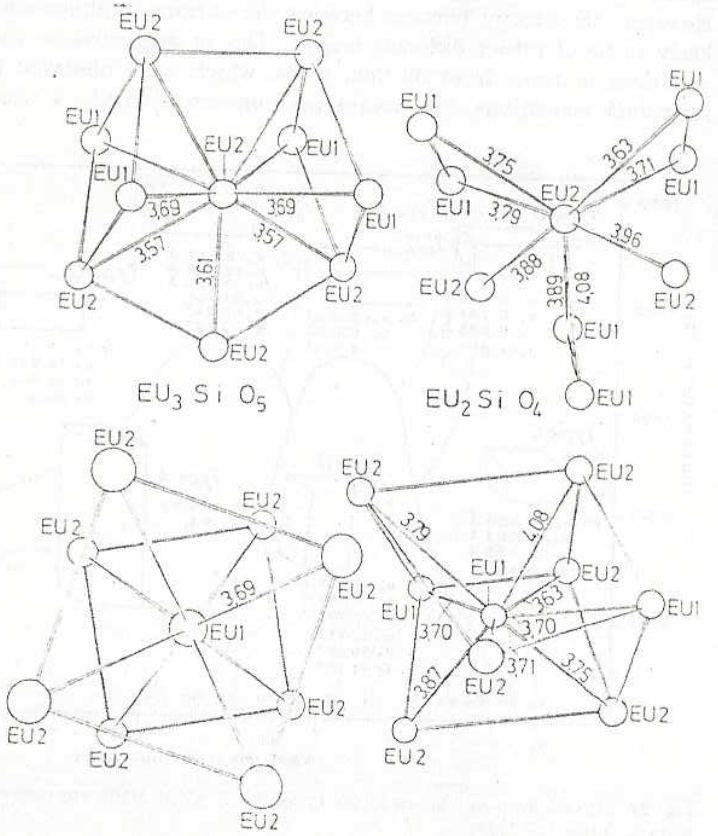

Fig. 22b. Metal to metal distances of closest neighbours in $Eu_3(SiO_4)O$ and $Eu_2(SiO_4)$

$(O—Eu_6)$octahedra run parallel to the fourfold axis. The silicon-bonded oxygens O(2) are in the general positions. The Si—O(2) distance is equal to 1.64 Å for all four bonds because Si is located in the special position on $(0,0,0)$. As shown in Fig. 22b the metal to metal distances are close to the values known from EuO (Eu—Eu = 3.67 Å), which is also ferromagnetic with a Curie temperature of 77 °K. Eu(1) has eight nearest Eu(2) neighbours at equal distances of 3.69 Å. The polyhedron is close to a antisquare prism. Eu(2) is surrounded by nine next metal neighbours in the shape of a distorted cube with one additional Eu(2) attached to one cube edge. Four Eu(2) are at 3.57 Å, four Eu(1) at 2.69 Å and one Eu(2) is at 3.61 Å.

3. Structures Containing Isolated Groups (Si_2O_7), or (Si_3O_{10}), + (SiO_4)

Compounds $1\,RE_2O_3 \cdot 2\,SiO_2$ are known from all binary rare-earth silicate systems. They show extensive polymorphism. The polymorphism is characterized by transition temperatures between 1300—1500 °C and by boundaries at europium and holmium along the series of trivalent rare earths. Seven polymorphic forms were observed; all are of type $RE_2(Si_2O_7)$ with one exception, $RE_4(Si_3O_{10})(SiO_4)$, which occurs with the medium-sized rare earths. Ternary compounds of type $Alk._3RE(Si_2O_7)$ crystallize with two different structures, which also contain (Si_2O_7) double-tetrahedra groups.

It is the configuration of the (Si_2O_7)double-tetrahedra groups in all these disilicate structures which is of special interest from several points of view. One aspect concerns the systematics of all possible double-tetrahedra configurations of anions $(X_2O_7)^{-n}$ and the packing with a certain number of individual cations providing charge balance. This viewpoint has recently been followed up in (*86*). Another aspect involves the double π-bonding theory, as developed in (*78*) for $(XO_4)^{-n}$tetrahedra ions (X = Si,P,S,Cl). Many helpful quantitative data might be introduced into this discussion in terms of the bonding lengths and angles observed for the (Si_2O_7)groups in rare-earth disilicate structures. A third aspect of the disilicate polymorphs is that concerning lanthanide periodicity. The (Si_2O_7)configuration is apparently determined by the bonding and polarizing forces of the surrounding cations. Thus, any periodicity of the rare-earth electronic structures, such as variation in ionic size or discontinuity in chemical bonding properties, along the series of trivalent rare earths should be reflected in the changing configuration of the (Si_2O_7)

Table 14. *Cell dimensions and densities of all observed polymorphic forms of the rare-earth disilicates. Standard deviations of the refined values are given in parentheses in units of the last decimal place.* ϱ_0, *pyknometer data at 20 °C. Z, formula units per unit cell volume, V.*

Structure type A (tetragonal, $P\,4_122-P4_1$)

	$La_2Si_2O_7$	$Pr_2Si_2O_7$	$Nd_2Si_2O_7$	$Sm_2Si_2O_7$	$Eu_2Si_2O_7$
a[Å]	6.7945(9)	6.7657(6)	6.7405(6)	6.6933(8)	6.6727(7)
c[Å]	24.871 (8)	24.608 (4)	24.524 (4)	24.384 (9)	24.338 (3)
V[Å^3]	1148.1 (9)	1126.4 (2)	1114.3 (2)	1092.4 (3)	1083.6 (9)
Z	8	8	8	8	8
ϱ_0[g cm^{-3}]	5.11 (9)	5.26 (6)	5.38 (6)	5.67 (7)	5.68 (9)
ϱ_c[g cm^{-3}]	5.15	5.30	5.44	5.70	5.79

Structure type B (triclinic, $P\bar{1}-P1$)

	$Eu_2Si_2O_7$	$Gd_2Si_2O_7$	$Tb_2Si_2O_7$	$Dy_2Si_2O_7$	$Ho_2Si_2O_7$	$Er_2Si_2O_7$
a[Å]	6.716 (3)	6.624 (5)	6.623 (5)	6.639 (2)	6.664 (5)	6.583(5)
b[Å]	6.762 (3)	6.679 (5)	6.684 (5)	6.691 (2)	6.674 (5)	6.609(5)
c[Å]	12.321 (7)	12.132 (9)	12.101 (9)	12.152 (3)	12.110 (9)	12.000(9)
α[°]	94.36 (4)	94.10 (8)	93.97 (7)	94.03 (3)	94.07 (8)	94.50 (8)
β[°]	90.02 (3)	89.79 (9)	89.85 (9)	89.81 (2)	89.97 (8)	90.57 (8)
γ[°]	91.75 (4)	91.60 (7)	91.55 (6)	91.69 (3)	91.66 (7)	91.79 (9)
V[Å^3]	557.7 (1)	535.2 (7)	534.4 (6)	538.2 (1)	537.1 (6)	520.3 (7)
Z	4	4	4	4	4	4
ϱ_0[g cm^{-3}]	5.54 (6)	5.82 (7)	5.93 (5)	6.06 (7)	6.11 (4)	6.28 (9)
ϱ_c[g cm^{-3}]	5.62	5.99	6.04	6.09	6.15	6.42

Structure type C (monoclinic, $C2/m-C2-Cm$)

	$Ho_2Si_2O_7$	$Er_2Si_2O_7$	$Tm_2Si_2O_7$	$Yb_2Si_2O_7$	$Lu_2Si_2O_7$
a[Å]	6.875 (5)	6.841 (5)	6.818 (7)	6.789 (6)	6.760 (6)
b[Å]	9.184 (9)	9.135 (9)	9.104 (9)	9.067 (9)	9.051 (9)
c[Å]	4.697 (4)	4.694 (6)	4.679 (5)	4.681 (4)	4.685 (7)
β[°]	101.69 (6)	101.70 (7)	101.75 (8)	101.84 (7)	101.86 (6)
V[Å^3]	290.5 (3)	287.3 (2)	284.4 (4)	282.1 (3)	280.6 (1)
Z	2	2	2	2	2
ϱ_0[g cm^{-3}]	5.62 (6)	5.78 (5)	5.82 (4)	6.01 (7)	6.02 (4)
ϱ_c[g cm^{-3}]	5.68	5.81	5.91	6.06	6.10

Structure type E (orthorhombic, $Pnam-Pna2_1$)

	$Eu_2Si_2O_7$	$Gd_2Si_2O_7$	$Tb_2Si_2O_7$	$Dy_2Si_2O_7$	$Ho_2Si_2O_7$
a[Å]	13.9142(9)	13.8665(9)	13.797 (2)	13.7275(9)	13.7934(9)
b[Å]	5.0553(4)	5.0532(4)	5.036 (1)	5.0303(3)	5.0371(4)
c[Å]	8.3486(7)	8.3008(8)	8.200 (2)	8.2050(6)	8.2524(8)
V[Å^3]	587.25 (3)	581.64 (4)	573.35 (9)	566.58 (4)	573.36 (5)
Z	4	4	4	4	4
ϱ_0[g cm^{-3}]	5.22 (8)	5.38 (6)	5.56 (7)	5.75 (4)	5.69 (5)
ϱ_c[g cm^{-3}]	5.33	5.51	5.63	5.78	5.82

Structure type D (monoclinic $P2_1/a$)

	$Ho_2Si_2O_7$	$Er_2Si_2O_7$
a[Å]	5.957 (2)	5.588 (2)
b[Å]	10.842 (3)	10.793 (3)
c[Å]	4.696 (2)	4.689 (2)
α[°]	90.0	90.0
β[°]	95.72 (3)	95.82 (4)
γ[°]	90.0	90.0
V[Å$_3$]	283.6 (1)	281.4 (1)
Z	2	2
ϱ_0[g cm^{-3}]	5.76 (4)	5.82 (7)
ϱ_c[g cm^{-3}]	5.82	5.93

Structure type F (triclihic $P\bar{1}-P1$),

	$Sm_2Si_2O_7$	$Eu_2Si_2O_7$
a[Å]	8.513 (3)	8.517 (1)
b[Å]	12.867 (4)	12.848 (2)
c[Å]	5.374 (2)	5.385 (1)
α[°]	91.34 (3)	91.65 (2)
β[°]	92.06 (4)	92.24 (2)
γ[°]	90.43 (3)	90.44 (2)
V[Å$_3$]	588.2 (2)	588.56 (9)
Z	4	4
ϱ_0[g cm^{-3}]	5.10 (5)	5.30 (5)
ϱ_c[g cm^{-3}]	5.26	5.33

Structure type G (pseudoorthorhombic, $P2_1/n$)

	$La_2Si_2O_7$	$Ce_2Si_2O_7$	$Pr_2Si_2O_7$	$Nb_2Si_2O_7$	$Sm_2Si_2O_7$
b[Å]	8.794 (2)	8.722 (1)	8.674 (1)	8.630 (2)	8.564 (7)
c[Å]	13.201 (2)	13.056 (2)	12.996 (2)	12.945 (2)	12.855 (9)
a[Å]	5.409 (1)	5.401 (1)	5.405 (1)	5.391 (1)	5.383 (5)
α,β,γ[°]	90.0	90.0	90.0	90.0	90.0
V[Å^3]	627.95 (8)	615.09 (7)	609.40 (7)	602.37 (7)	592.61
Z	4	4	4	4	4
ϱ_0[g cm^{-3}]	4.61 (6)	4.81 (7)	4.86 (6)	5.01 (6)	5.11 (7)
ϱ_c[g cm^{-3}]	4.71	4.84	4.90	5.04	5.23

After Ref. (*21*)

$Eu_2(Si_2O_7)$ and $Sm_2(Si_2O_7)$ of sufficient size and quality have not been successful so far. Thus, this is the only structure in the field of disilicate polymorphs, which has not yet been worked out. However, its cell dimensions and powder diffraction intensities (*21*) suggest a strong similarity with structure type G, which has already been determined. A better approach to an understanding of the polymorphism of the rare-earth disilicates will be achieved by giving extensive information about the structural details of all the polymorphic forms. This is provided below following the alphabetical sequence of structure types from A to G.

3.1.1. Structure Type A, (La, ... Eu)$_2$(Si_2O_7), 'RE Di A'

Single crystals of the low-temperature form of $Pr_2(Si_2O_7)$ were obtained by sintering the compound at temperatures at which the modification of type G is stable. These crystals were cooled to below the transition temperature of about 1350 °C. After annealing for a few hours, single

Table 15. *Atomic parameters of A-type* $Pr_2(Si_2O_7)$

Atom	x	y	z	B[Å^2]
Pr 1	0.76635(7)	0.29698(7)	0.99312(2)	1.09 (2)
Pr 2	0.52041(7)	0.16681(7)	0.14075(2)	1.01 (2)
Pr 3	0.33792(7)	0.91768(7)	0.99347(3)	1.02 (2)
Pr 4	0.12165(7)	0.76307(7)	0.13275(3)	1.06 (2)
Si 1	0.8522 (4)	0.7634 (4)	0.0085 (1)	0.78 (4)
Si 2	0.5985 (4)	0.6548 (4)	0.1067 (1)	0.71 (4)
Si 3	0.2623 (4)	0.3762 (4)	0.0147 (1)	0.79 (4)
Si 4	0.0091 (4)	0.2912 (4)	0.1141 (1)	0.67 (4)
O 1	0.8951(10)	0.6156(10)	0.9578 (3)	0.89 (8)
O 2	0.7207(10)	0.9412(10)	0.9835 (3)	1.03 (9)
O 3	0.0458(10)	0.8439(10)	0.0404 (3)	0.87 (8)
O 4	0.7181(10)	0.6252(10)	0.0511 (3)	0.84 (8)
O 5	0.4799(13)	0.5167(13)	0.1333 (3)	1.48(11)
O 6	0.4328(10)	0.8590(10)	0.0877 (3)	1.10 (9)
O 7	0.7530(10)	0.8124(10)	0.1467 (3)	0.96 (9)
O 8	0.3262(10)	0.5715(10)	0.9834 (3)	1.10 (9)
O 9	0.4456(10)	0.2375(10)	0.0338 (3)	0.98 (9)
O 10	0.1249(10)	0.2404(10)	0.9746 (3)	1.05 (8)
O 11	0.1207(10)	0.4291(10)	0.0668 (3)	1.12 (9)
O 12	0.9685(10)	0.4559(10)	0.1604 (3)	1.03 (9)
O 13	0.1573(11)	0.1247(11)	0.1403 (3)	1.15 (9)
O 14	0.8124(12)	0.2054(12)	0.0867 (3)	1.34(10)

After Ref. (*26*), however more accurate values as obtained recently by a LSQS refinement on 1004 independent reflections measured with the same crystal and identical experimental conditions as described in Ref. (*26*)

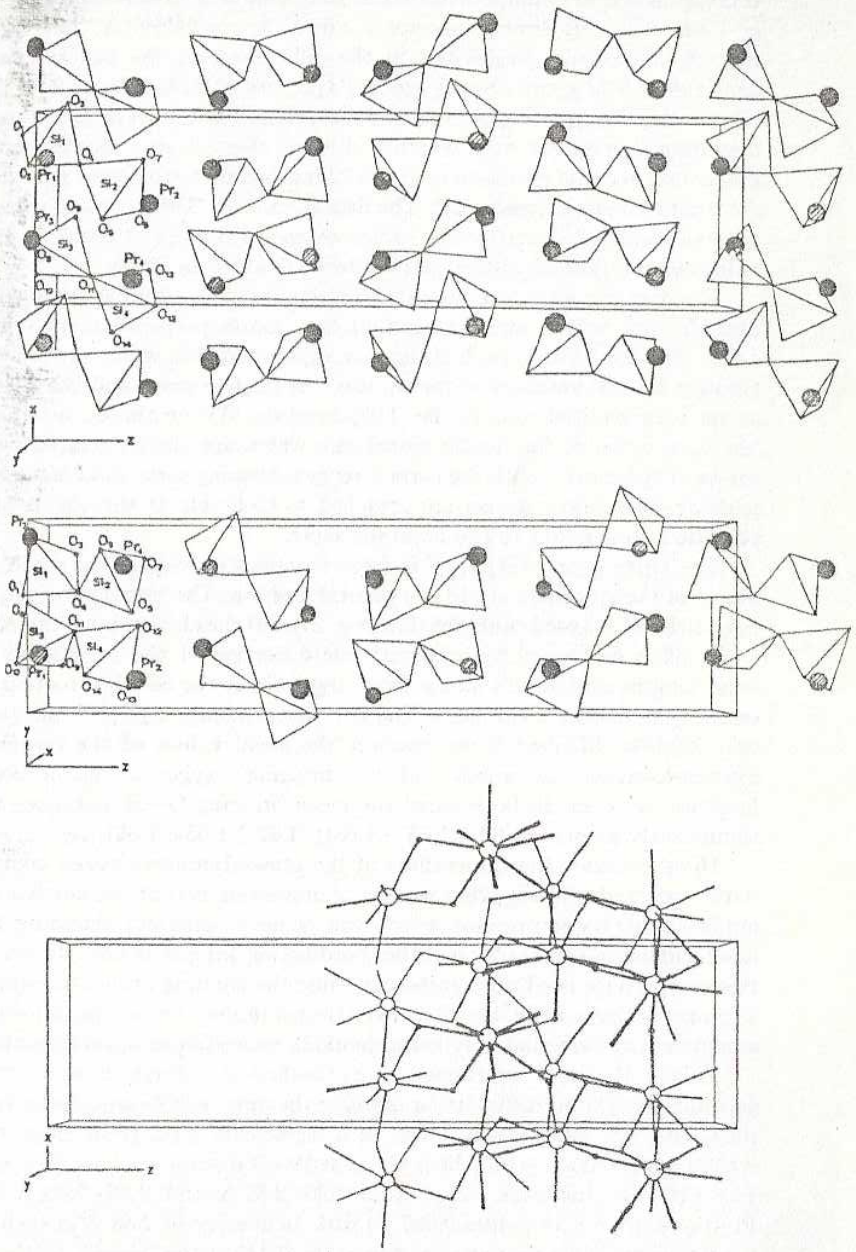

Fig. 26. Crystal structure of A-type $Pr_2(Si_2O_7)$

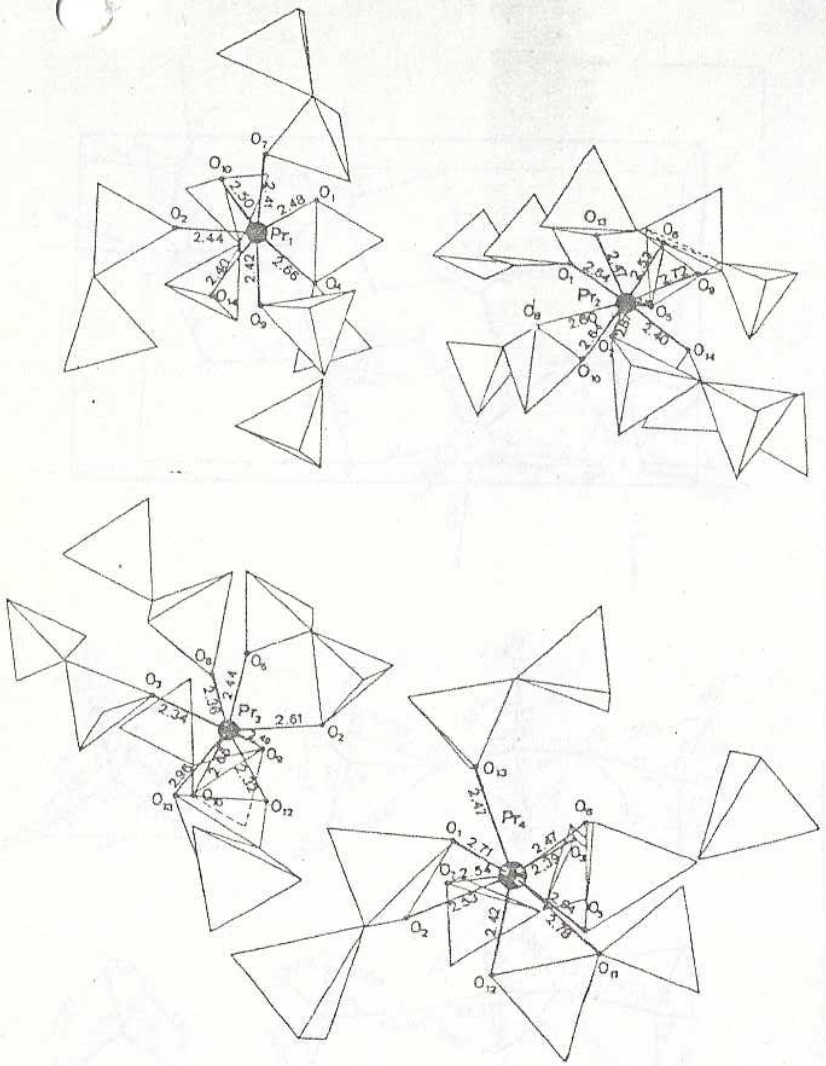

Fig. 28. Oxygen coordination around the rare earth cations in A-type $Pr_2(Si_2O_7)$

Therefore O(11) was considered to belong to the second shell; this is supported by its function as the bridging oxygen in a double tetrahedron with a reduced charge contribution as compared with the terminal oxygen atoms of the polyhedron. The arrangement of the closest seven oxygen atoms at a mean distance of 2.48 Å of the first shell of Pr(1)

recalls the sevenfold-coordinated lanthanide ion in the B-type sesquioxide structure. It has the shape of a trigonal prism with the seventh oxygen atom coordinating through one face. An interesting feature of this polyhedron is the corner oxygen atom O(4) on the prism, which is the bridging oxygen of the first double-tetrahedra group. The distance Pr(1)—O(4) of 2.66 Å is about 0.16 Å larger than the next inner one O(10) with 2.52 Å.

In contrast to the result for Pr(1), the Pr(3)-oxygen coordination O(13) was considered to belong to the first shell because its distance of 2.96 Å is closer to the seven distances of the other oxygen atoms ranging from 2.32 to 2.66 Å than to the second shell which starts at 3.56 Å. Hence, Pr(3) has coordination number 8. The shape of the Pr(3) oxygen polyhedron is close to a dodecahedron, which is a common coordination type in lanthanide compounds.

This disilicate structure type A is also known from the corresponding pyrophosphate β—$Ca_2P_2O_7$ (*64*). A structure analysis was carried out also on the isomorphous compound $Sm_2(Si_2O_7)$ (*25*).

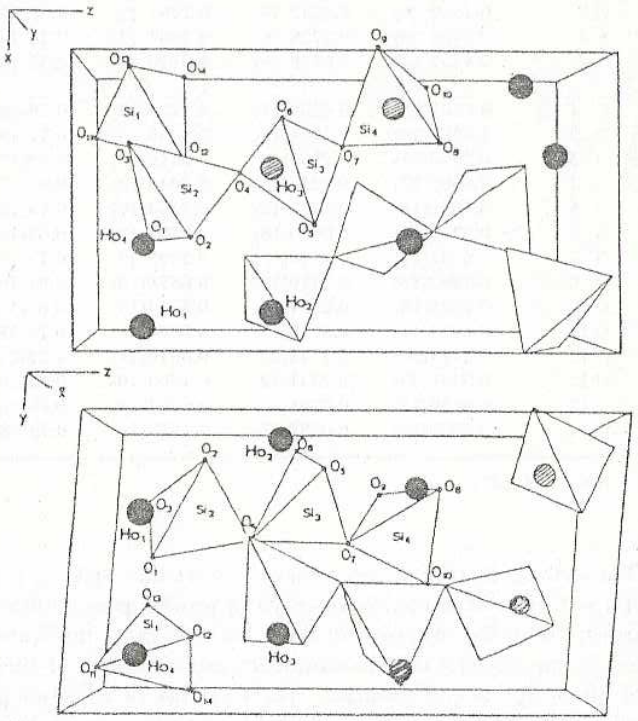

Fig. 29. Crystal structure of $Ho_4(Si_2O_{10})(SiO_4)$

The shape of the eightfold coordinated heavy atoms can hardly be described in terms of Cartesian geometry (Fig. 30). Their shape varies between a strongly distorted cube and a distorted type of dodecahedron. The mean values of the Ho—O distances are 2.42 Å, 2.42 Å, 2.47 Å, 2.46 Å, which gives an average value of 2.44 Å for all four crystallographically independent Ho cations.

The (SiO_4)tetrahedra show a high degree of distortion (Fig. 30) with Si—O distances varying between 1.78 and 1.54 Å. This is the largest difference ever observed in a (SiO_4)tetrahedron in silicate structures, in view of the fact that e.s.d. values are 0.007 Å in this investigation. These extreme Si—O values within the individual tetrahedra belonging to the (Si_3O_{10}) chain are fairly well balanced, however. The mean values of the four Si-O distances in the three tetrahedra are 1.64 Å, 1.63 Å, and 1.65 Å. Another extreme value seems to be given in this configuration by the 118.2° angle at the bridging Si(2)—O(4)—Si(3) between the first and the middle tetrahedron in the (Si_3O_{10}) chain-like group. The other bridging angle Si(3)—O(7)—Si(4) is 133.2°, thus quite regular as compared to the observed angles for other disilicate groups, e.g. 129° and 133° in the Pr Di A structure. The degree of distortion seems also to be extremely high in the isolated (SiO_4)tetrahedra in this structure with two long Si—O distances of 1.72 and 1.70 Å, which are compensated by two extremely short Si—O distances of 1.56 Å. This single tetrahedron also shows the largest deviations from the ideal tetrahedral angle with 120.8° for O(11)—Si(1)—O(14) and 98.2° for O(11)—Si(1)—O(13).

At this point, it seems worthwhile to comment on the transition characteristics observed for polymorphic compounds of types RE Di E and RE Di B. The reconstructive type of transition, which had been suggested because of the extremely low rate of transformation and the fact that the pure B-type phase had never been observed after transition from the E-type modifications, is best understood in the light of the given structural information. The E → B transition appears to be mainly determined by the breaking of Si—O—Si bonds of the double-tetrahedra groups in the E-type structure to achieve the (Si_3O_{10}) configuration present in the RE Di B-type structure, and vice versa, on the pattern $2\,(Si_2O_7) \rightleftarrows (Si_3O_{10}) + (SiO_4)$.

An isotypic compound is likely to exist with the digermanate structures of the large rare-earth cations, as has been described recently for the La analogue (*65*). These structural data on the La digermanate were extremely helpful to identify the oxygen positions in the Ho disilicate structure as given in Table 16. Earlier suggestions (*21*) that there might be a close structural relation to $Cd_2P_2O_7$ or $K_2Cr_2O_7$ have to be rejected from the present point of view since both of the latter structure types contain double-tetrahedra groups (X_2O_7).

3.1.3. Structure Type C, (Ho. ... Lu)$_2(Si_2O_7)$, 'RE Di C'

Disilicate structure type C is the only one in the family of disilicate structures which is stable from room temperature up to the melting point of the compounds. Its range of stability along the rare-earth series is extended beyond the radius of the smallest rare-earth Lu^{3+}, to Sc^{3+} with r = 0.68 Å (*17, 66*). This structure type has also been named after the mineral thortveitite.

The latest crystal structure analysis, carried out on the Yb analogue (*24*), gave essentially the same result as that published for thortveitite, $Sc_2(Si_2O_7)$ (*67*). These authors concluded, from arguments derived from crystal chemistry concerning the different bond lengths and temperature vibrations of individual oxygen atoms, that space group C2/m is the correct one rather than the other possible space groups C2 or Cm. The data on $Sc_2(Si_2O_7)$ originally gave rise to a most stimulating discussion as to the possibility of 180° angles for the bridging Si—O—Si in silicate structures. This linear bridge has now been confirmed for $Yb_2(Si_2O_7)$. Considerable thermal motion of the bridging oxygen is however indicated by the B-value of 1.02 Å^2 as compared to 0.50 Å^2 and 0.54 Å^2 of the terminal oxygens. The structural analysis was carried out with 1220 single-crystal diffractometer intensity data. The final R value of 5.4%, corresponds to e.s.d.'s for the cation-oxygen distances of about 0.005 Å. The refined values of the atomic parameters are given in Table 17.

Table 17. *Atomic parameters of* $Yb_2(Si_2O_7)$

Atom	x	y	z	B[Å^2]
Yb	0.5	0.80687(2)	0.0	0.25
Si	0.7189(3)	0.5	0.4125(6)	0.37
O(1)	0.5	0.5	0.5	1.02
O(2)	0.8831(5)	0.5	0.7151(15)	0.50
O(3)	0.7361(5)	0.6504(4)	0.2197(11)	0.54

After Ref. (*24*).

The wide range of stability of this structure type is likely to be explained by the nearly closest hexagonal packing of the oxygens (Fig. 31) containing rare-earth cations in the octahedra holes and silicons in the tetrahedra holes in alternating parallel layers (*001*). The (SiO_4) tetrahedra show a very low degree of distortion as compared to other disilicate configurations (Fig. 32). The mean value of the Si—O bond length is 1.63 Å and the variation is ±0.01 Å. Also the octahedral oxy-

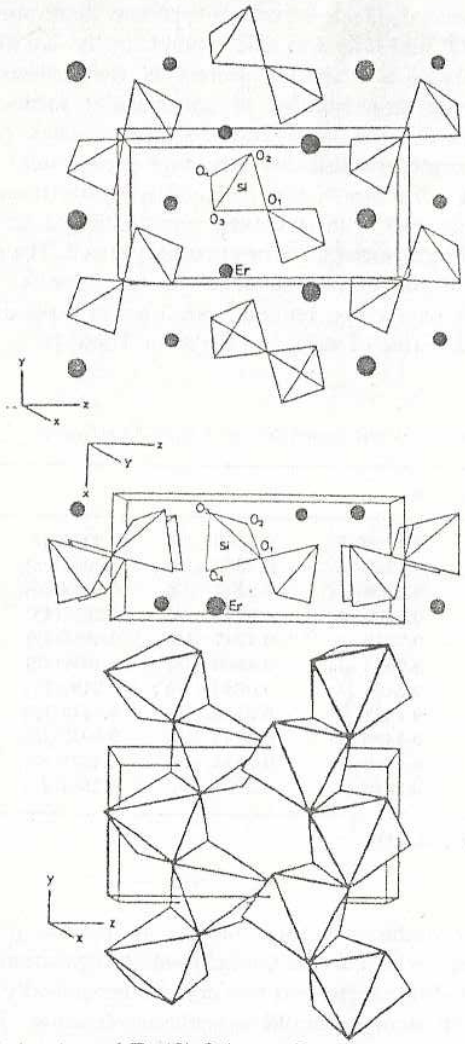

Fig. 33. Crystal structure of $Er_2(Si_2O_7)$ type D

ture has recently been refined from 1860 independent observations (*hkl*) for $Er_2(Si_2O_7)$ (*24*) which gave a final R value of 6.2% for the three-dimensional data. The atomic parameters and their standard deviations are listed in Table 18.

Table 18. *Atomic parameters of D-type* $Er_2(Si_2O_7)$

Atom	x	y	z	B[Å^2]
Er	0.88829(8)	0.09318(6)	0.34934(5)	0.29
Si	0.3601 (4)	0.6442 (3)	0.3871 (3)	0.33
O(1)	0.5	0.5	0.5	0.91
O(2)	0.2052 (8)	0.8653 (7)	0.4486 (6)	0.64
O(3)	0.1235 (9)	0.4583 (8)	0.3191 (6)	0.63
O(4)	0.6184 (9)	0.7522 (7)	0.2984 (6)	0.56

After Ref. (*24*).

The interesting unit in this structure (Fig. 33) is the (Si_2O_7) double-tetrahedra group. Its centrosymmetry and 180° Si—O—Si angle follow directly from the space group $P2_1/b$. Fourfold general positions and two-fold special positions at the centers of symmetry are possible in this space group. Since the unit cell with $Z = 2$ contains only two pyrosilicate groups, they necessarily occupy these special positions. Evidence for the linearity of the Si—O—Si bond, therefore does not depend on the accuracy of the intensity data applied during the structure refinement, as was the case with C-type $Sc_2(Si_2O_7)$ and $Yb_2(Si_2O_7)$. Thus, the structure of $Er_2(Si_2O_7)$ appears to provide further evidence for the possible existence of (Si_2O_7)groups with a Si—O—Si angle equal to 180°.

Also in this case the thermal motion of the bridging oxygen is considerably stronger than of the terminal oxygens (see Table 18). The bond lengths and valence angles in the double-tetrahedra group are given in Fig. 34.

The mean Si—O terminal O length is 1.62 Å. These terminal oxygen atoms of the (Si_2O_7) group form strongly distorted octahedra around the Er atoms similar to those around the Yb atom in $Yb_2(Si_2O_7)$. The bridging oxygen atom O(1) is not bonded to the Er cation. The mean Er—O distance in the octahedron is 2.27 Å. With the subgroup relation of space group $P2_1/b$ to space group $C2/m$ of structure type C, some structural features are correlated, namely, the staggered orientation of the double tetrahedra with the 180° Si—O—Si bridging angle and the sixfold oxygen coordination around the heavy atoms. However, in structure type D the orientation of the (Si_2O_7) groups relative to each other, and the connection of the Er—O octahedra are different. The (Si_2O_7) groups in structure type D are mutually directed along $[011]$ and $[0\bar{1}1]$. Consequently, the coordination of the heavy atoms does not result in a network-forming feature, as in structure type C, but in a ribbon-like arrangement along the b axis.

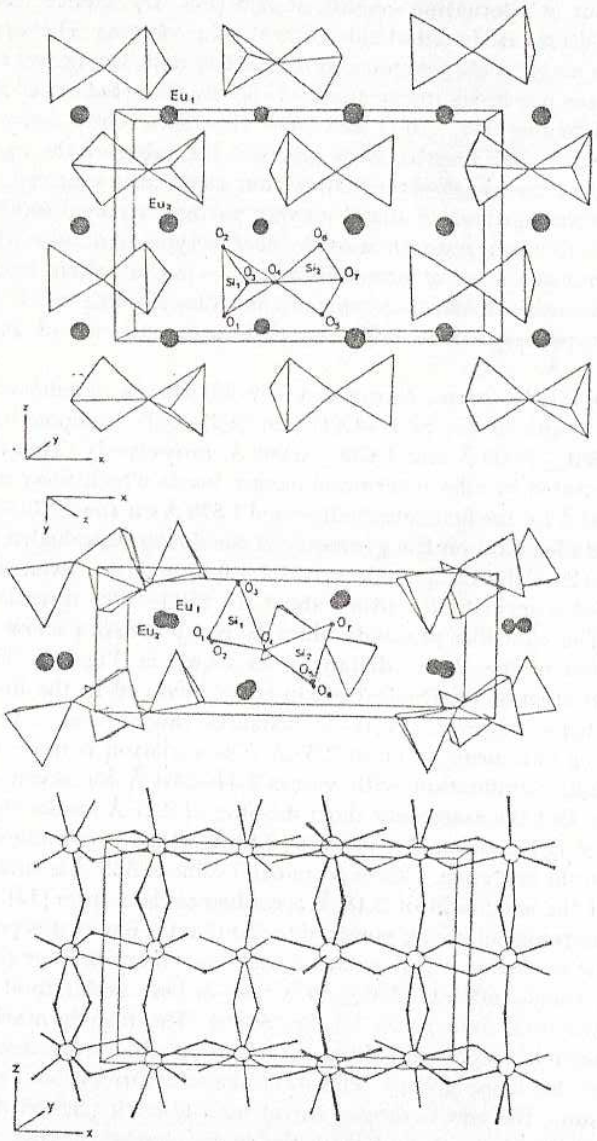

Fig. 35. Crystal structure of E-type $Eu_2(Si_2O_7)$

rules give the impression of a B-centred subcell which has just 1/4 of the volume of the supercell of corresponding space group symmetry $Pna2_1$-Pnam.

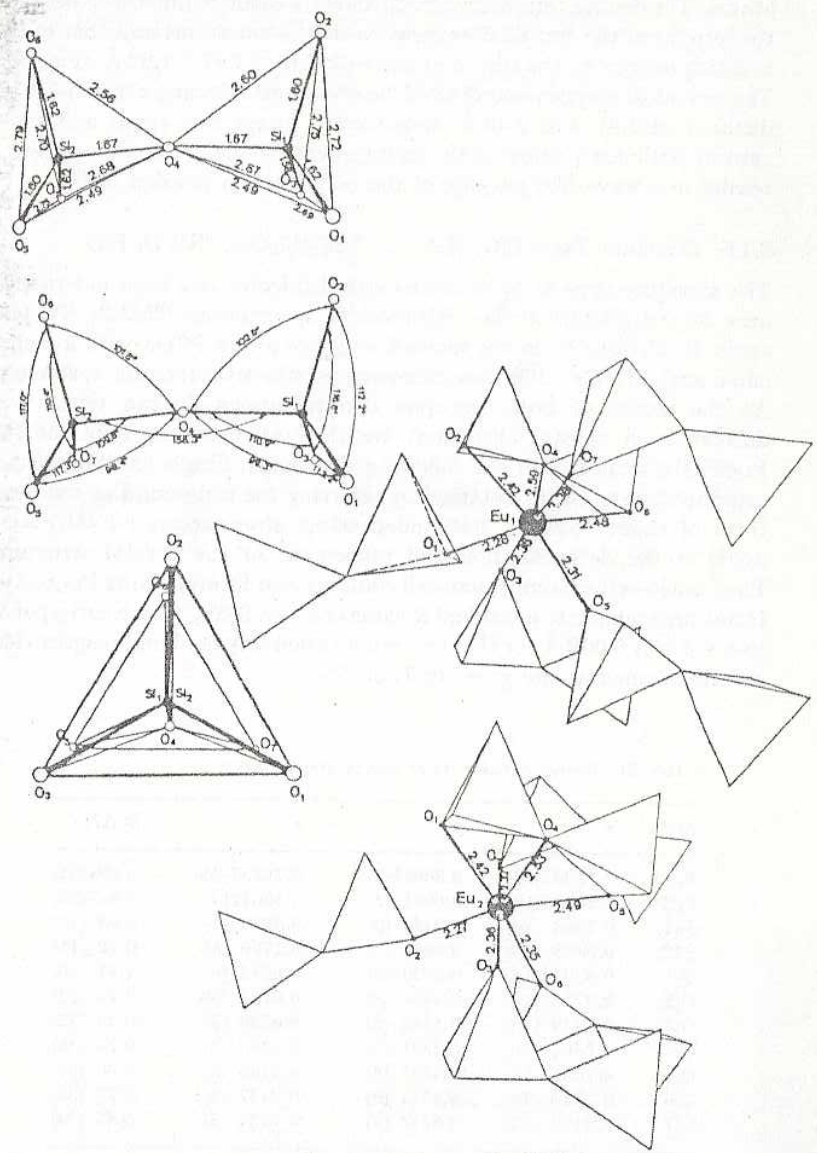

Fig. 36. Cation-oxygen coordination in E-type $Eu_2(Si_2O_7)$

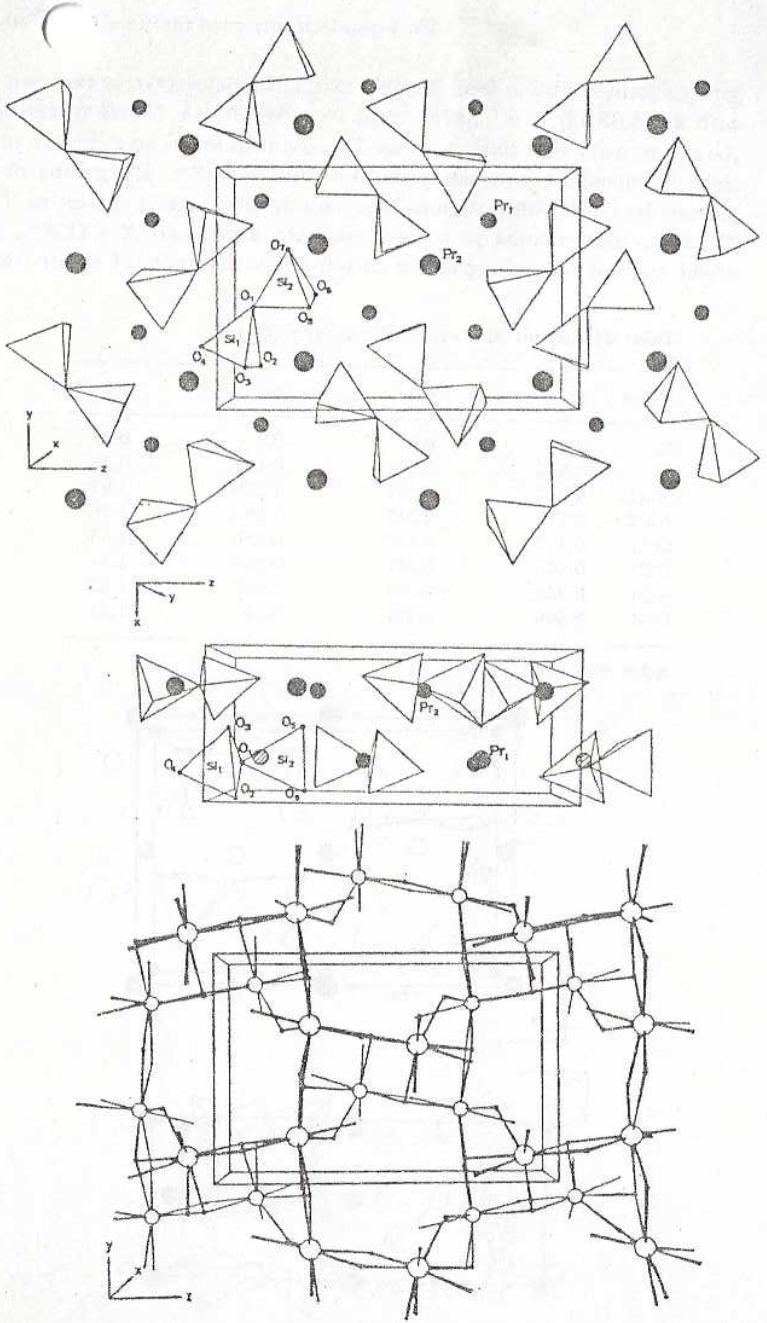

Fig. 37. Crystal structure of G-type $Pr_2(Si_2O_7)$

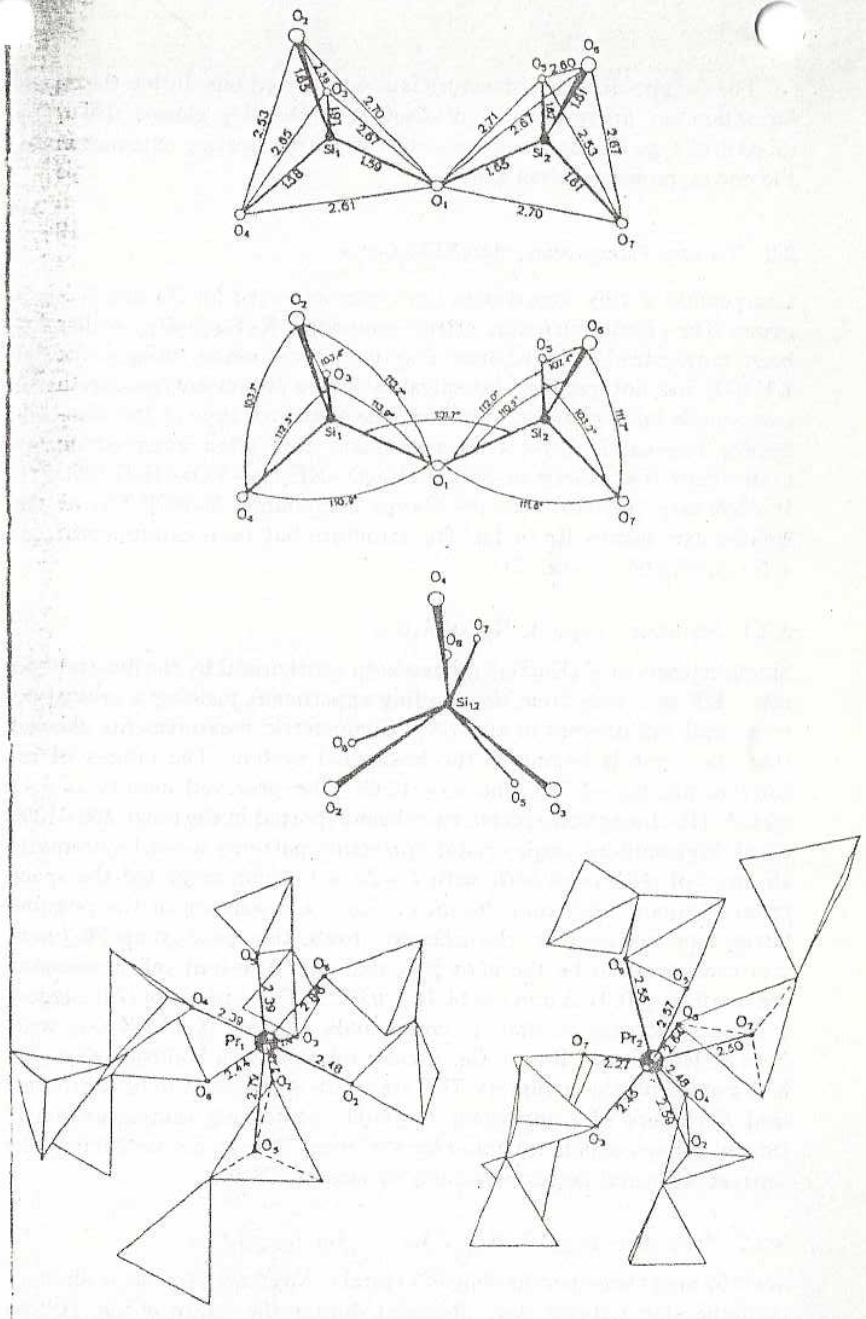

Fig. 38. Cation-oxygen coordination in G-type $Pr_2(Si_2O_7)$

The structure consists of isolated (Si_2O_7) groups, scandium-oxygen polyhedra in the shape of slightly distorted octahedra, and two independent sodium cations with Na(1) in a fivefold oxygen coordination and Na(2) in a fourfold coordination. The main structural motif is created by the isolated Sc—O octahedra with the Sc in the position *0,0,0* (Fig. 39). These octahedra are linked both by the (Si_2O_7) double-tetrahedra groups of eclipsed configuration and by Na—O polyhedra. The structure shows a high degree of similarity to the sheet-like silicates of vermiculite, nontronite and sanbornite, which also show two types of cores along the *c* axis. The degree of distortion in the Sc—O octahedron is fairly low (Fig. 40) with an average value for the Sc—O distances of 2.10 Å ± 0.03 Å. The (Si_2O_7) double-tetrahedra group is characterized by a plane of symmetry which relates the individual SiO_4 tetrahedra of the (Si_2O_7) group to each other. The mean Si—O bond length of the terminal oxygens is 1.62 Å, the distance to the bridging oxygen 1.68 Å. The angle Si—O—Si of the eclipsed (Si_2O_7) configuration is 136°.

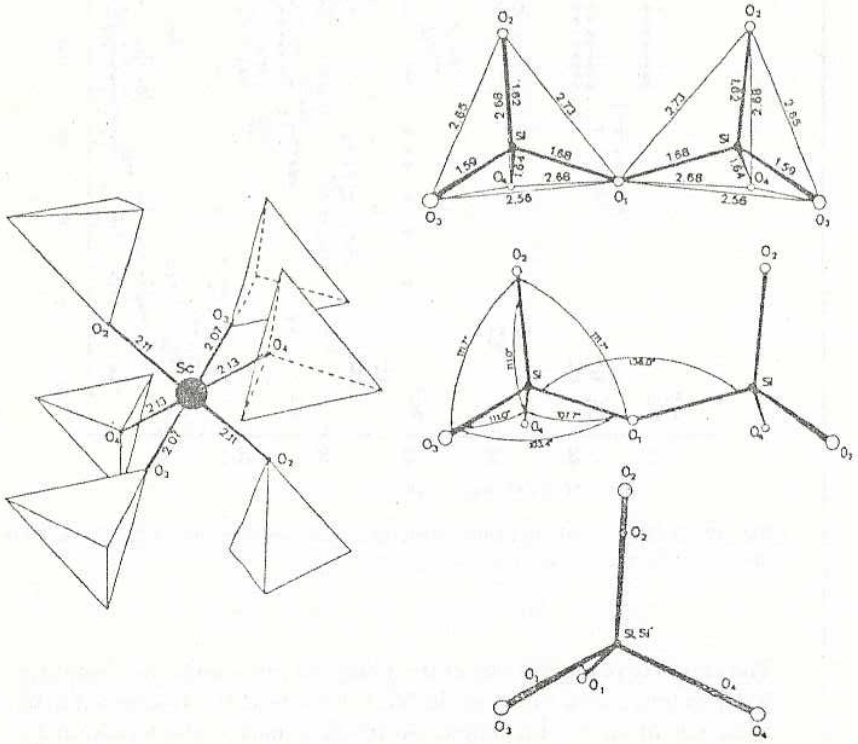

Fig. 40. Cation-oxygen coordination in $Na_3Sc(Si_2O_7)$

4. Polymorphism and Structural Data

Rare-earth silicates of composition 1 $RE_2O_3 \cdot 1\ SiO_2$, 7 $RE_2O_3 \cdot 9\ SiO_2$ and 1 $RE_2O_3 \cdot 2\ SiO_2$ were found in the binary systems RE_2O_3—SiO_2, with RE including the series of trivalent rare earths La^{3+} to Lu^{3+}. The disilicates $RE_2O_3 \cdot 2\ SiO_2$ show extensive polymorphism. Seven different structures, here named RE Di A, ... RE Di G, were observed of types $RE_2(Si_2O_7)$ and $RE_4(Si_3O_{10})(SiO_4)$. The structures contain (Si_2O_7)-douple tetrahedra of either the staggered or the eclipsed configuration and in one case, (RE Di B), almost linear (Si_3O_{10})groups plus isolated (SiO_4) tetrahedra. Oxyorthosilicates 1 $RE_2O_3 \cdot SiO_2$ show two different structures of type $RE_2(SiO_4)O$, named RE Oxy A and RE Oxy B. These structures contain isolated (SiO_4)tetrahedra plus isolated, not silicon-bonded oxygens. Compounds 7 $RE_2O_3 \cdot 9\ SiO_2$ were observed to crystallize in only one structure with the complete series of trivalent rare earths. This structure is of the apatite type $RE_{9.33}\square_{0.66}(SiO_4)_6O_2$, showing $^2/_3$ cation deficiency per cell.

The ranges of stability of the various structural types over the rare-earth series are shown below Fig. 41. Structures of the ternary rare-earth silicate compounds and the sesquioxides (*85*) are included for comparison.

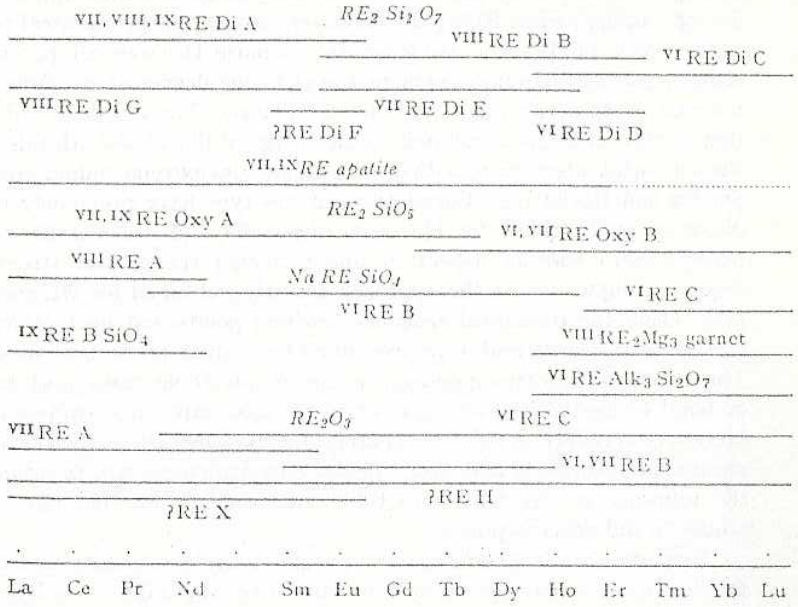

Fig. 41. Stability ranges of structural types along the rare-earth series

Table 22. *Data on cation-oxygen coordination in rare-earth disilicate crystal structures containing* (Si_2O_7) *or 2* $(Si_2O_7) \equiv (Si_3O_{10}) + (SiO_4)$ *configurations. For symbols used and definitions as given in e. g. chapter 4.1*

Compound				RE—O coordination		Si—O coordination								
Mol. composition	Structure type	Coordination formula	mean e.s.d. (M—O)	^{CN}RE	$\langle\bar{d}\rangle$ [Å] (RE—O)	Δd_{max} [Å] $(d-\langle\bar{d}\rangle)$	^{cn}O	$\langle\bar{d}\rangle$ [Å] (Si—O)	Δd_{max} $(d-\langle\bar{d}\rangle)$	^{cn}O	$\bar{d}_{ter}$ [Å]—Si—O—Si—[Å] $\bar{d}_{brl}$ [°]		^{cn}O	^{cn}O
$1\ Pr_2O_3 \cdot 2\ SiO_2$	RE Di A	$^{VII}Pr\ ^{VIII}Pr\ ^{IX}Pr_2(Si_2O_7)_2$	0.007 Å	^{VII}Pr	2.48 Å	+0.18 Å −0.07	3.7	1.63 Å	+0.04 Å −0.02	3.5	1.62	1.65 Å 128.5°	1.63	3.7	3.0
				^{IX}Pr	2.58	+0.14 −0.19	3.7	1.63	+0.03 −0.04	3.5					
				^{VIII}Pr	2.52	+0.44 −0.19	3.6	1.63	+0.01 −0.04	3.5	1.62	1.65 Å 133.1°	1.62	3.5	3.0
				^{IX}Pr	2.59	+0.35 −0.20	3.2	1.63	+0.04 −0.03	3.3					
$1\ Ho_2O_3 \cdot 2\ SiO_2$	RE Di B	$^{VIII}Ho_4(Si_3O_{10})(SiO_4)$	0.009 Å	^{VIII}Ho	2.42 Å	+0.30 Å −0.18	3.5	1.64 Å	+0.08 Å −0.08	3.5					
				^{VIII}Ho	2.42	+0.42 −0.17	3.6	1.64	+0.14 −0.08	3.3	1.60	1.66 Å 118.2°		3.5	3.0
				^{VIII}Ho	2.47	+0.43 −0.30	3.5	1.63	+0.12 −0.09	3.3		1.69 Å			4.0
				^{VIII}Ho	2.46	+0.33 −0.30	3.3	1.65	+0.06 −0.08	3.8		132.2°	1.65	3.5	
$1\ Yb_2O_3 \cdot 2\ SiO_2$	RE Di C	$^{VI}Yb_2(Si_2O_7)$	0.005 Å	^{VI}Yb	2.24 Å	+0.04 Å −0.03	3.0	1.63 Å	+0.01 Å −0.01	2.8	1.63	1.63 Å 180.0°	1.63	3.0	2.0
$1\ Er_2O_3 \cdot 2\ SiO_2$	RE Di D	$^{VI}Er_2(Si_2O_7)$	0.005 Å	^{VI}Er	2.26 Å	+0.05 Å −0.03	2.3	1.62 Å	+0.01 Å −0.01	2.3	1.62	1.63 Å 180.0°	1.62	2.3	2.0
$1\ Eu_2O_3 \cdot 2\ SiO_2$	RE Di E	$^{VII}Eu_2(Si_2O_7)$	0.008 Å	^{VII}Eu	2.41 Å	+0.18 Å −0.13	3.1	1.62 Å	+0.05 Å −0.02	3.3	1.61	1.67 Å 158.3°	1.62	3.0	4.0
				^{VII}Eu	2.40	+0.12 −0.13	3.1	1.63	+0.06 −0.01	3.3					
$1\ Pr_2O_3 \cdot 2\ SiO_2$	RE Di G	$^{VIII}Pr_2(Si_2O_7)$	0.009 Å	^{VIII}Pr	2.57 Å	+0.29 Å −0.17	3.8	1.61 Å	+0.04 Å −0.03	3.3	1.62	1.62 Å 131.2 Å	1.61	3.7	2.0
				^{VIII}Pr	2.51	+0.13 −0.24	3.8	1.62	+0.03 −0.01	3.3					

between the oxygens in the coordination spheres increase as the size of the rare-earth cations decreases. These forces eventually become large enough to make the structure energetically unstable. At this point the coordination number of the cation is reduced in order to minimize the potential energy from its short-range configuration and a new structure is initiated. This electrostatic principle of a compromise between a maximum of spherical shielding for the cation and a minimum of repulsion amongst the coordination anions, obviously results in a different number of stable crystal structures for compounds of different composition. As was shown in detail, silicates of composition $1\ RE_2O_3 \cdot 2\ SiO_2$ show the highest number of polymorphic forms amongst all the rare-earth silicates. The very sensitive configuration of the (Si_2O_7)groups is likely to be responsible for the seven different structure types. The double tetrahedra generally have a less spherical character than isolated (SiO_4)tetrahedra or isolated oxygens, even when these include all possibilities of distortion between staggered and eclipsed orientation. This shortcoming prohibits to provide extensive spherical shielding around the larger rare-earth cations and coordination with oxygens distributed almost equi-

4.1. Configuration of the (SiO_4)Tetrahedra

The size of most of the trivalent rare-earth ions is far beyond what is required for the stability of octahedral oxygen coordination. For this reason, closest packing of the oxygens with Si and RE cations accommodated in tetrahedral and octahedral holes was not found in any of the larger rare-earth silicate structures. The anionic part of the structures represented by single oxygens, (SiO_4)tetrahedra or by (Si_2O_7)-, (Si_3O_{10})-groups seems to be adapted by the rare-earth cations in such a way as to achieve as much spherical shielding as is allowed by the degree of distortion possible in the individual (SiO_4)tetrahedra. The electrostatic bonding character (75%) and the strong polarizing forces of the rare-earth cations against oxygen result in extreme distortion of the individual (SiO_4)tetrahedra from the ideal tetrahedral configuration. The ideal symmetry of point group T_d, which would correspond to a tetrahedron showing equal Si—O distances and 109° 28′ of the O—Si—O angles, was always found to be reduced to C_1.

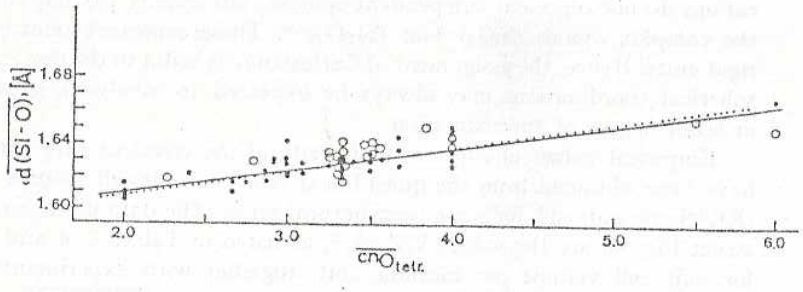

Fig. 43. Variation of mean bond lengths $<\overline{d(Si-O)}>$ with mean coordination number of the oxygens $\overline{cn O_{tetr.}}$ of individual (SiO_4) tetrahedra in the asymmetric unit of RE-silicate structures, which have been refined to a level corresponding to e.s.d.'s (Si—O) ≤ 0.01 Å (white balls). Black balls and solid line represent corresponding data from (*82*), dotted line data from (*54*)

In order to achieve a better understanding of the appreciable variation in Si—O bond lengths, the following correlations were carried out. The average coordination numbers of the silicon-bonded oxygens of individual (SiO_4)tetrahedra were correlated with the mean Si—O distances in the tetrahedra. As Fig. 43 shows, there is rather poor correlation between these values in most cases. Better correlation was found between the variation in the individual Si—O bond lengths Δd,

and the variation in charge balance Δp_o on the oxygens. This correlation is based on the following assumptions. According to Pauling's electrostatic valence principle (*73*), the individual bond strength of an oxygen surrounded by 'cn' cations of valency z_i to a single cation i with coordination number CN at the center of a polyhedron, is given by $s_i = \frac{z_i}{CN_i}$. The degree of charge balance p_o on any individual oxygen is then given by the 'cn' contributions s_i reaching the oxygen from 'cn' cations of the coordination shells to which it belongs. Thus, the sum over the single bond strengths $p_o = \sum_{i=1}^{cn} s_i$ should show a value for oxygens in ionic crystals close to 2.0.

The electrostatic valence principle recently was applied to a large number of silicate structures with some success (*83*, *84*). There, the variations Δd (Si—O) and Δp_o of the individual Si—O bonds were correlated. However, in the computations it is assumed that all contributions to the charge balance of the oxygen are controlled solely by the quotient $\frac{z_i}{CN_i}$. The author neglects the fact that the spherical density distribution of electrostatic forces, arising from the $z \cdot$ e-fold charged cation, decreases with $\frac{z \cdot e}{d^2}$, where d is the individual oxygen-cation distance in a given coordination polyhedron. This means that the local charge balance on any oxygen should be strongly dependent on the individual cation-oxygen distances. This point must not be neglected in the case of the rare-earth silicate structures. The RE—O distances have been shown in Tables 22 and 23 to vary considerably within a given coordination polyhedron.

Following Gauss' law, a qualified correction term for Pauling's electrostatic valence rule seems to be given by the quotient $\frac{<\bar{d}>^2}{d_i^2}$. It presents a simple dimensionless number. In this term d_i is the individual oxygen-cation distance and $<\bar{d}>$ is the mean cation-oxygen distance in a given coordination polyhedron. Thus, the charge balance on an individual oxygen is given by the value.

$$p_o = \sum_{i=1}^{cn} s_i \quad [\text{v.u.}]$$

in valence units [v.u.] with

$$s_i = \frac{z_i}{CN_i} \left(\frac{<\bar{d}>}{d_i} \right)^2 [\text{v.u.}]$$

A strong and nearly linear correlation is given in Fig. 44 for all binary rare-earth silicate structures on the basis of this term for the variation

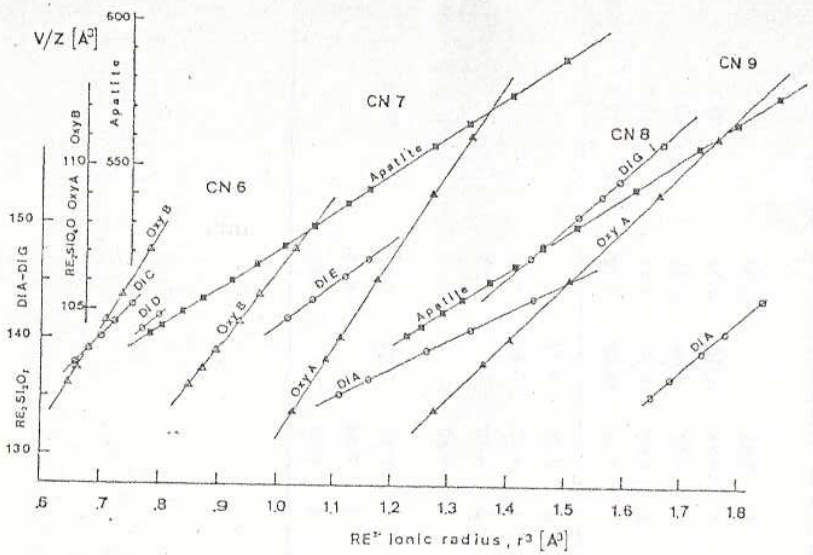

Fig. 45. Plot mol. volume, V/Z[Å³] vs RE^{3+} ionic radii, r^3[Å³] of isostructural series of RE-silicate compounds

sponding line in Fig. 45, a second known value r ($^{CN}RE_{i+n}$) had to be introduced. In isostructural series where experimental structural data are available on one compound only, the value V/Z [Å]³ for the remaining members of the series has been made consistent on the assumption that the relative size of the RE^{3+} ions within a given series of identical coordination is the same as in other isostructural compounds of different coordination number. This seems to be proved by the two series for CN 6 and CN 8 of cubic C-type RE_2O_3, 'RE'OCl (*48*) and RE-pyrochlores (*54*), respectively. Thus, the unknown ionic radii r (RE_{i+n}) were supplied in terms of the quotients $r^3(RE_i)/r^3(RE_{i+n})$ from other isostructural series with different coordination numbers, which are fully supported by experimental data on structure, i.e. for at least two compounds in a given series. In this way, the slope of the linear relations in Fig. 45 has been determined for the isostructural series of compounds $RE_2(SiO_4)$ O (Oxy A, Oxy B) and oxyapatites $RE_{9.33}\square_{0.67}(SiO_4)_6O_2$. For polymorphic disilicates $RE_2Si_2O_7$ the following structural data have been taken into account: DiA = $(Pr_2(Si_2O_7)$ (*26*), $Sm_2(Si_2O_7)$ (*25*), DiC = $Yb_2(Si_2O_7)$ (*24*), $Sc_2(Si_2O_7)$ (*67*); DiD = $Er_2Si_2O_7$ (*24*), $Y_2(Si_2O_7)$ (*22*, *23*); DiE = $Gd_2(Si_2O_7)$ (*24*), $Eu_2(Si_2O_7)$ (*27*); DiG = $Nd_2(Si_2O_7)$ (*24*), $Pr_2(Si_2O_7)$ (*20*)).

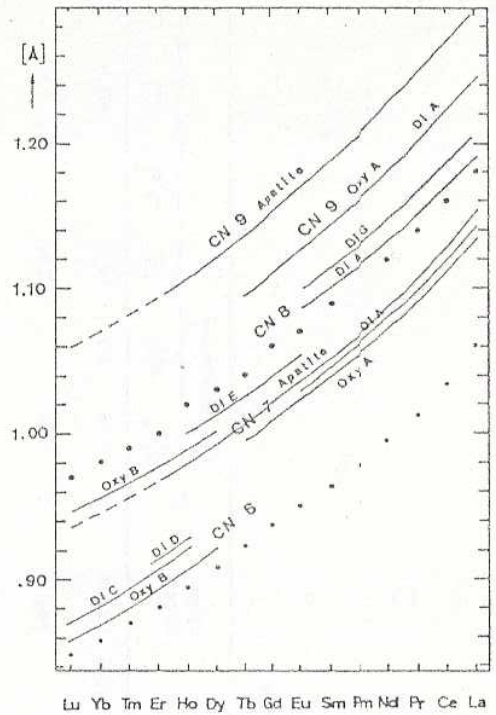

Fig. 46. Effective ionic radii [Å] of trivalent rare earths in different oxygen coordination, CN 6, 7, 8, 9, as derived from structural data, employed in the relation mol. volume vs. r^3 (RE^{3+}) (Fig. 45) for isostructural series of compounds $RE_2(SiO_4)O$ (OxyA, OxyB), $RE_2(Si_2O_7)$ (DiA, ... DiG) and apatite-like $(RE_{9.33}\square_{0.67})(SiO_4)_6O_2$. The symbols • and ● represent the $r(RE^{3+})$ values for CN 6 and CN 8 from Refs. (*48*) and (*54*), respectively

The empirical set of RE^{3+} ionic radii with different coordination numbers resulting from this procedure is presented in Fig. 46. The lines representing individual coordination in a given silicate structure type correspond to an experimental error of ± 0.01 Å. Thus, the agreement between r (RE^{3+}) values of the same coordination number in different structure types is fairly good. The data on the ninefold coordinated RE^{3+} cations of apatite $(RE_{3.33}+\square_{0.67})RE_6(SiO_4)_6O_2$ are of special character because of the cation deficiency $^{IX}(3\ ^1/_3\ RE+\ ^2/_3\ \square)$ in the (4*f*) position of this structure. The rare-earth silicate lines are on a generally higher level than the corresponding data from the simpler oxides (*48*) (*54*) of CN 8 and CN 6.

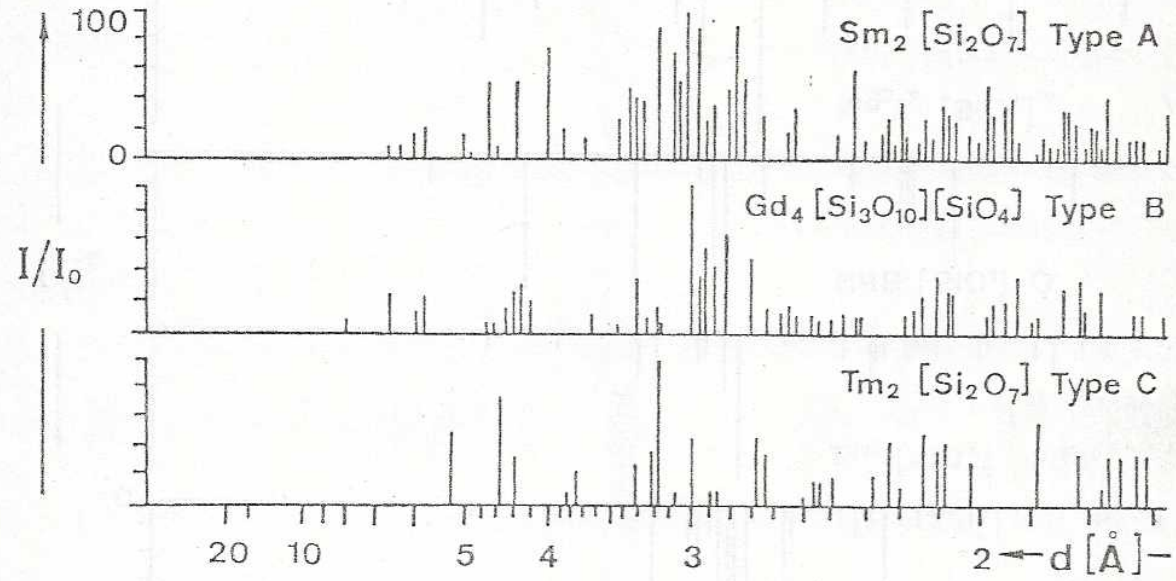
100
0
$Sm_2[Si_2O_7]$ Type A
$Gd_4[Si_3O_{10}][SiO_4]$ Type B
$Tm_2[Si_2O_7]$ Type C
I/I_o
20 10 5 4 3 2 ← d [Å]

Fig. A 1

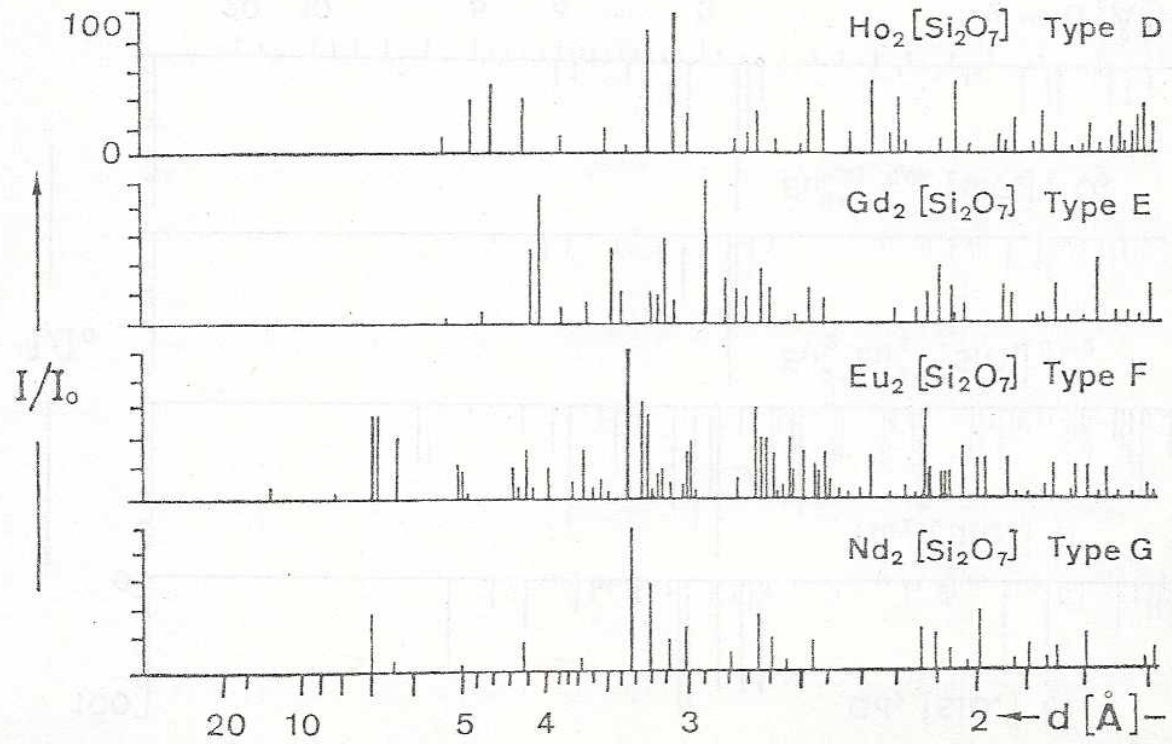
100
0
$Ho_2[Si_2O_7]$ Type D
$Gd_2[Si_2O_7]$ Type E
$Eu_2[Si_2O_7]$ Type F
$Nd_2[Si_2O_7]$ Type G
I/I_o
20 10 5 4 3 2 ← d [Å]

Fig. A 2

18. *Felsche, J., Hirsiger, W.:* J. Less-Common Metals *18*, 131 (1969).
19. — J. Appl. Cryst. *2*, 1380 (1969).
20. — Naturwissenschaften *57*, 127 (1970).
21. — J. Less-Common-Metals *21*, 1 (1970).
22. *Batalieva, N. G., Pyatenko, Yu. A.:* Zh. Strukt. Khim. *8*, 548 (1967).
23. — — Zh. Strukt. Khim. *11*, 921 (1968).
24. *Smolin, Yu. I., Shepelev, Yu. F.:* Acta Cryst. *B26*, 484 (1970).
25. — — Kristallografiya *15*, 256 (1970).
26. *Felsche, J.:* Z. Krist. *133*, 304 (1971).
27. — Naturwissenschaften *59*, 35 (1972).
28. — Acta Cryst. 1973 (in the press).
29. *Chichagov, A. V., Litvin, B. N., Belov, N. V.:* Kristallografiya *14*, 119 (1969).
30. — — — Geokhimiya *9*, 1044 (1968).
31. *Maksimov, B. A., Litvin, B. N., Ilyukhin, V. V., Belov, N. V.:* Kristallografiay *14*, 498 (1969).
32. *Ito, J.:* Mat. Res. Bull. *2*, 1093 (1967).
33. *Shafer, W. M., McGuire, T. R., Suits, J. C.:* Phys. Rev. Letters *11*, 251 (1963).
34. *Rau, R. C.:* Acta Cryst. *17*, 1483 (1964).
35. *Kaldis, E., Verreault, R.:* J. Less-Common Metals *20*, 177 (1970).
36. *Shafer, W. M.:* J. Appl. Phys. *36*, 1145 (1965).
37. *Bondar, I. A., Toropov, N. A., Koroleva, L. N.:* Izv. Akad. Nauk SSSR, Neorg. Mat. *1*, 561 (1965); *3*, 2034 (1967).
38. *Maksimov, B. A., Kharitonov, Yu. A., Ilyukhin, V. V., Belov, N. V.:* Dokl. Akad. Nauk SSSR *183*, 1072 (1968).
39. *Buisson, G., Michel, C.:* Mat. Res. Bull. *3*, 193 (1968).
40. *Felsche, J.:* Naturwissenschaften *58*, 565 (1971).
41. *Smolin, Yu. I.:* Kristallografiya *14*, 985 (1969).
42. *Harris, L. A., Finch, C. B.:* Am. Mineralogist. *50*, 1493 (1965).
43. *Felsche, J.:* J. Sol. State Chem. *5*, 266 (1972).
44. *Ito, J.:* Am. Mineralogist *53*, 890 (1968).
45. *Cochbain, A. G., Smith, G. V.:* Mineral. Mag. *36*, 411 (1968).
46. — Mineral. Mag. *36*, 654 (1968).
47. *Smolin, Yu. I., Shepelev, Yu. F.:* Izv. Akad. Nauk SSSR, Inorg. Mater. *5*, 1823 (1969).
48. *Templeton, D. H., Dauben, C. H.:* J. Am. Chem. Soc. *76*, 5237 (1954).
49. *McCarthy, G. J., White, W. B., Roy, R.:* J. Inorg. Nucl. Chem. *29*, 253 (1967).
50. *Grisafe, D. A., Hummel, F. A.:* Am. Mineralogist *55*, 1131 (1970).
51. *Schwarz, H.:* Inorg. Nucl. Chem. Letters *3*, 231 (1967).
52. *Blasse, G., de Vries, J.:* J. Inorg. Nucl. Chem. *29*, 1541 (1967).
53. *Posner, A. S., Perloff, A., Diorio, A. F.:* Acta Cryst. *11*, 308 (1958).
54. *Shannon, R. D., Prewitt, C. T.:* Acta Cryst. *B25*, 925 (1969).
55. *Chichagov, A. V., Belov, N. V.:* Geokhim. SSSR *12*, 1456 (1968).
56. *Chichagov, A. V., Ilyukhin, V. V., Belov, N. V.:* Dokl. Akad. Nauk SSSR *177*, 574 (1967).
57. *Maksimov, B. A., Ilyukhin, V. V., Belov, N. V.:* Kristallografiya *12*, 214 (1967).
58. *Voronkov, A. A., Pyatenko, Yu. A.:* Kristallografiya *12*, 214 (1967).
59. *Busch, G., Kaldis, E., Verreault, R., Felsche, J.:* Mat. Res. Bull. *5*, 9 (1970).
60. *Felsche, J.:* Naturwissenschaften *58*, 218 (1971).
61. *Eysel, W., Hahn, Th.:* Z. Krist. *131*, 322 (1970).
62. *Weidenborner, J. E., Stemple, N. R., Okaya, Y.:* ACA-Abstract, p. 69 (1965).
63. *Glasser, L. S. D., Glasser, F. P.:* Acta Cryst. *18*, 453 (1965).
64. *Webb, N.:* Acta Cryst. *21*, 942 (1966).

65. *Smolin, Ju. I., Shepelev, Yu. F., Upalova, T. V.:* Soviet Phys. "Doklady" (English Transl.) *14*, 630 (1970).
66. *Shannon, R. D., Prewitt, C. T.:* J. Sol. State Chem. *2*, 199 (1970).
67. *Cruickshank, Lynton, H., Barclay, G. A.:* Acta Cryst. *15*, 491 (1962).
68. *Bayer, G., Felsche, J., Hirsiger, W.:* Glastechn. Ber. *42*, 317 (1969).
69. *Felsche, J., Hirsiger, W.:* Glastech. Ber. *45*, 173 (1972).
70. *Bondar, I. A., Tenisheva, T. F., Toropov, N. A., Shepelev, Yu. F.:* Dokl. Akad. Nauk SSSR *160*, 1069 (1965).
71. *Skshal, S. M., Simonov, V. I., Belov, N. V.:* Dokl. Akad. Nauk SSSR *184*, 337 (1969).
72. *Naray-Szabo, T.:* Phys. Chem. Glass *4*, 38A (1963).
73. *Pauling, L.:* J. Am. Chem. Soc. *51*, 1010 (1929).
74. *Zachariasen, W. H.:* Acta Cryst. *16*, 385 (1968).
75. *Pant, A. K., Cruickshank, D. W. J.:* Z. Krist. *125*, 1 (1967).
76. *Clark, J. R., Appleman, D. E., Papike, J. J.:* Contr. Mineral. Petrology *20*, 81 (1968).
77. *Voronkov, M. G.:* Dokl. Akad. Nauk SSSR *138*, 106 (1961).
78. *Cruickshank, D. W. J.:* J. Chem. Soc. *1077*, 5486 (1961).
79. *Brown, G. E., Gibb, G. V., Ribbe, P.:* Am. Mineralogist *54*, 1044 (1969).
80. *Neumann, H., Bergstol, S., Nilssen, B.:* Norsk Geol. Tidsskr. *46*, 327 (1966).
81. *Toropov, N. A., Bondar, I. A., Lazarev, A. N., Smolin, Yu. I.:* Rare Earth Silicates and Their Analogues, Akad. Nauk SSSR ('NAUKA'), Leningrad, 1971 (in russ.).
82. *Brown, G. E., Gibbs, G. V.:* Am. Mineralogist *54*, 1528 (1969).
83. *Baur, W. H.:* Am. Mineralogist *56*, 1573 (1971).
84. — Trans. Am. Cryst. Ass. *6*, 125 (1970).
85. *Foex, M., Traverse, I. P.:* Bull. Soc. Mineral. Crist. *89*, 184 (1966).
86. *Brown, I. D., Calvo, C.:* J. Sol. State Chem. *1*, 173 (1970).
87. *Strunz, H.:* Mineralogische Tabellen, Leipzig: Akad. Verlagsgesellschaft 1970.
88. *Bandurkin, G. A., Dzhurinskii, B. F.:* Dokl. Akad. Nauk SSSR *168*, 1315 (1966).
89. *Gschneider, K. A.:* J. Less-Common Metals *25*, 405 (1971).
90. *Felsche, J., Kaldis, E.:* J. Sol. State Chem. *5*, 49 (1972).

Received July 11, 1972.